Reactivity of Low-Valent Iron and Cobalt Complexes with Fluoroalkenes

Karine Ghostine

Thesis submitted to the University of Ottawa

in partial fulfillment of the requirements for the

Master of Science, Chemistry

Department of Chemistry and Biomolecular Sciences

Faculty of Science

University of Ottawa

Abstract

Fluorocarbons are versatile molecules that are used in multiple industries ranging from pharmaceuticals to refrigerants, insecticides and advanced materials. More particularly hydrofluorocarbons (HFCs) and hydrofluoroolefins (HFOs) are current replacements for ozone-depleting chlorofluorocarbons (CFCs) that were used for decades as refrigerants, propellants, solvents and blowing agents. However, syntheses of HFCs and HFOs involve energy-intensive processes and toxic compounds such as heavy metals and anhydrous HF. Development of more sustainable, energy efficient and "greener" synthesis of small fluorocarbons is needed, which draws attention to organometallic catalysis, especially with abundant, inexpensive and non-toxic transition metals. One approach to new organometallic routes to hydrofluorocarbons involves the formation and functionalization of fluorometallacycles. Previous work in the 1990's by Baker *et al.* demonstrated the catalytic hydrodimerization of tetrafluoroethylene (TFE) using Ni catalysts with π-acidic phosphite ligands. They also demonstrated the hydrogenolysis of the d^6 ferracyclopentane, $Fe(CO)_4(1,4\text{-}C_4F_8)$, **2-1**, under high pressure and temperature with different additives to give mixtures of different hydrofluorocarbons. Since that time the reactivity of d^8 fluorometallacyles has been extensively studied, leading to fundamental understanding and new catalytic applications. However less attention has been paid to d^6 systems, the synthesis and reactivity of which are the focus of this Thesis.

Following introduction and background in **Chapter 1**, **Chapter 2** presents the synthesis and characterization of a series of new NHC-, phosphine- and nitrogen-ligand-substituted Fe(II) perfluorometallacycles derived from complex **2-1**. This led to the discovery of the first example of a fluorinated metallacyclocarbene obtained from *in situ* C_α–F bond activation that afforded

FeF(triphos)(1,4-C_4F_7), **2-6**, (triphos = bis(2-diphenylphosphinoethyl)phenylphosphine) during the P-based linear tridentate ligand substitution reaction. [Fe(triphos)(1,4-C_4F_7)(NCMe)]$^+BPh_4^-$, **2-7**, and Fe(OTf)(triphos)(1,4-C_4F_7), **2-8**, were derived from **2-6** by treatment with $NaBPh_4$ in acetonitrile and Me_3Si-OTf, respectively (Tf = triflate, SO_2CF_3). The same phenomenon was not observed with hard-donor N-based linear tridentate ligand, terpy', (terpy' = 4′-(4-methylphenyl)-2,2′:6′,2″-terpyridine), presumably because of the less Lewis acidic metal center. Fluoride abstraction from Fe(terpy')(CO)(1,4-C_4F_8), **2-9**, by a Lewis acid, however allowed for C_α–F bond activation to give the cationic iron monocarbonyl carbene complex, [Fe(terpy')(CO)(1,4-C_4F_7)]$^+OTf^-$, **2-10**. **Chapter 3** investigates further the reactivity of these new Fe(II) perfluorometallacycle complexes. The lack of reactivity of the mono- and di-substituted Fe carbonyl perfluorometallacycles with Lewis acids confirmed that C_α–F bond activation only occurs when there is enough π-backbonding into the C_α–F anti-bonding orbital, as π-acceptor phosphines and carbonyl ligands can compete for the metal back-bonding. Indeed, C_α–F abstraction is only observed with Fe(terpy')(CO)(1,4-C_4F_8), **2-9**, due to the poor acceptor ability of the nitrogen ligand. On the other hand, the lack of electron density on the metal center can cause the Fe center to act as an internal Lewis acid, promoting C_α–F migration as observed *in situ* during the triphos substitution reaction. These results show that d^6 [Fe] perfluorometallacycles do not share similar reactivity with d^8 [Ni] perfluorometallacycles. Moreover, the study of the character of the Fe=C^F bonds suggests a nucleophilic carbene for **2-6**, while **2-7, 2-8** and **2-10** all displayed electrophilic carbene character. Furthermore, hydrogenolysis of Fe(OTf)(triphos)(1,4-C_4F_7), **2-8**, and [Fe(triphos)(1,4-C_4F_7)(NCMe)]$^+BPh_4^-$, **2-7**, at low pressure and room temperature, generated exclusively $H(CF_2)_3CFH_2$, HFC-347pcc, and iron hydrides, confirming a previous hypothesis that attributed formation of this

hydrofluoroalkane to an Fe carbene intermediate. In contrast, $[Fe(terpy')(CO)(1,4\text{-}C_4F_7)]^+OTf^-$, **2-10**, reacts with H_2 to yield HF and an unidentified iron complex, showing that the nature of the ancillary ligands greatly influences the reactivity. **Chapter 4** explores the reactivity of phosphine-substituted cobalt(I) carbonyl hydride complexes towards TFE to expand our work on d^6 perfluorometallacycles. The most electron-rich ligands prevented metallacycle formation or slowed it down possibly due to strong π-backbonding into the CO ligands, making it harder to generate an open coordination site. Indeed, a mixture of the Co-tetrafluoroethyl complex, derived from insertion of TFE into Co–H, and the zerovalent dimer/hydrogenated TFE products, derived from the reaction of the Co–H with the 16e- $CoL_n(CO)_{3-n}(CF_2CF_2H)$ intermediate, were obtained with the bulkiest ligands, $CoH(dcppe)(CO)_2$ and $CoH(Pcp_3)(CO)_3$ (dcppe = 1,2-bis(dicyclopentylphosphino)ethane, cp = cyclopentyl). With the slightly less bulky P^iBu_3 ligand, further reactivity of the insertion product with TFE slowly formed a d^6 metallacycle hydride complex. In contrast, with the dppe and tripod cobalt carbonyl hydrides, metallacycle product formation was evident even at short reaction times with insertion/hydrogenation ratios of 1:1, showing that using less electron-rich, steric bulky ligands prevented the bimolecular Co dimer formation, but left enough room for binding a second equivalent of TFE for metallacycle formation. Finally, **Chapter 5** summarizes the findings of this Thesis and discusses future directions based on this work.

Acknowledgments

Firstly, I would like to express my sincere gratitude to my supervisor, Professor R. Tom Baker for his immense knowledge, guidance and continuous support for the last two years. Your passion and motivation for chemistry kept me moving forward. I truly feel lucky to have had the opportunity to work with you. I have learned so much during these past few years.

To all current and former members of the Baker research group, you have contributed for making grad school such a fun experience. I also want to thank my labmates for their insightful comments and encouragements. Your support throughout this experience is truly appreciated.

I would like to thank the amazing staff at the University of Ottawa, who helped making this work possible, Glenn Facey, Eric Ye, Bulat Gabidullin, and Peter Pallister.

Thanks to my cousins for being my personal cheerleaders throughout this process. Last but not least, I would like to thank my loving parents and friends for their endless support and understanding. Thanks for believing in me.

Table of Contents

List of Figures

Appendices

List of Schemes

Chapter 1

Chapter 2

Chapter 3

Chapter 4

Chapter 5

List of Tables

Chapter 1

Chapter 3

List of Compounds

Metal complexes:

2-1	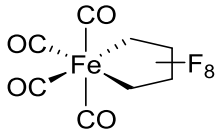	**2-9**	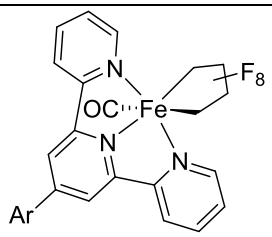	**4-5**	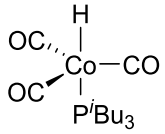
2-2a	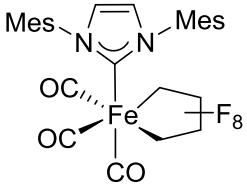	**2-10**	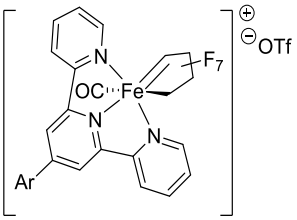	**4-6**	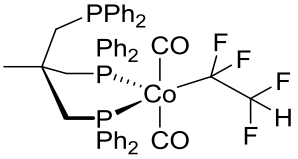
2-2b	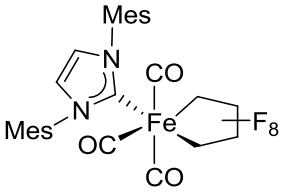	**3-1**	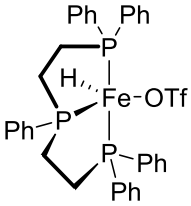	**4-7**	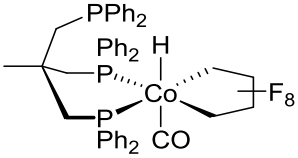
2-3	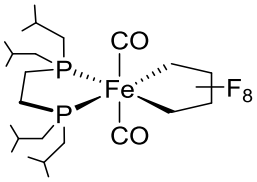	**3-2**	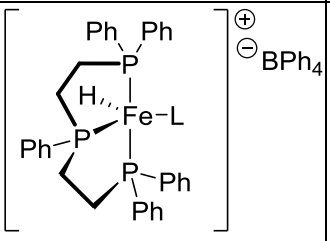 L= MeCN or PPh_3	**4-8**	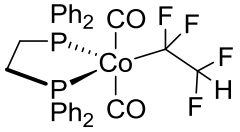
2-4	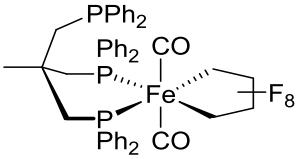	**3-3**	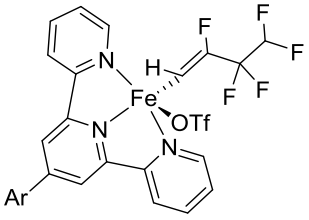	**4-9**	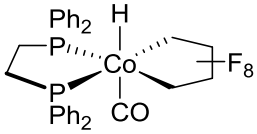

2-5	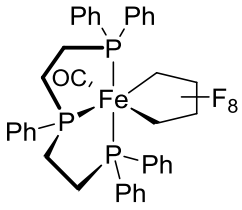	**4-1**	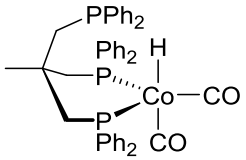	**4-10**	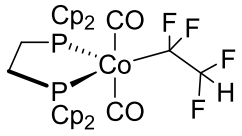
2-6	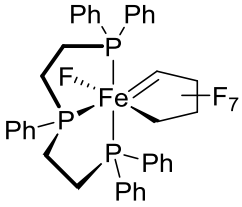	**4-2**	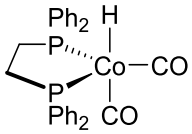	**4-11**	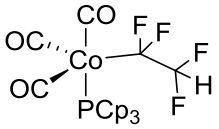
2-7	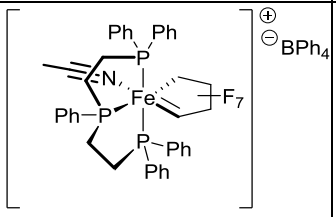	**4-3**	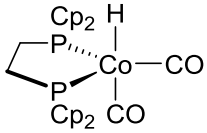	**4-12**	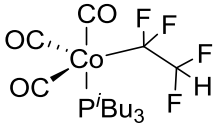
2-8	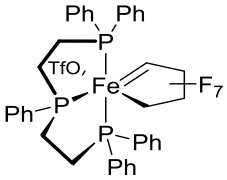	**4-4**	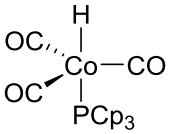	**4-13**	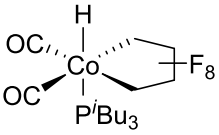
				4-14	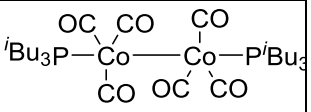

List of Abbreviations and Symbols

BDE	Bond dissociation energy
Bu	Butyl
ca.	Approximately
Cp	Cyclopentadienyl
CFC	Chlorofluorocarbon
cod	1,5-Cyclooctadiene
d	Days
Pcp_3	Tricyclopentylphosphine
dcppe	1,2-Bis(dicyclopentylphosphino)ethane
P^iBu_3	Triisobutylphosphine
dibpe	1,2-Bis(diisobutylphosphino)ethane
dibpp	1,3-Bis(diisobutylphosphino)propane
DME	1,2-Dimethoxyethane
dmpe	1,2-Bis(dimethylphosphino)ethane
dppb	1,4-Bis(diphenylphosphino)butane)
dppe	1,2-Bis(diphenylphosphino)ethane
dppf	1,1′-Ferrocenediyl-bis(diphenylphosphine)
dppp	1,3-Bis(diphenylphosphino)propane
dvtms	Divinyltetramethyldisiloxane
Et	Ethyl
h	Hour
HCFC	Hydrochlorofluorocarbon
HCFO	Hydrochlorofluoroolefin
HFCB	Hexafluorocyclobutene
HFC	Hydrofluorocarbon
HF	Hydrofluoric acid
HFO	Hydrofluoroolefin
HFP	Hexafluoropropene

Hz	Hertz
IAd	1,3-Di(1-adamantyl)imidazolium
IMes	1,3-Dimesitylimidazol-2-ylidene
FT-IR	Fourier Transform Infrared Spectroscopy
kcal	Kilocalorie
L	Ligand
M	Metal
Me	Methyl
NHC	*N*-heterocyclic carbene
NMR	Nuclear magnetic resonance
OTf	Triflate
PDI	Tridentate pyridinediimine
Pr	Propyl
psig	Pounds per square inch gauge
py	Pyridine
R^F	Fluoroalkyl group
RT	Room temperature
Terpy’	4′-(4-Methylphenyl)-2,2′:6′,2″-terpyridine
TFE	Tetrafluoroethylene
THF	Tetrahydrofuran
TMNO	Trimethylamine N-oxide
Triphos	Bis(2-diphenylphosphinoethyl)phenylphosphine
Tripod	1,1,1-Tris(diphenylphosphinomethyl)ethane
UV-vis	Ultraviolet–visible spectroscopy
VDF	1,1-Difluoroethylene
Xantphos	4,5-Bis(diphenylphosphino)-9,9-dimethylxanthene

List of Contributions

Presentations:

(1) Ghostine, K.; Das, U. K.; Baker, R. T. (2017) A Pinch of Iron: Amine Borane Dehydrogenation Catalysis Using Iron SNS and CNS Pincer Complexes. 100th Canadian Chemistry Conference (CSC). (poster presentation)

(2) Ghostine, K.; Baker, R. T.; (2018) First-Row Fluorometallacycles: Synthesis and Reactivity. 101st Canadian Chemistry Conference (CSC). (oral presentation)

Publications:

(1) Ghostine, K.; Elsby, M.; Das, U. K.; Gabidullin, B. M.; Baker, R. T. Iron-SNS and -CNS complexes: Synthesis, reactivity and amine-borane dehydrogenation catalysis, manuscript in preparation.

(2) Ghostine, K.; Gabidullin, B. M.; Baker, R. T. Perfluoroferracyclocarbene Complexes, manuscript in preparation.

(3) Ghostine, K.; Daniels, A.; Gabidullin, B. M.; Baker, R. T. Perfluorocobaltacycle Hydrides, manuscript in preparation.

Chapter 1

Introduction

1.1 Hydrofluorocarbon Compounds as Chlorofluorocarbon Replacements

Fluorine forms the strongest single bond to carbon with 115 kcal/mol C–F BDE in F–CH_3 (vs 104.9 kcal/mol C–H BDE in methane), in part due to the electronegativity difference between carbon and fluorine (2.5 vs 4) which makes the bond highly polar.[1] Fluorinated compounds are versatile materials that often exhibit thermal stability and chemical inertness, not to mention dielectric strength, water-repellency, and the famous slipperiness of Teflon.[2] Fluorocarbons are useful in multiple industries ranging from pharmaceuticals to refrigerants, insecticides and materials.

Chlorofluorocarbons (CFCs) were used for decades as refrigerants, propellants, solvents and blowing agents due to their stability and physical properties. However, their production on an enormous scale was accompanied by atmospheric release that damaged the Earth's ozone layer. Following the Montreal Protocol,[3] CFCs were replaced by hydrochlorofluorocarbons (HCFCs), and then by hydrofluorocarbons (HFCs). HFCs have no ozone-depleting potential, because they do not contain C–Cl bonds and they degrade in the troposphere.[2]

CFCs were synthesized industrially using the Swarts Process,[4] in which chlorine atoms are replaced by fluorine in the presence of a Lewis acid such as SbF_5 or SbF_3Cl_3. A similar process was developed for the synthesis of hydrofluorocarbons using Cr(III)-based heterogeneous catalysts. For instance, the original synthesis of 1,1,1,2-tetrafluoroethane (HFC-134a), one of the world's most popular refrigerants, involves fluorination of trichloroethylene in the presence of CrF_3/O_2, and also gives by-products such as HFC-125, HCFC-133a, and HCFO-1121 (Figure 1.1), which are separated by distillation.[5] An alternative synthesis consists of

treating HCFC-133a with HF in presence of alkali metal fluorides.[6] HFC-125, a more fluorinated derivative, can be prepared by the hydrofluorination of tetrafluoroethylene using chromium oxyfluoride.[7]

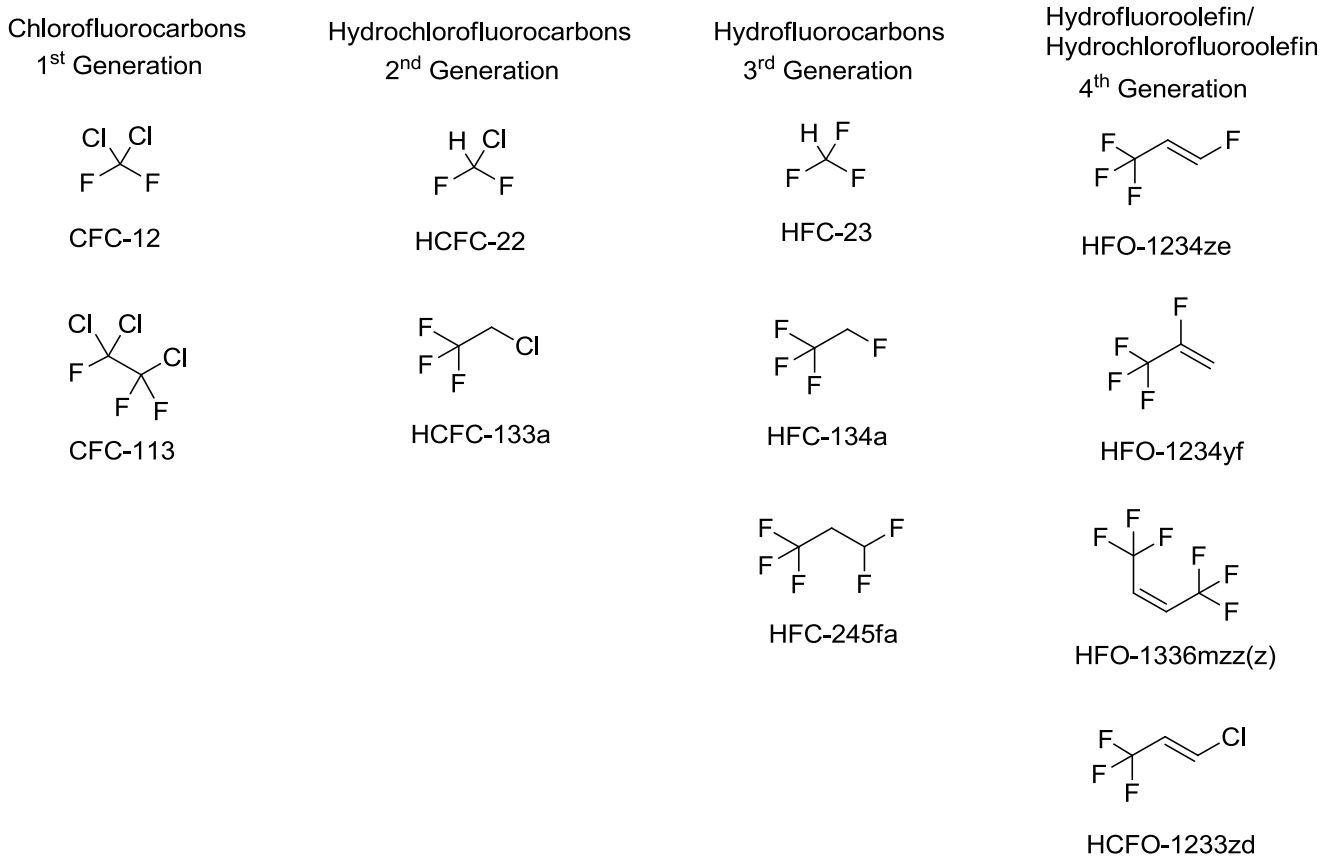

Figure 1.1. Examples of important CFCs, HCFCs, HFCs and HFOs/HCFOs.

While HFCs have negligible impact on the ozone layer, they are greenhouse gases due to the C–F bonds that absorb infrared radiation. However, a 4th-generation of olefinic refrigerants, hydrofluoroolefins and hydrochlorofluoroolefins, has emerged which shows greatly reduced greenhouse gas potential. The presence of the double bond makes it impossible for the molecule to reach the stratosphere and the oxidized products fall from the troposphere, thus preventing significant build-ups over time.

2,3,3,3-Tetrafluoropropene (HFO-1234yf), one of the most promising HFC replacements, can be made via different synthetic routes. One method involves hydrogenation of $CF_3CF=CHF$ (HFP) over a Pd/C catalyst, followed by defluorination over γ-alumina.[8] An alternative would be chlorotrifluoroethylene (CTFE) and a methyl halide heating at high temperatures to form $C_3H_2ClF_3$ isomers which are then exposed to HF to yield the desired HFO, as well as minor by-products. HCl and HF are removed by scrubbing and unreacted intermediates by distillation.[9] 1,3,3,3-tetrafluoropropene (HFO-1234ze), another popular HFO, was synthesized from 1,1,1,3,3-pentafluoropropane (HFC-245fa) or 3-chloro-1,1,1,3-tetrafluoropropane (HCFC-244fa). However, preparing this HFC and HCFC is a long process,[10] and alternative syntheses include heating vinyl fluoride ($H_2C=CFH$) with a Pd catalyst[11] or combining 1,2-dichloroethylene and CCl_4 in the presence of a ruthenium or rhodium catalyst.[12] However, both these methods give multiple products, necessitating additional purification steps.

In summary, the synthesis of fluorinated compounds as CFC replacements involves energy-intensive processes and sometimes toxic compounds.[13]

1.2 Fluoroorganometallic Chemistry

Development of more sustainable, energy efficient and "greener" synthesis of small fluorocarbons is needed, which has drawn attention to organometallic catalysis, especially with abundant, inexpensive and non-toxic transition metals. The reactivity of fluoroolefins with transition metals is discussed below.

1.2.1 Coordination of Fluoroolefins

The high electronegativity of fluorines has a depletive effect on the electron density in the olefin's π-bond, and thus on their σ-donor ability, making them more likely to react with late low-valent metals due to their strong π-backbonding ability. Indeed, for fluoroolefins, retro-

dative bonding from the metal is highly important and will depend on the metal's oxidation state and the ancillary ligands (Figure 1.2).[14] The fluoroolefin–metal bond might be considered a typical olefin–metal π-bond, in which filled metal d-orbitals are back-bonding into the olefin's π-antibonding orbital or the bonding may be more consistent with a bis(σ-bonded) three-membered ring. Moreover, intermediate situations are probable, where the bonding mode is not strictly as an olefin or a metallacyclopropane.[15]

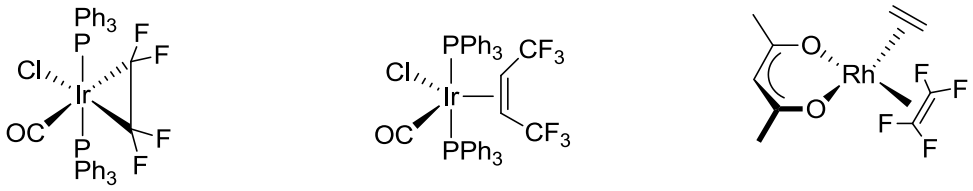

Figure 1.2. Examples of fluoroolefin complexes.

1.2.2 Oxidative Coupling of Fluoroolefins

The cyclization reaction to afford a metallacyclopentane is induced by oxidative coupling of two olefins at the metal center (Scheme 1.1) which increases the formal oxidation state of the metal by two units. Although alkynes typically undergo this reaction more easily than alkenes, the latter can be activated by electron-withdrawing substituents or ring strain. Tetrafluoroethylene favors this reaction because of the conversion of the sp^2 C–F bond to a less electronegative sp^3 C–F bond that relieves the repulsion between the fluorine lone pairs and the C=C π-bond. Nevertheless, simple alkenes can undergo oxidative coupling if the metal is π basic enough.[16]

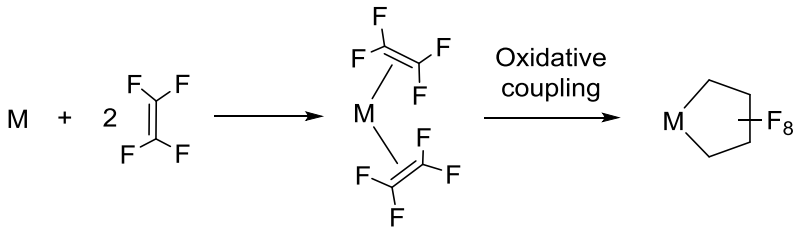

Scheme 1.1. Fluoroolefin oxidative coupling to a metallacyclopentane.

Many factors determine the formation of a five-membered ring metallacycle vs the olefin-type complex (three-membered ring).[17] For example, σ-donor and π-acceptor ligands can affect the type of ring formed, as well as sterics.

1.2.3 Transition Metal Perfluorometallacyclopentane Complexes

The very first example of a perfluorometallacycle, $Fe(CO)_4(1,4\text{-}C_4F_8)$ (Figure 3), was introduced by Stone in 1961[18] by addition of tetrafluoroethylene (TFE) to low-valent $Fe(CO)_5$.[19] Nobel prize-winner Geoff Wilkinson had prepared the complex earlier but misassigned it as the bis(olefin) complex.[19] Its synthesis and reactivity will be discussed in detail in the next sections. Shortly thereafter, Stone reported a new cobalt metallacyclopentane as a product of the reaction between cyclopentadienylcobalt dicarbonyl and TFE.[20] After preparing these d^6 iron and cobalt metallacyclopentanes, Stone expanded the reactivity to zerovalent nickel and TFE.[21] For instance, tetrakis(triethylphosphine)nickel reacts rapidly with tetrafluoroethylene to yield a stable nickelacyclopentane which contrasts with previous chemistry involving platinum. Indeed, reaction of zerovalent platinum or palladium complexes such as $Pt(PR_3)_4$ and L_nPd with TFE forms exclusively stable metallacyclopropane products.[22,23] In addition, $Pt(cod)_2$ and TFE yielded a diplatinum TFE-bridged complex $(cod)Pt(\mu\text{-}\eta^2\text{-}C_2F_2)_2Pt(cod)$.

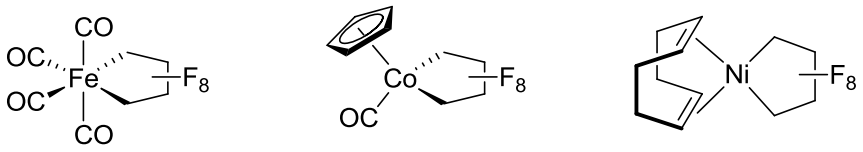

Figure 1.3. First reported perfluorometallacycles.

Since then, a lot of studies have been done on perfluoronickelacycles such as widening the scope of the ancillary ligands and studying their effects.[21,24] Ogoshi *et al.* recently reported multiple examples of nickel metallacyclopropane and -pentane complexes.[24] The size of the metallacycle formed was associated with the steric bulk of the ancillary ligands: the bulkiest ligands favoured formation of the metallayclopropane (Scheme 1.2).

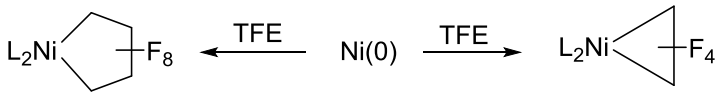

L_2 = 2 Et_3P
2 Ph_2PMe
2 $Bu^n{}_3P$
$Ph_2P(CH_2)_2PPh_2$
2 $(MeO)_3P$
2,2'-bipyridyl
2 Ph_3P
2 4-picoline

L_2 = 2 PCy_3
2 $^iPr_3$
$Cy_2P(CH_2)_2PCy_2$
$Cy_2P(CH_2)_4PCy_2$

Scheme 1.2. Ligand effects on perfluoronickelacycle formation.

Ruthenium metallacycles were also prepared. For example, $Ru(CO)_2(PPh_3)_2(1,4\text{-}C_4F_8)$ was generated from $Ru(CO)_2(PPh_3)_3$ and TFE.[25] In addition, reduction of $RuCl_2(PPh_3)_4$ with NaH in MeCN in the presence of TFE gave a ruthenacyclopentane complex (Figure 1.4).[26]

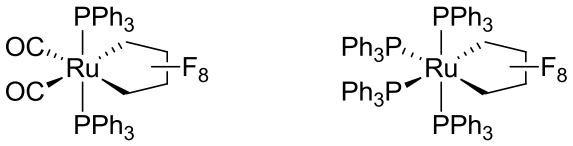

Figure 1.4. Ruthenacyclopentane complexes.

Although perfluorometallacyclopentanes are usually prepared by oxidative coupling of TFE, Vicic and colleagues recently reported an alternative synthesis from dinuclear fluoroalkylzinc reagents $(MeCN)_2Zn[\mu\text{-}(CF_2)_n]_2Zn(NCMe)_2$ and nickel(II) precursors.[27] The first step is the preparation of the dizinc reagent from diethyl zinc and 1,4-diiodooctafluorobutane. The zinc complex can then readily transmetalate to nickel in the presence of L ligands to form a mononuclear perfluoronickelacycle (Scheme 1.3).

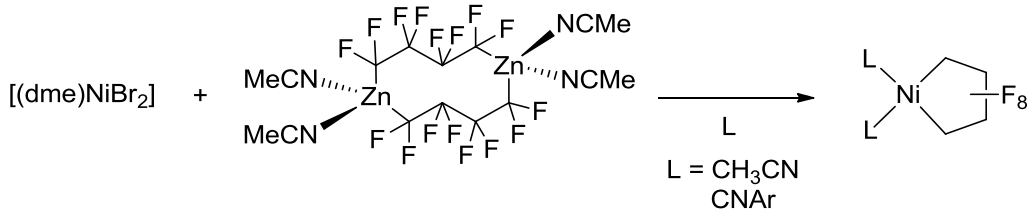

Scheme 1.3. Synthesis of perfluoronickelacycles via a transmetallation reaction.

However, less attention has been paid to iron and cobalt fluorometallacycle complexes, the synthesis and reactivity of which will be the focus of this thesis.

1.2.4 TFE Insertion into Metal Hydrides

Fluoroolefins are susceptible to nucleophilic attack due to their electrophilic nature, therefore making it possible to insert the fluoroolefin into a reactive metal hydride bond. This reaction was first reported in 1961 by Stone with manganese pentacarbonyl hydride and tetrafluoroethylene (Scheme 1.4),[28] followed by other examples involving π-cyclopentadienyl molybdenum and tungsten tricarbonyl hydrides,[29] and rhenium pentacarbonyl hydride.[30]

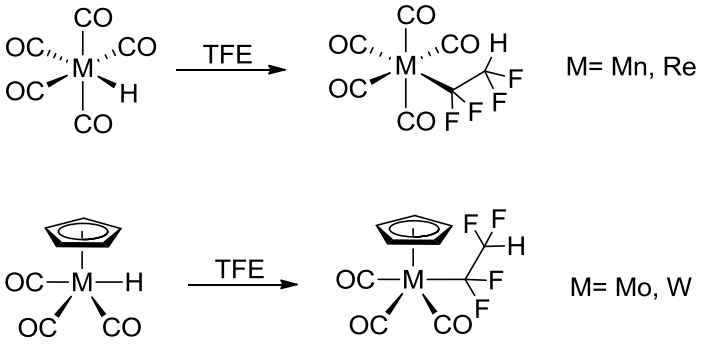

Scheme 1.4. Insertion of TFE into metal hydrides.

Althought insertion of non-fluorinated olefins into M–H might induce polymerization, TFE forms a stable fluoroalkyl that does not insert additional TFE as demonstrated by Roper on iridium complexes (Scheme 1.5).[31] Indeed, upon heating, $IrH(CO)(PPh_3)_3$ is converted to $IrH(C_2F_4)(CO)(PPh_3)_2$ under pressure of TFE. When the latter was treated with more TFE under much more vigorous conditions, the fluoroolefin inserted into the metal–hydride bond and the coordination of a second equivalent of TFE occurred without a second insertion.

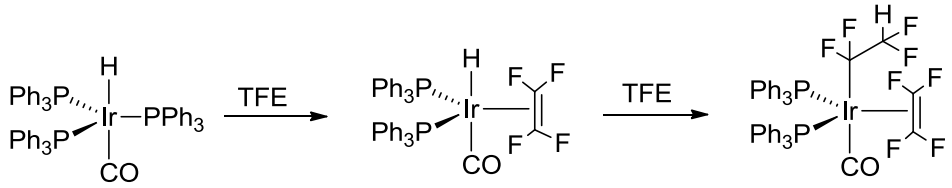

Scheme 1.5. Insertion of TFE into Ir–H bond and coordination of a second equivalent.

1.2.5 TFE Insertion into Metal-Metal Bonds

It has been reported that tetrafluoroethylene can insert into a metal–metal bond. Indeed, dicobalt octacarbonyl reacts with TFE to yield the ethanediyl-bridged complex, $(CO)_4Co(\mu\text{-}\eta^2\text{-}C_2F_4)Co(CO)_4$.[32] Similar reactivity was observed with TFE and germanium–manganese[33] and tin–manganese[34] bonds.

1.2.6 C–F Bond Activation of Fluorinated Ligands Mediated by Transition Metals

Selective carbon–fluorine bond activation of perfluoroorganometal complexes can provide novel synthetic routes to fluorinated organic molecules. The weakening of the C–F bond at the α-position was first reported by Reger and Dukes for the synthesis of a metal difluorocarbene by treating a d^4 Mo–CF_3 complex with strong Lewis acid SbF_5.[35] X-ray crystallographic studies of the Mo–CF_3 precursor showed a longer C_α–F bond distance than the average sp^3 carbon–fluorine bond, thus explaining its reactivity. Selective activation of the C_α–F bond was further demonstrated on a longer fluoroalkyl chain complex. Indeed, Mo=$CFCF_2CF_3$ was obtained upon treatment of Mo–$CF_2CF_2CF_3$ with a Lewis acid.[35] C–F bond activation was also reported for perfluorometallacyclopropane complexes. In the case of $(PPh)_3Pt(C_2F_4)$[36] and $(PMe_3)_3Ni(C_3F_6)$,[37] the fluorinated fragment undergoes rearrangement to form the vinyl product after fluoride abstraction. Moreover, our group recently reported fluoride abstraction from fluorocobaltacyclobutanes.[38] In this case, it was proposed that fluoride abstraction occurred at the β-position when $CpCo(PPh_2Me)(C_3F_6)$ was treated with stoichiometric Me_3SiOTf or a catalytic amount of $HNTf_2$ yielding the *trans*-vinyl and isomerization/ring contraction metallacyclopropane, respectively. Similar results were later published with the $Ni(C_3F_6)$(dppe) complex (Scheme 1.6).[39]

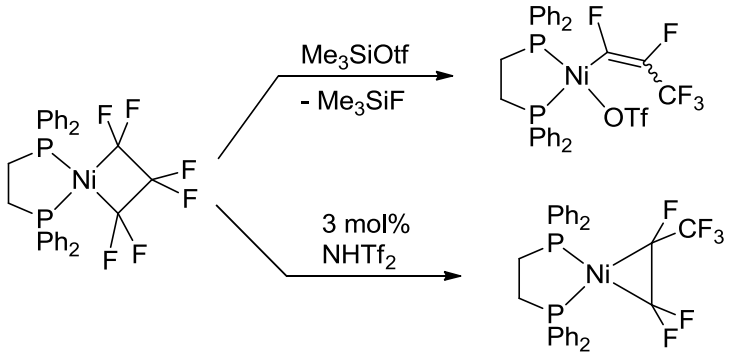

Scheme 1.6. C–F activation in $Ni(C_3F_6)$(dppe).

The high stability of perfluorometallacyclopentanes was established with the very first example reported, $Fe(CO)_4(1,4\text{-}C_4F_8)$ (synthesis and reactivity discussed in Section 1.4).[40] Their reactivity, however, remained largely unexplored until Burch and coworkers reported C_α–F bond activation of $Ni(PEt_3)_2(CF_2)_4$ in the presence of 1 equivalent of BF_3.[41] They suggested that the α-F was abstracted from the metallacycle, leading to a transient carbene intermediate (not observed), followed by phosphine ligand migration to the 'carbene' carbon to generate a phosphine-functionalized metallacycle. Moreover, addition of a second equivalent of BF_3 yielded a second C_α–F activation. In order to isolate the product, dppe was used to displace the tetrafluoroborate ligands, affording the final dicationic species (Scheme 1.7).

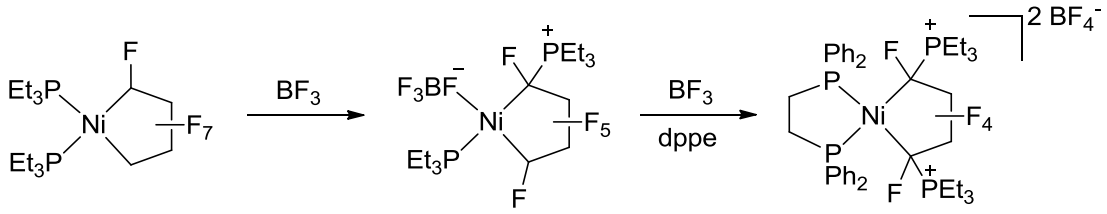

Scheme 1.7. Cα−F abstraction in a bis(phosphine) nickel perfluorocyclopentane.

Similar reactivity, α-F abstraction and ligand migration, was also demonstrated recently in the Baker group with $L_2Ni(CF_2)_4$ (L = PPh_3, PPh_2Me, pyridine) and Me_3SiOTf, where the displaced L donor is installed on the α-C and the triflate group coordinates to the metal.[42] The [P,S^{iPr}]-ligated metal perfluorocyclopentane also undergoes C_α–F bond activation in the presence of Me_3SiOTf, followed by selective ligand migration (Scheme 1.8). The resulting metallabicyclic product undergoes interesting Ni–C bond cleavage reactions with water and isonitrile ligands.[43]

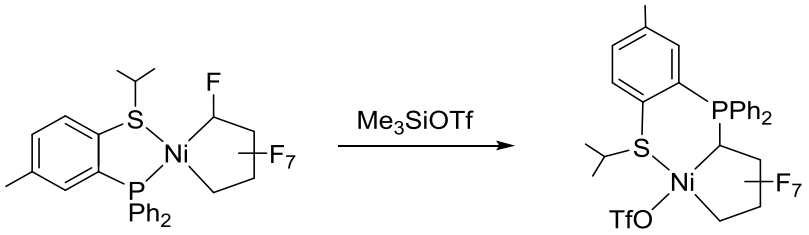

Scheme 1.8. [P,S^{iPr}]-ligated metal perfluorocyclopentane C_α–F activation by TMS-OTf.

In contrast, activation of the C_α–F bond in pseudo-three-coordinate NHC-perfluoronickelacyclopentane using Me_3SiOTf yielded a cyclobutyl ring via $C_\alpha F_2$ migration, without NHC ligand migration[44] (discussed in section 1.3.2) (Scheme 1.9). Upon heating the perfluorocyclobutyl-containing complex, perfluorocyclobutene was produced, most likely through β-fluoride elimination.

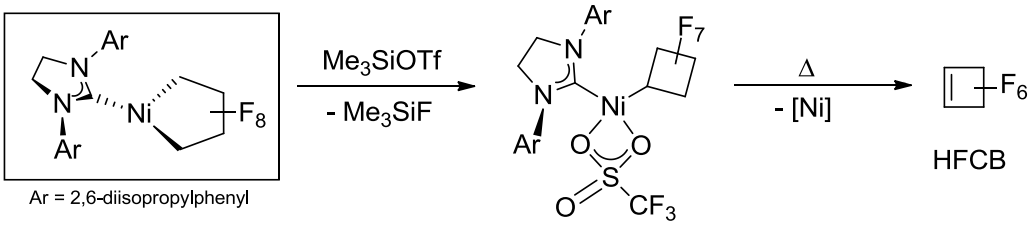

Scheme 1.9. Cα–F abstraction in 3-coordinate nickelacycle causes ring contraction.

Since the NHC ligand remains bound to the metal, C–F bond functionalization using Brønsted acids was also studied. Reaction of the low-coordinate compound with trifluoroacetic acid yielded HF and a trifluoroacetate-substituted metallacycle whereas reaction with less acidic trimethylbenzoic acid gave primarily the Ni–C^F bond cleavage product (Scheme 1.10).[44] Interestingly, the latter product was exceedingly stable with no β-F elimination observed after heating at 80°C for 12 h.

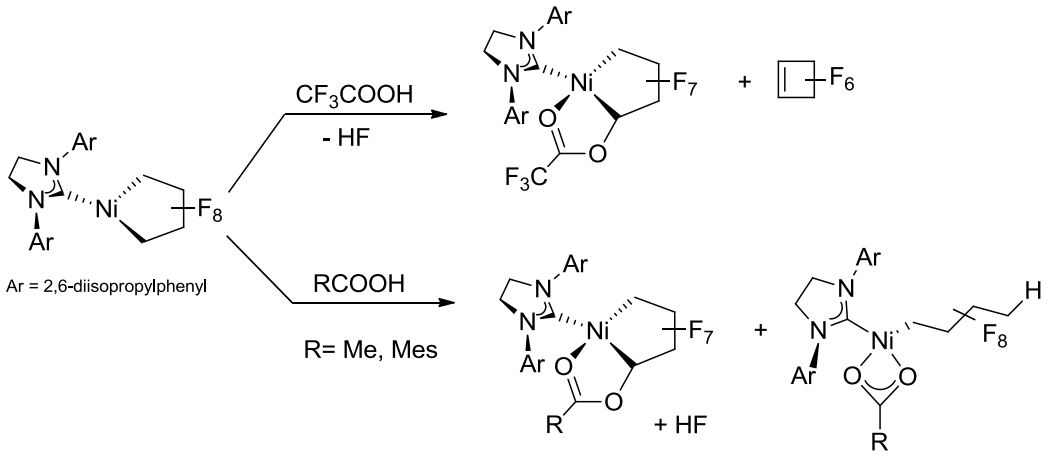

Scheme 1.10. Reactivity of NHC–perfluorometallacyclopentane with Brønsted acids.

1.3 Hydrogenolysis of Perfluorometallacycle Complexes

Modification of fluorometallacycles, often facilitated by activated C–F bonds and ring strain, represents an unconventional, yet appealing, method towards the synthesis of small functionalized fluorocarbons. Hydrogenolysis of the metallacycle M–C is one way to achieve ring-opening and production of new fluorocarbons.

1.3.1 Nickel Complex-Catalyzed Hydrodimerization of Tetrafluoroethylene

While at Du Pont, Baker *et al.* developed a catalytic method for the hydrodimerization of tetrafluoroethylene (Scheme 1.11).[45] As shown below, the perfluoronickelacyclopentane is formed by oxidative coupling of two TFE molecules to the NiL_4 complex with loss of two phosphite ligands. Next, addition of H_2 is proposed to give the dihydrogen intermediate, followed by protonation of the α-carbon and formation of a nickel hydride. Finally, the HFC chain is released via reductive elimination to yield HFC-338pcc and reform NiL_4. The hydrogenolysis of the robust Ni–C^F bond required high temperatures and pressures and was only observed when π-acidic phosphite ligands were employed. In contrast, Werner *et al.* demonstrated that nickelacycles, $Ni(C_4F_8)L_2$, where L= PPh_3, or L_2= Dppp, Dppe do not undergo

hydrogenolysis in the presence of H_2 at 20 atm.[26] More recently, our group showed that the low-coordinate NHC nickel complex discussed above greatly increases the rate of Ni–C^F bond hydrogenolysis (7 psig and 25°C vs. 700 psig and 100°C).[44]

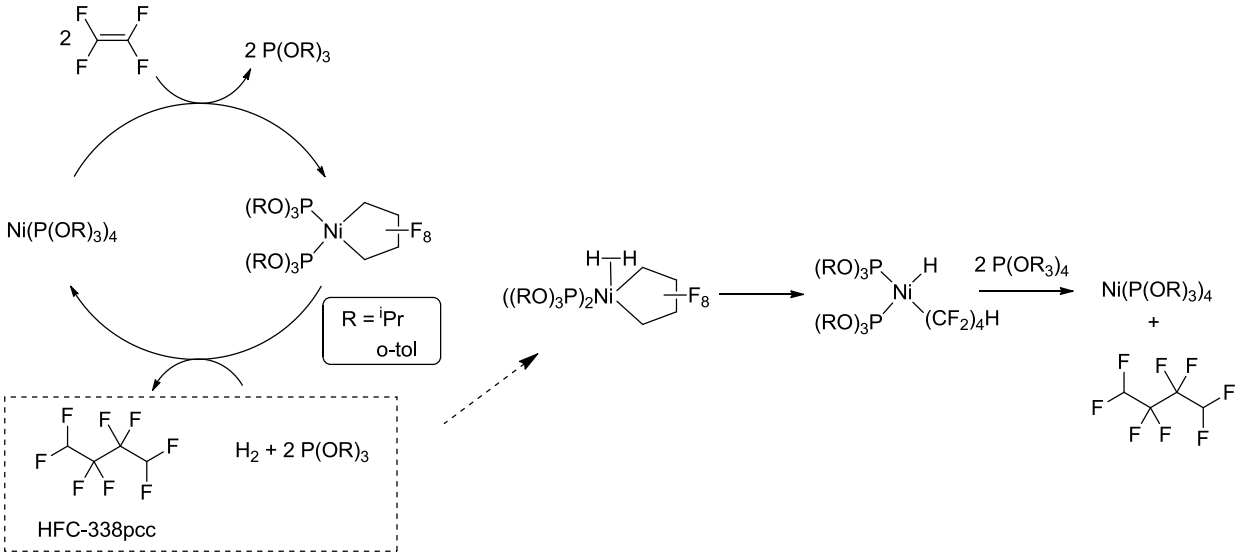

Scheme 1.11. Catalytic hydrodimerization of tetrafluoroethylene using [Ni] with a focus on the hydrogenolysis of nickel perfluorometallacycle complex.

1.3.2 Hydrogenolysis of $Fe(CO)_4(1,4\text{-}C_4F_8)$

Baker and coworkers have also shown that the $Fe(CO)_4(1,4\text{-}C_4F_8)$ complex undergoes slow hydrogenolysis of the Fe–C^F bond under harsh conditions to yield hydrofluorocarbons[46] with decreased selectivity vs the nickel complexes. Without any additives, hydrogenolysis gave both HFC-338pcc and HFC-347pcc (Scheme 1.12).

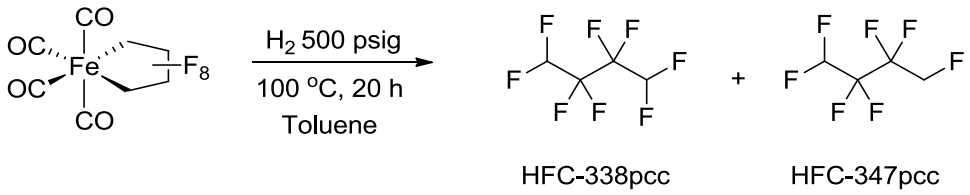

Scheme 1.12. Hydrogenolysis of $Fe(CO)_4(1,4\text{-}C_4F_8)$.

The proposed mechanism for this reaction involves loss of CO to generate a vacant coordination site to allow formation of the dihydrogen intermediate. From there, it can follow two different paths that lead to different products (Scheme 1.13). The dihydrogen intermediate can protonate one of the α-carbons to form the iron alkyl hydride complex, which undergoes reductive elimination to yield the HFC-338pcc. On the other hand, one of the α-fluorines can get protonated to release HF and form an iron metallacycle carbene hydride. Another dihydrogen molecule then adds to the Fe–H and Fe–C to generate the saturated Fe dihydrogen metallacycle, which after α-carbon protonation and reductive elimination gives HFC-347pcc.

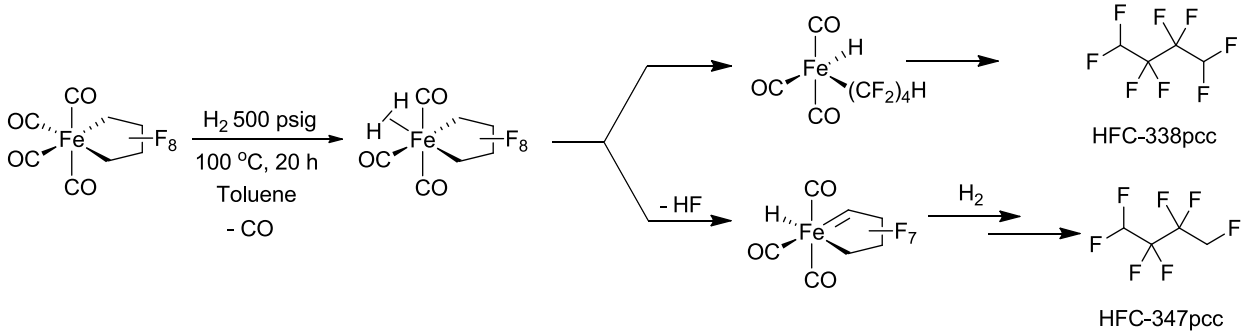

Scheme 1.13. Proposed mechanisms for the hydrogenolysis of $Fe(CO)_4(1,4\text{-}C_4F_8)$.

Although the carbene intermediate was proposed, it has never been observed. As such, further studies on the reactivity of these carbene complexes could lead to a better understanding of the hydrogenolysis process and potentially new catalysis involving the carbene intermediate.

Interestingly, the use of different additives had a significant impact on the Fe–C^F bond hydrogenolysis rate and selectivity (Table 1.1). For example, addition of PPh_3 increased conversion from 49% to 84.5%, but decreased the selectivity by also forming isomers of $C_4H_4F_6$ including one with three hydrogens on the terminal carbon. All runs were performed at 500 psig (3550 kPa) H_2 for 20 hours at 100°C unless noted otherwise. Catalysts such as $RuHCl(PPh_3)_3$ and

$RhCl(PPh_3)_3$ increased the rate as well as gave a good selectivity. A 100% conversion was obtained with these rhodium and ruthenium complexes (runs 6 and 11). However, decreasing the hydrogenolysis time from 20 to 10 hours, decreased the conversion using $RhCl(PPh_3)_3$, but improved the selectivity, while increasing both selectivity and conversion using $RuHCl(PPh_3)_3$ (runs 7 and 10). In addition, switching gas from H_2 to H_2/CO for the rhodium catalyst significantly decreased the conversion.

Table 1.1. Vapor and liquid phase analysis for the hydrogenolysis of $Fe(CO)_4(1,4\text{-}C_4F_8)$.[46]

Run No.	Additives	% Conv.	Vapor phase analysis			Liquid phase analysis		
			$H(CF_2)_4H$/ $H(CF_2)_3CFH_2$	$C_4H_4F_6$ isomers	Perfluoro-cyclobutene*	$H(CF_2)_4H$	$H(CF_2)_3CFH_2$	$CH_2F(CF)_2CH_2F$
1	None	49	97.5	-	1.5	59.5	38	-
2	PPh_3	84.5	90	6.5	3.5	13.5	71.5	15
3	$P(O\text{-}p\text{-}tol)_3$	15	96	0.5	0.5	64	26	-
4	Pd/Carbon	16	88.5	9	2.5	4.5	80.5	15
5	Rh/Carbon	25	42.5	-	47.5	18	16	6
6	$RhCl(PPh_3)_3$	100	72	6	15.5	4.5	78	17.5
7[a]	$RhCl(PPh_3)_3$	93	90.5	6.5	3	8.5	77	14.5
8	$RhCl(PPh_3)_3$	98	89	9.5	1	1	73.5	25.5
9[b]	$RhCl(PPh_3)_3$	5	93.5	1.5	1.5	12.5	83.5	4
10	$RuHCl(PPh_3)_3$	97.5	46.5	28.5	2	7	62	31
11[a]	$RuHCl(PPh_3)_3$	100	92	3.5	2.5	3.5	90.5	6
12	$[Rh(COD)(DPPB)]BF_4$	88	86.5	0	12.5	37	63	-

[a]10 h, [b] 500 psig (3550 kPa) H_2/CO *Injection of $Fe(CO)_4(1,4\text{-}C_4F_8)$ into the GC-MS gave perfluorocyclobutene

1.4 Iron Fluorometallacylopentane Complexes

Although, the iron carbonyl perfluorometallacylopentane complex was the first reported perfluorometallacycle,[19] very few studies have been reported regarding its reactivity. Iron

pentacarbonyl reacts with a host of fluorinated compounds such as *n*-perfluoropropyl iodide,[18] 1,1-dichlorodifluoroethylene,[47] chlorotrifluoroethylene and HFP. The perfluoroalkyl iodide undergoes oxidative addition, yielding a perfluoropropyliron complex, whereas the liquid olefins gave complexes of the type (olefin)$Fe(CO)_4$. Reaction with 1,1-difluoroethylene (VDF) was also attempted, but appeared to form olefin or vinylic iron products instead of a metallacycle.[48] To date, only tetrafluoroethylene is reported to give the iron metallacyclopentane product.

1.4.1 Synthesis of $Fe(CO)_4(1,4\text{-}C_4F_8)$

The reaction of TFE with $Fe_3(CO)_{12}$, $Fe_2(CO)_9$ or $Fe(CO)_5$ gives $Fe(CO)_4(1,4\text{-}C_4F_8)$ when heated under pressure.[19,18] This complex was characterized by mass spectrometry and infrared, and nuclear magnetic resonance spectroscopy. Interestingly, Wiggans *et al.* reported that irradiation of TFE and $Fe(CO)_5$ affords the olefin complex, $(C_2F_4)Fe(CO)_4$, but prolonged irradiation leads exclusively to the metallacycle product $Fe(CO)_4(1,4\text{-}C_4F_8)$.[47] An enhanced procedure for the synthesis of $Fe(CO)_4(1,4\text{-}C_4F_8)$ was then published in 1970 by Wiggans and coworkers[40] due to the inconvenience of the previously published high-pressure synthesis that resulted in very low yields.[19] This new procedure consisted of UV irradiation of a solution containing a mixture of pentacarbonyliron and dodecacarbonyltri-iron with TFE to give a 49% yield of the cyclic compound (Scheme 1.14). The polymerization of TFE was observed without solvent. When the reaction is performed with pentacarbonyliron or dodecacarbonyltri-iron alone, the yield was still good, but the reaction was slower. It was also noted that the reaction mixture had to be vigorously stirred during irradiation or a significant amount of nonacarbonyldi-iron is formed which affects the yield. However, when vigorously stirred, the nonacarbonyldi-iron also affords $Fe(CO)_4(1,4\text{-}C_4F_8)$.

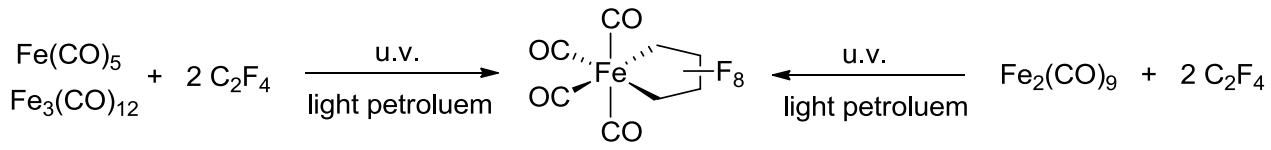

Scheme 1.14. Synthesis of $Fe(CO)_4(1,4\text{-}C_4F_8)$.

The ^{19}F NMR spectrum of the $Fe(CO)_4(1,4\text{-}C_4F_8)$ complex has two resonances (barely resolvable triplets, $^2J_{FF}$ = 2 Hz) at -70.6 and -136.9 ppm. Additionally, the crystal structure of the iron metallacyclopentance was obtained (Figure 1.5).[48] It displays a pseudo-octahedral geometry, with Fe–C^F bond distances of 2.024(3) and 2.010(3) Å.

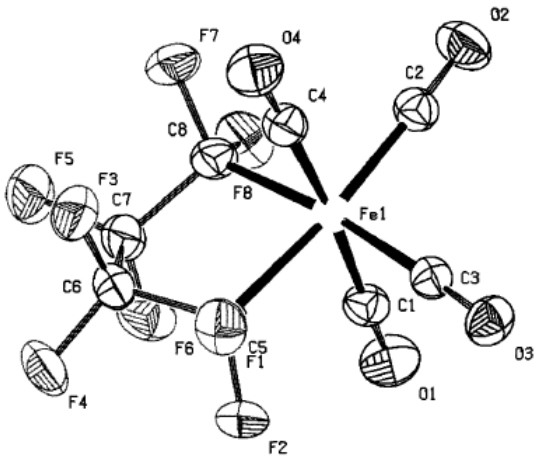

Figure 1.5. ORTEP diagram of $Fe(CO)_4(1,4\text{-}C_4F_8)$.

1.4.2 Reactivity of $Fe(CO)_4(1,4\text{-}C_4F_8)$

$Fe(CO)_4(1,4\text{-}C_4F_8)$ is incredibly stable for a transition metal bonded to an organo-group by σ-bonds. It is stable indefinitely at room temperature. However, perfluorocyclobutene is formed when the complex is heated at 160°C for 12 days, presumably via CO loss and fluoride shift from the CF_2 group to the metal (Scheme 1.15). In addition, treatment with bromine for 120 hours at 70°C afforded perfluorocyclobutane and treatment with iodine at 150°C for 4

hours releases four equivalents of carbon monoxide per molecule, which confirmed that it contains an $Fe(CO)_4$ group.[18]

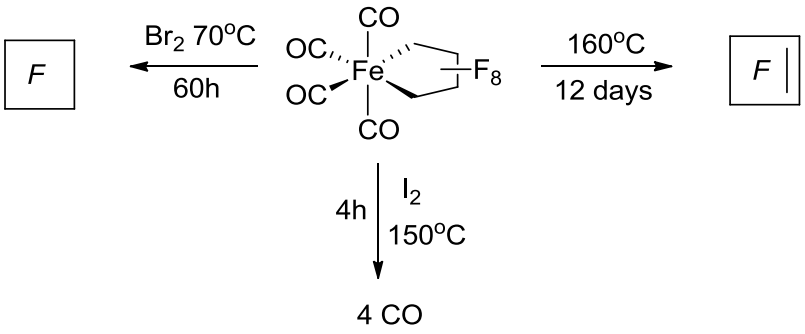

Scheme 1.15. Reactivity of $Fe(CO)_4(1,4\text{-}C_4F_8)$.

The high stability and lack of reactivity of $Fe(CO)_4(1,4\text{-}C_4F_8)$ can be attributed to the electronegative (electron-withdrawing) fluorine substituents on the carbon atoms, resulting in strong Fe–C^F bonds. The latter removes electron density from the metal more efficiently than alkyl groups, which lead to an enhanced stability, thus making it harder to liberate the metallacycle from the iron.[18]

1.4.3 Ligand Substitutions on $Fe(CO)_4(1,4\text{-}C_4F_8)$

Over the past years, the only other reactivity that was explored with the iron carbonyl perfluorometallacyclopentane complex involved ancillary ligand substitution (Table 1.2). Indeed, it has been reported that when irradiated, or heated at 80°C, in the presence of one equivalent of triphenylphosphine, triphenyl-phosphite, triphenylarsine or triphenylstibine, one CO ligand is replaced to afford the new monosubstituted $Fe(CO)_3(1,4\text{-}C_4F_8)L$ complexes, in which the metallacycle remains intact. No reaction was observed for triphenylbismuth. On the other hand, triethyl-phosphite gave a mixture of the mono- and disubstituted complexes and pyridine yielded only the disubstituted complex $Fe(CO)_2(1,4\text{-}C_4F_8)L_2$. For bidentate phosphine

ligands such as 1,2-bis(diphenylphosphino)ethane (dppe), both the expected chelated dicarbonyl product as well as the dppe-bridged dimer $[Fe(CO)_3(1,4\text{-}C_4F_8)]_2[\mu\text{-}(Ph_2PCH_2)_2]$ are obtained (Scheme 1.16). 2,2'-Bipyridine and *o*-phenanthroline also afforded the chelated dicarbonyl complex.[40]

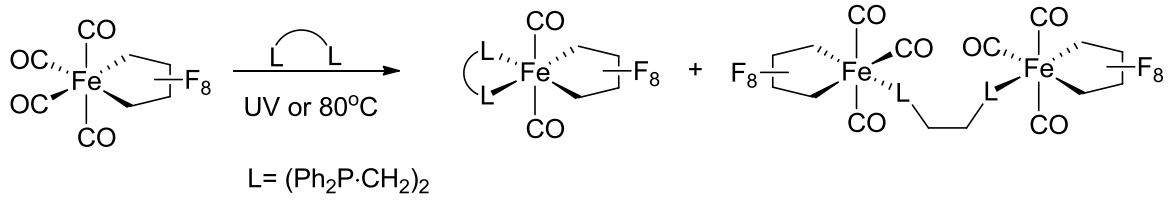

Scheme 1.16. Synthesis of $[Fe(CO)_3(1,4\text{-}C_4F_8)]_2[\mu\text{-}(Ph_2PCH_2)_2]$.

Table 1.2. Preparation of mono- and disubstituted iron carbonyl perfluorometallacycles.

Entry	Ligand	Complex	Yield (%)
1	PPh_3	$Fe(CO)_3(1,4\text{-}C_4F_8)PPh_3$	53
2	$AsPh_3$	$Fe(CO)_3(1,4\text{-}C_4F_8)AsPh_3$	70
3	$SbPh_3$	$Fe(CO)_3(1,4\text{-}C_4F_8)SbPh_3$	66
4	$P(OPh)_3$	$Fe(CO)_3(1,4\text{-}C_4F_8)[P(OPh)_3]$	73
5	$P(OEt)_3$	$[Fe(CO)_3(1,4\text{-}C_4F_8)P(OEt)_3]$	24
		$Fe(CO)_2(1,4\text{-}C_4F_8)[P(OEt)_3]_2$	36
6	Pyridine	$Fe(CO)_2(1,4\text{-}C_4F_8)py_2$	52
7	$Ph_2P\text{-}CH_2CH_2\text{-}PPh_2$	$Fe(CO)_2(1,4\text{-}C_4F_8)$(dppe)	63
		$[Fe(CO)_3(1,4\text{-}C_4F_8)]_2(\mu\text{-dppe})$	17
8	2,2'-Bipyridine	$Fe(CO)_3(1,4\text{-}C_4F_8)$bipy	82
9	*o*-Phenanthroline	$Fe(CO)_3(1,4\text{-}C_4F_8)$o-phen	71

Substitution of one carbonyl group on the $Fe(CO)_4(1,4\text{-}C_4F_8)$ complex by an L ligand can occur at the axial or equatorial position with respect to the fluorocarbon moiety. The

configuration can be easily determined based on the ^{19}F NMR and infrared spectra. For the complex with an axial L ligand, the fluorine atoms of each CF_2 group are nonequivalent. And four peaks with a large geminal coupling constant (ca. 220 Hz)[49] would be expected in the ^{19}F spectrum. However, no large coupling constant was observed in the spectra of the monosubstituted products. Alternatively, an equatorial L ligand would give rise to two different signals for the α-CF_2 groups, and large coupling when L = P ligand also supports the presence of a CF_2 group *trans* to P.[50] Moreover, the infrared spectrum suggested a structure where two carbonyl groups are *trans*. In summary, the structure of the monosubstituted complexes has L in the equatorial position.[40]

The three possibilities for the structure of the non-chelated disubstituted complexes are illustrated below (Figure 1.6). The infrared spectra show two strong bands in the carbonyl region, excluding the structure with two *trans* carbonyl groups. The ^{19}F NMR spectrum displayed a triplet (coupling 21.5 Hz) and a singlet of the same intensity. The simplicity of the spectrum provides evidence for the structure where two CO ligands are *cis* with the L ligands *trans* to each other. When a chelating ligand is used to form the disubstituted product, spectroscopic analysis suggests formation of the complex where both ligands L are *trans* to the fluorocarbon moiety and with *trans* CO ligands.[40]

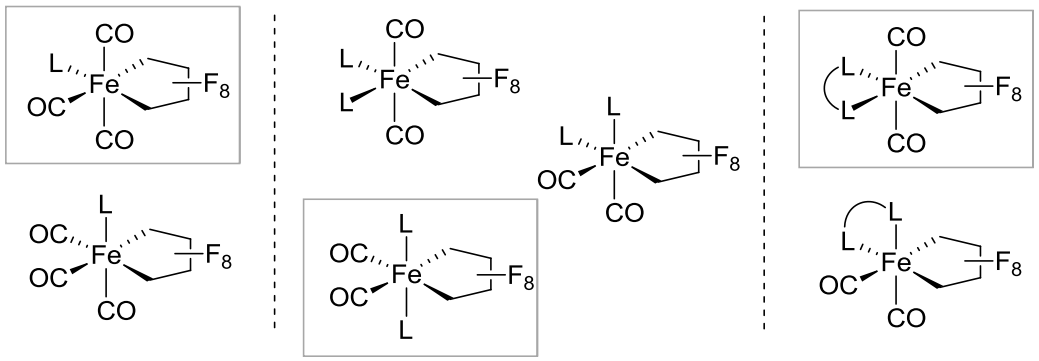

Figure 1.6. Possible structures of the mono- and disubstituted complexes with preferred isomers in boxes.

Lindner *et al*. published the crystal structure of the $Fe(CO)_3(1,4\text{-}C_4F_8)PPh_3$ complex (Figure 1.7). It was shown that the metallacycle ring has a twist conformation, where C6 and C7 are disordered. However, the conformational chirality was taken into account in the structure calculations.[51] The Fe–C5 and Fe–C8 bond distances are 2.141(4) and 2.107(4) Å, respectively. Slightly longer $Fe–C_\alpha^F$ bonds than in the $Fe(CO)_4(1,4\text{-}C_4F_8)$ complex can be explained by a more electron-rich metal center caused by the triphenylphosphine ligand. The crystal structure of $Fe(CO)_2(1,4\text{-}C_4F_8)$(dppe) was obtained by a previous member of the Baker group, and showed $Fe–C_\alpha^F$ bond distances of 2.008(8) and 1.991(9) Å. $Fe–C_\alpha^F$ bonds in this case are shorter than the $Fe–C_\alpha^F$ bonds of $Fe(CO)_4(1,4\text{-}C_4F_8)$, possibly due to the fact that the dppe group is a better σ-donor than CO, thus leaving more electron density on the iron, which can be used for back-bonding to the metallacycle. This phenomenon would cause shorter bonds due to stronger interactions.

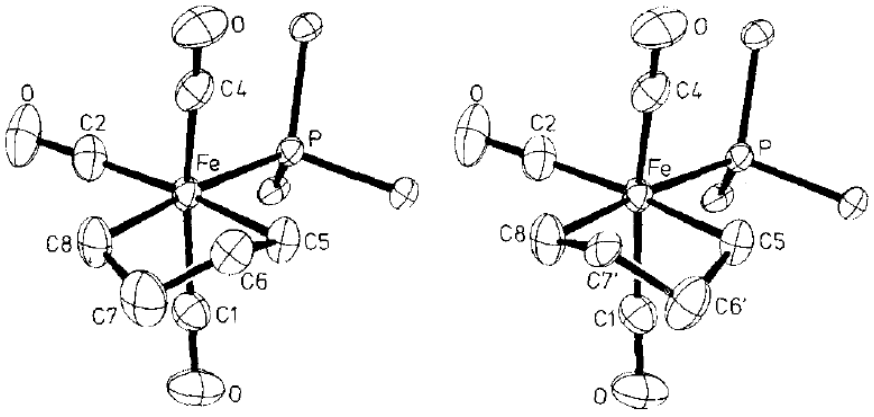

Figure 1.7. Crystal structure of the enantiomers of $Fe(CO)_3(PPh_3)(1,4\text{-}C_4F_8)$.

1.5 Transition Metal Carbene Complexes

The first metal carbene complex $(CO)_5Cr{=}C(OMe)(Me)$ was synthesized in 1964 by Fischer and Maasböl.[52] This class of compounds, now known as Fischer-type metal carbenes, can be described as σ-donation of the filled lone pair orbital of the singlet-carbene to an empty d-orbital of the metal, and π-back-donation of a filled metal d-orbital to an empty carbene *p*-orbital (Figure 1.8). They are usually known to be low-valent late transition-metal carbenes with heteroatom substituents, which are good π-donors, and display electrophilic reactivity at the carbon carbene.[53] A few years later, Schrock carbenes (or alkylidenes) were introduced by the synthesis of $(Me_3CCH_2)_3Ta{=}CH(CMe_3)$ which showed that Schrock carbenes behave differently than Fischer carbenes.[54] Indeed, the metal–carbene bonding of the latter class of compounds is usually discussed as a covalent interaction between a triplet carbene and a triplet metal (Figure 1.8). They are known to be high-valent early-transition-metal alkylidenes with H or alkyl substituents and show nucleophilic reactivity at the carbene carbon.

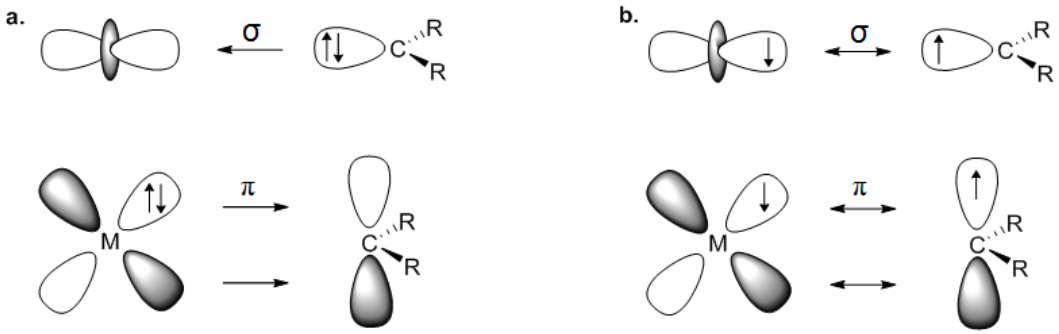

Figure 1.8. Schematic representation of the orbital interactions in (a) Fischer-type carbene complexes (b) Schrock-type carbene complexes.

However, the classification of metal carbene complexes is not limited to these two types. While a lot of attention has been drawn on the reactivity of metal carbene complexes such as Schrock carbenes, Fischer carbenes and metal *N*-heterocyclic carbene complexes, less effort has focused on metal fluorocarbenes.

1.5.1 Metal Fluorocarbenes

Metal fluorocarbenes are in some ways intermediate between Fischer and Schrock carbenes. For instance, as we move across the second row of the periodic table (N, O, F), electronegativity increases as π-donor ability decreases. Fluorine-substituted carbenes are similar to their N- or O-substituted analogues with low-valent metals (Fischer-type), but due to the reduced π-donor effect, they can be compared to Schrock carbenes, especially for metal carbenes such as M=CF(CF_3) for which the singlet-triplet splitting of the free carbene has been estimated to be just 9 kcal/mol.[55] The carbene behavior can also depend on the oxidation state of the metal. For example, $[Ru]^{II}$=CF_2 possesses an electrophilic carbene, whereas $[Ru]^{0}$=CF_2 displays nucleophilic nature.[56]

The first metal fluorocarbenes, $[(\eta^5\text{-}C_5H_5)Mo{=}CF_2(CO)_3]SbF_6$, $C_5H_5)Mo{=}CF_2(CO)_2(PPh_3)]SbF_6$, and $[(\eta^5\text{-}C_5H_5)Mo{=}CF(C_2F_5)(CO)_3]SbF_6$, were synthesized in 1978 by fluoride abstraction, but could not be isolated.[35] Since then, many metal fluorocarbene complexes, most of them based on precious metals, have been reported, and only a few were isolable.[56] However, early reports of first-row metal fluorocarbenes consisted of iron and manganese complexes with limited reactivity studies. The iron and manganese difluorocarbenes (Figure 1.9) were prepared by fluoride abstraction from $[CpFe(CF_3)(CO)_2]$ and $[Mn(CF_3)(CO)_5]$ respectively, using BF_3 as a Lewis acid.[57] These carbenes show extreme sensitivity to moisture, readily undergoing hydrolysis to afford HF and $[CpFe(CO)_3]^+$ or $[Mn(CO)_4]^+$. Substitution of a carbonyl for triphenylphosphine to give $CpFe{=}CF_2(CO)(PPh_3)]BF_4$ resulted in a more stabilized carbene due to the increased electron density on the metal center. Moreover, the latter features a metal-carbene bond of 1.724 Å.[58]

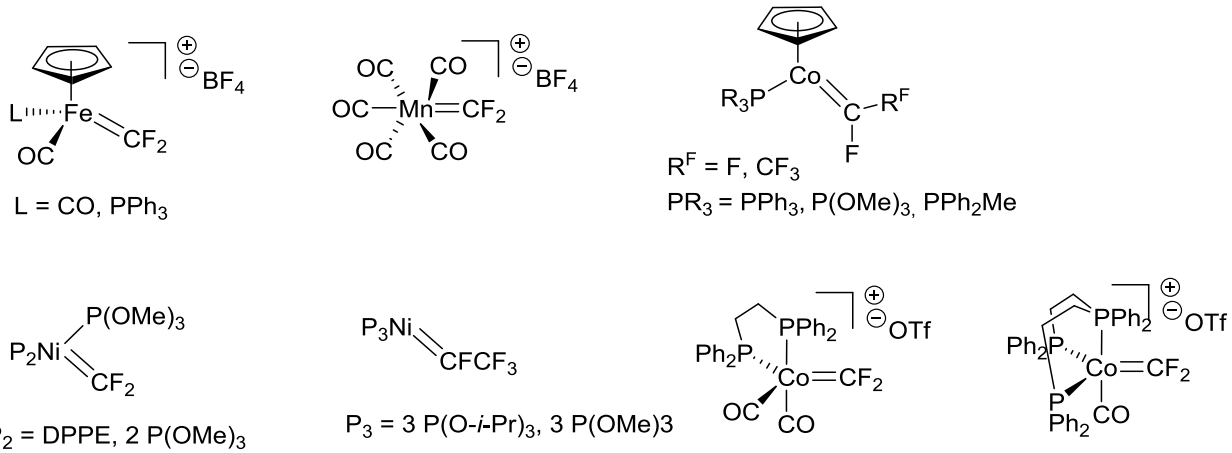

Figure 1.9. First-row metal fluorocarbenes reported.

Our group has recently reported the first examples of cobalt and nickel fluorocarbenes and conducted reactivity studies. The first isolable cobalt carbene complexes,

[CpCo=CFR^F(PR$_3$)], were synthesized from [CpCo(CO)$_2$] by oxidative addition of the iodofluoroalkanes to form [CpCo(CF$_2$R)(CO)I], followed by carbonyl substitution with the appropriate ligand and finally a two-electron reduction.[59] Interestingly, these carbenes exhibit nucleophilic reactivity in reactions with H^+ and Me^+, as well as by their stability towards water, despite the fact that they feature some Fischer-type carbene characteristics. Cobalt-carbene bond distances for PR$_3$ = PPh$_3$ and R^F = F or R^F = CF$_3$ are 1.740 and 1.751 Å, respectively. The short metal-carbene bond distances can be explained by strong π-interactions between the cobalt and the carbene carbon. Moreover, the CpCo=CF(CF$_3$)(PPh$_2$Me) complex reacts with *para*-substituted phenylacetylenes to give a partially fluorinated cobaltcyclobutene complexes via a 1,4 diradical intermediate.[60] In addition, CpCo=CF(R^F)(PPh$_2$Me), where R^F=F or CF$_3$, reacts with TFE to form the metallacyclobutane product via formal [2+2] cycloaddition.[38] Alternatively, the synthesis of cobalt carbene complexes can be performed by introduction of the :CF$_2$ group directly to the metal using the Ruppert-Prakash reagent (Me$_3$SiCF$_3$) activated by a catalytic amount of NaI.[61] Furthermore, the P$_2$Co and P$_3$Co carbene complexes in Figure 1.9 were synthesized by fluoride abstraction of Co(CO)$_4$(CF$_3$) by Me$_3$SiOTf.[62] The P$_3$Co carbene complex features a Co–C$_{carbene}$ bond distance of 1.7395 Å. It was also suggested that two or more phosphine ligands were necessary to stabilize these cationic difluorocarbene complexes.

Lastly, the first isolable nickel fluorocarbenes were prepared by a two-electron reduction of Ni(CF$_3$)(dppe)[OC(O)CF$_3$] with potassium graphite, in the presence of P(OMe)$_3$ to yield Ni=CF$_2$(dppe)[P(OMe)$_3$], and the dppe group could be exchanged for two P(OMe)$_3$ groups using CuCl. These [Ni]=CF$_2$ complexes undergo cycloaddition reactions with TFE much faster than their [Co]=CF$_2$ counterpart through a dissociative process.[39] Moreover, it has been reported that nickel fluoro(trifluoromethyl)carbene complexes, ([P$_3$Ni]=CFCF$_3$) (Figure 1.9), react with TFE

or 1,1-difluoroethylene to afford both metallacyclobutane and perfluorocarbene metathesis products ($P_3Ni{=}CF_2$ and $CH_2{=}CFCF_3$). The nickel carbene starting material for this fluoroalkane metathesis was prepared from $Ni[P\text{-}(O\text{-}i\text{-}Pr)_3]_4$ and $Cd(CF_2CF_3)_2 \cdot DME$.

1.5.2 Metallacycle Carbenes

There is precedent for the formation of metallacycle carbene complexes; Jones and coworkers synthesised and isolated manganese and iron metallacycle carbene complexes.[52,53] They showed that under photolytic conditions, alkoxy-substituted cyclopropyl and cyclobutyl complexes of $(\eta^5\text{-Cp})Fe(CO)_2$ undergo α-elimination to give respectively ferracyclopentenones and ferracyclopentenes (Scheme 1.17)**.** Formation of the ferracarbene seems to be driven by a combination of methoxy stabilization and strain relief.

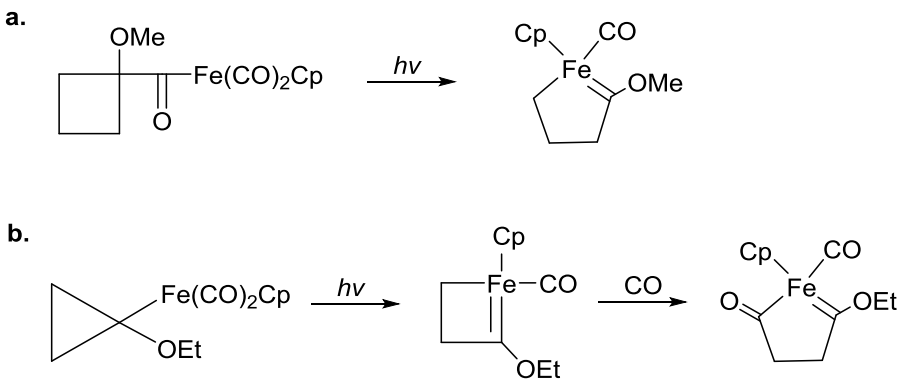

Scheme 1.17. Cyclic carbene formation from (a) methoxy-cyclobutyl-acyl complex of $(\eta^5\text{-Cp})Fe(CO)_2$ via decarbonylation-C-C bond insertion (b) ethoxy cyclopropyl complex of $(\eta^5\text{-Cp})Fe(CO)_2$ via C-C bond insertion.

Similar reactivity was observed with the α-methoxy-benzocyclobutyl complex and the β-dialkylamino-cyclobutyl complex (Scheme 1.18). The crystal structure of the $(\eta^5\text{-Cp})Fe(CO)[{=}C(OMe)CH_2C_6H_4]$ complex indicates an Fe–C(2) distance for the carbene of 1.827 Å, whereas that for the l-carbonyl-l-(η^5-cyclopentadienyl)-2-(diisopropylamino)-l-ferracyclopentene complex is 1.927 Å. The longer bond for the amine-substituted carbene can be explained by the

single bond iminium resonance form shown in Scheme 1.18.[63] However, the Fe–C(5) bond of 2.044 Å is slightly longer than the Fe–C(2) carbene and a similar conclusion can be drawn for the methoxycarbene complex which has an Fe–C(7a) distance of 1.958 Å (Scheme 1.18). Similar results were obtained with manganese analogues.[64]

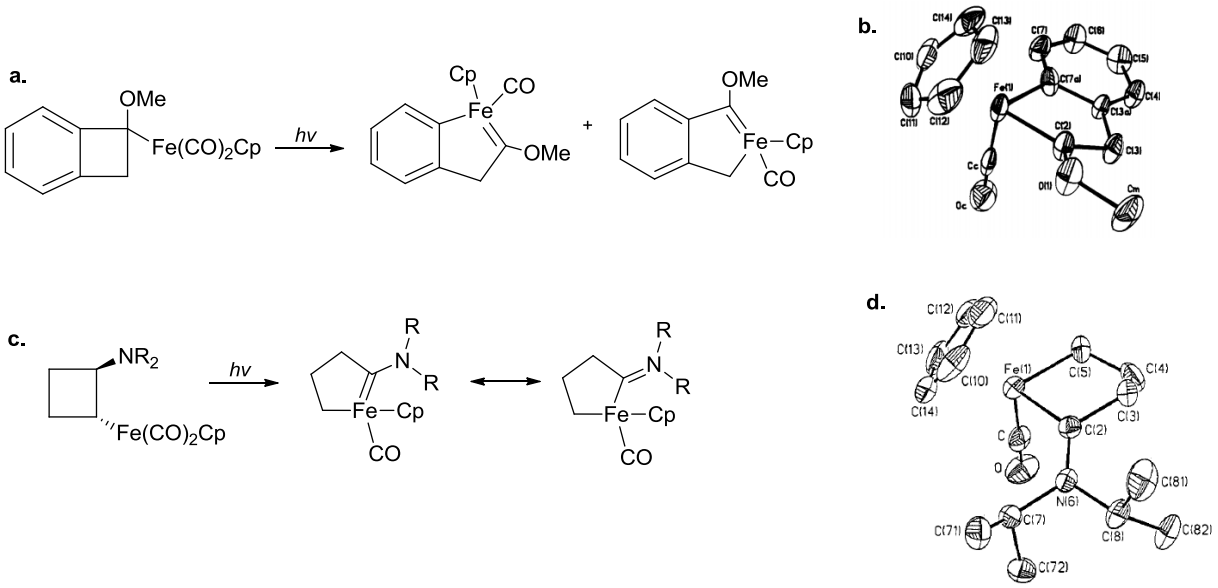

Scheme 1.18. (a) Formation of (η^5-Cp)Fe(CO)[=C(OMe)$CH_2C_6H_4$]) (b) ORTEP drawing of **(a)** (c) Formation of (η^5-Cp)Fe(CO) [=C(N^iPr_2)$(CH_2)_3$]) (d) ORTEP drawing of **(c)**.

1.6 Scope of this Thesis

The objective of this Thesis is to further investigate d^6 perfluorometallacyclopentane complexes in order to get a deeper understanding of their reactivity. Chapter 2 focuses on the synthesis and characterization of a series of new Fe(II) perfluorometallacycles derived from the first perfluorometallacycle reported $Fe(CO)_4$(1,4-C_4F_8), **2-1**, which led to the discovery of the first examples of a fluorinated metallacyclocarbenes. The nature, electrophilic or nucleophelic, and reactivity of these carbenes will be explored in chapter 3 as well as the reactivity of the Fe(II) perfluorometallacycles synthesized. This includes studying selective C_α–F bond activation and hydrogenolysis of these metallacycles. Chapter 4 discusses the reactivity of a series of

phosphine-substituted cobalt(I) carbonyl hydride complexes towards fluoroolefins. Lastly, Chapter 5 summarizes the findings of this Thesis and discusses future directions.

1.7 References

(1) Blanksby, S. J.; Ellison, G. B. *Acc. Chem. Res.* **2003**, *36* (4), 255–263.

(2) Lemal, D. M. *J. Org. Chem.* **2004**, 69, 1–11.

(3) Norman, C. S.; Decanio, S. J.; Fan, L. *Glob. Environ. Chang.* **2010**, *18*, 330–340.

(4) Wang, Z. Reagents, Swarts reaction. In Comprehensive Organic Name Reactions and Reagents, **2010**.

(5) May, P.; Ruh, R. P.; Davis, R. A. US patent 2,885,427,**1959**.

(6) Gumprecht, W. H. US patent 4,311,863, **1982**.

(7) Halasz, S. P. von. CA patent 1,196,345, **1985**.

(8) Rao, V. N. M.; Sievert, A. C.; Nappa, M. J. World patent WO 2008/030440 A2, **2008**.

(9) Van Der Puy. US patent 8,071,826, **2011**.

(10) Potts, J. E.; Ashcraft, A. C.; Wise, E. W.; Va, W. US patent 3,472,826, **1969**.

(11) Mukhopadyay, S.; Nair, H. K.; S, T. H.; Puy, V. Der. US patent **2008**, 7,345,209.

(12) Nair, H. K.; Singh, R. R.; Wajek, D.; Poss, A. J. World patent WO 2013/122790 A1, **2013**.

(13) Egorova, K. S.; Ananikov, V. P. *Organometallics* **2017**, *36*, 4071–4090.

(14) Cramer, R.; Kline, J. B.; Roberts, J. D. *J. Am. Chem. Soc.* **1968**, *21* (9), 2519–2524.

(15) Parshall, G. W.; Jones, F. N. *J. Am. Chem. Soc.* **1965**, 87, 5356.

(16) Crabtree, R. H. The Organometallic Chemistry of the Transition Metals, 6th Ed.; John Wiley & Sons, Inc: Yale University, New Haven, Connecticut, 2014.

(17) Stone, F. G. A. *Pure Appl. Chem.* **1972**, *30*, 551.

(18) Manuel, T. A.; Stafford, S. L.; Stone, F. G. A. *J. Am. Chem. Soc.* **1961**, *104* (2), 2–3.

(19) Hoehn, H. H.; Pratt, L.; Watterson, K. F.; Wilkinson, G.; *J. Chem. Soc.* **1960**, No. 2738, 2738–2745.

(20) Coyle, T. D.; Kings, R. B.; Pitcher, E.; Stafford, S. L.; Teichel, P.; Stone, F. G. A. *J. Inorg. Nucl. Chem.* **1961**, *20* (1–2), 172–173.

(21) Cundy, C. S.; Green, M.; Stone, F. G. A. *J. Chem. Soc. A Inorg. Phys. Theor.* **1970**, 1647–1653.

(22) Green, M.; Osborn, R. B. L.; Rest, A. J.; Stone, F. G. A. *J. Chem. Soc. A Inorg. Phys. Theor.* **1968**, 502, 2525–2530.

(23) Mukhedkar, V. A.; Mukhedkar, A. J. *J. Inorg. Nucl. Chem.* **1981**, *43* (11), 2801–2805.

(24) Ohashi, M.; Shibata, M.; Saijo, H.; Kambara, T.; Ogoshi, S. *Organometallics* **2013**, *32* (13), 3631–3639.

(25) Procedures, G. *Inorg. Chim. Acta* **1977**, *22*, 0–3.

(26) Gasafi-Martin, W.; Oberendfellner, G.; Werner, K. Von. *Can. J. Chem.* **1996**, *74* (11), 1922–1924.

(27) Kaplan, P. T.; Xu, L.; Chen, B.; Mcgarry, K. R.; Yu, S.; Wang, H.; Vicic, D. A. *Organometallics* **2013**, *32*, 7552–7558.

(28) Treichel, P. M.; Pitcher, E.; Stone, F. G. A.; Pitcher, E. *Inorg. Chem.* **1962**, *1* (3), 511–517.

(29) Treichel, P. M.; Morris, J. H.; Stone, F. G. A. *J. Chem. Soc.* **1963**, 720, 720–723.

(30) Wilford, J. B.; Stone, F. G. A. *Inorg. Chem.* **1965**, *4* (1), 2–6.

(31) Burrell, A. B.; Roper, W. R. *Organometallics* **1990**, *3* (3), 1905–1910.

(32) Beveridge, A. D.; Clark, H. C. *J. Organomet. Chem.* **1967**, No. 11, 601.

(33) Clark, H. C.; Cotton, J. D.; Tsai, J. H. *Inorg. Chem.* **1966**, *5* (8), 1407–1415.

(34) Clark, H. C.; Tsai, J. H. *Inorg. Chem.* **1966**, *5* (8), 1407–1415.

(35) Reger, D. L.; Dukes, M. D. *J. Organomet. Chem.* **1978**, *153* (1), 67–72.

(36) Ohashi, M.; Shibata, M.; Ogoshi, S. *Angew. Chem. Int. Ed.* **2014**, *53* (49), 13578–13582.

(37) Xu, W.; Sun, H.; Xiong, Z.; Li, X. *Organometallics* **2013**, *32* (23), 7122–7132.

(38) Harrison, D. J.; Lee, G. M.; Leclerc, M. C.; Korobkov, I.; Baker, R. T. *J. Am. Chem. Soc.* **2013**, *135* (49), 18296–18299.

(39) Harrison, D. J.; Daniels, A. L.; Korobkov, I.; Baker, R. T. *Organometallics* **2015**, *34* (24), 5683–5686.

(40) Fields, R.; Germain, M. M.; Haszeldine, R. N.; Wiggans, P. W. *J. Chem. Soc. A Inorg. Phys. Theor.* **1970**, *9* (1964), 1964–1969.

(41) Burch, R. R.; Calabrese, J. C.; Ittel, S. D. *Organometallics* **1988**, *7* (7), 1642–1648.

(42) Giffin, K. A.; Korobkov, I.; Baker, R. T. *Dalton Trans.* **2015**, *44* (45), 19587–19596.

(43) Giffin, K. A.; Harrison, D. J.; Korobkov, I.; Baker, R. T. *Organometallics* **2013**, *32* (24), 7424–7430.

(44) Andrella, N. O.; Sicard, A. J.; Gorelsky, S. I.; Korobkov, I.; Baker, R. T. *Chem. Sci.* **2015**, *6* (11), 6392–6397.

(45) Baker, R. T.; Beatty, R. P.; Farnham, W. B.; Robert, D.; Wallace, L. US patent 5,670,679*,* **1997**.

(46) Baker, R. T.; Beatty, P. R.; Farnham, B. W.; Wallace, L. R. US patent 5,545,769, **1996**.

(47) Fields, R.; Germain, M. M.; Haszeldine, R. N.; Wiggans, P. W. *Chem. Commun.* **1967**, 24, 243–244.

(48) Granville, S. L. University of Ottawa MSc thesis, **2010**.

(49) Pitcher, E.; Stone, F. G. A. *Spectrochim. Acta* **1961**, *18* (5), 585–594.

(50) Appleton, T. G.; Clark, H. C.; Manzer, L. E. *Coord. Chem. Rev.* **1973**, *10*, 335–422.

(51) Lindner, E.; Schauss, E.; Hiller, W.; Fawzi, R. *Angew. Chem. Int. Ed.* **1984**, *23*, 711–712.

(52) Fischer, E. O.; Maasböl, A. *Angew. Chem.* **1964**, *76* (14), 645–645.

(53) Frenking, G.; Solà, M.; Vyboishchikov, S. F. *J. Organomet. Chem.* **2005**, *690* (24–25), 6178–6204.

(54) Schrock, R. R. *J. Am. Chem. Soc.* **1974**, *96* (21), 6796–6797.

(55) Dixon, D. A. *J. Phys. Chem.* **1986**, *90* (1), 54–56.

(56) Brothers, P. J.; Roper, W. R. *Chem. Rev.* **1988**, *88* (7), 1293–1326.

(57) Richmond, T. G.; Crespi, A. M.; Shriver, D. F. *Organometallics* **1984**, *3* (2), 314–319.

(58) Crespi, A. M.; Shriver, D. F. *Organometallics* **1985**, *4* (10), 1830–1835.

(59) Harrison, D. J.; Gorelsky, S. I.; Lee, G. M.; Korobkov, I.; Baker, R. T. *Organometallics* **2013**, *32* (1), 12–15.

(60) Lee, G. M.; Leung, A. S. C.; Harrison, D. J.; Korobkov, I.; Hughes, R. P.; Baker, R. T. *Organometallics* **2017**, *36* (15), 2853–2860.

(61) Lee, G. M.; Harrison, D. J.; Korobkov, I.; Baker, R. T. *Chem. Commun.* **2014**, *50* (9), 1128–1130.

(62) Harrison, D. J.; Daniels, A. L.; Korobkov, I.; Baker, R. T. *Organometallics* **2015**, *34* (18), 4598–4604.

(63) Stenstrom, Y.; Koziol, A. E.; Palenik, G. J.; Jones, W. M. *Organometallics* **1987**, *6* (10), 2079–2085.

(64) Crowther, D. J.; Zhang, Z.; Palenik, G. J.; Jones, W. M. *Organometallics* **1992**, *11*, 622–628.

Chapter 2

Synthesis and Characterization of Iron Perfluorometallacycle Complexes

2.1 Introduction

As discussed in chapter 1, the synthesis and reactivity of iron fluorometallacycles have not been studied extensively. The very first example of a perfluorometallacycle, $Fe(CO)_4(1,4\text{-}C_4F_8)$ (**2-1**, Figure 1.3), was introduced by Stone in 1961[1] by addition of tetrafluoroethylene (TFE) to low-valent $Fe(CO)_5$. Limited reactivity studies showed that this cyclic compound is highly stable. CO substitutions by monodentate ligands resulted in the di-or monosubstituted structure, and bidentate ligand substitutions gave the chelated or bridged complexes, depending on the nature of the ligand.[2] Moreover, while at Du Pont Baker *et al*. proposed a metallacycle carbene intermediate during the hydrogenolysis of **2-1**. This chapter discusses further investigations on ligand substitutions and metallacyclocarbene formation from **2-1**.

Before working with the initial iron carbonyl precursors, multiple attempts at the synthesis of iron perfluorometallacycle were made starting from different low-valent iron complexes. A 14-electron, low-coordinate iron(0) compound, [(IMes)Fe(dvtms)], was the first complex to be studied in this research (IMes = 1,3-Dimesitylimidazol-2-ylidene; dvtms = divinyltetramethyldisiloxane). It was successfully prepared following a literature procedure[3] by the reduction of $FeCl_2$ in the presence of dvtms and IMes. As oxidative coupling of TFE was not observed with [(IMes)Fe(dvtms)], attempts at replacing the vinyl groups by phosphine ligands were made in order to have a more electron-rich precursor. Bidentate ligands such as DCPPE, DMPE, DIPPE, DIBPP, DPPF, Xantphos, and monodentate ligands like PMe_2Ph, $P^tBu_2{}^nBu$, $PEt_2{}^iBu$, $P(o\text{-}tol)_3$, as well as a series of phosphite ligands, were combined with the low-

coordinate Fe(0) compound. However, only dmpe coordinated to the metal by displacing the dvtms group. Metallacycle formation was not observed, however, upon addition of TFE or VDF to the newly formed Fe(NHC)(dmpe) complex. Modification of this synthesis using IAd or IMe resulted in decomposition of the product. Direct preparation of (IMes)Fe($P)_2$ in a similar way as for (IMes)Fe(dvtms) was also unsuccessful. 16-electron complexes, (P_2)Fe(dvtms) were also synthesized and treated with fluoroolefins, but the desired product was not observed.

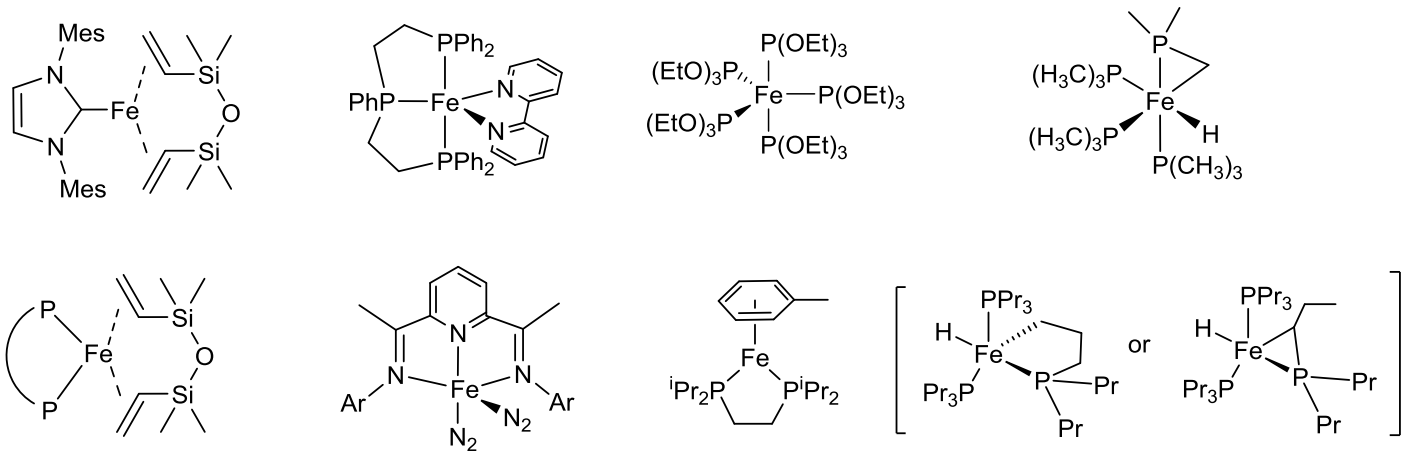

Figure 2.1. Examples of iron precursors tested for TFE oxidative coupling.

Moreover, addition of TFE to low-valent Fe[$P(OEt)_3$]$_5$, prepared via a known procedure,[4] did not yield a metallacycle. Ligand substitution to make the complex more electron rich also failed. This led to the synthesis of similar iron complexes involving phosphines: trimethylphosphine was reacted with $FeCl_2$ and reduced to yield $FeH(CH_2PMe_2)(PMe_3)_3$ via intramolecular C–H addition of the trialkylphosphine to the metal.[5] Unfortunately, addition of TFE or VDF resulted in decomposition of the complex. For this reason, other phosphine ligands (PCp_3, P^nPr_3) were tried, using a variety of different reduction methods (Na/Hg, Mg, Zn, KC_8, Na naphthalenide) and starting materials ($FeCl_2$, $FeBr_2$). The only successful synthesis was $FeCl_2$

reduced with magnesium powder in the presence of excess tripropylphosphine which also formed an iron hydride complex (see possible structure in Figure 2.1). However, due to the oily nature of the product, it was impossible to remove the excess tripropylphosphine which made it difficult to study the reactivity of the complex with TFE. Indeed, reacting free tripropylphosphine with TFE gave a host of different products as determined by ^{19}F NMR spectroscopy.

Furthermore, selected zerovalent phosphine and nitrogen ligand-based iron complexes were reproduced from the literature due to their potential to coordinate the electrophilic fluoroolefin by possibly offering an empty coordination site and by being electron-rich (Figure 2.1). Surprisingly, metallacycle formation was not detected upon addition of TFE or VDF to (triphos)Fe(bipy)[6] or (PDI)Fe(N_2)[7] under a variety of conditions. Lastly, [1,2-bis(diisopropylphosphino)ethane](η^6-toluene)iron(0) was prepared[8] and exposed to fluoroolefins with the idea that the toluene ligand would be easily displaced; however, this hypothesis was not realized.

Due to the unsuccessful syntheses of iron fluorometallacyclopentanes from selected low-valent and electron-rich iron precursors, the focus of this research was redirected towards the synthesis of iron metallacycles derived from iron carbonyl complexes.

2.2 Synthesis of Iron Perfluorometallacycle Complexes from $Fe_2(CO)_9$

Complex **2-1** can be synthesized in good yields from a mixture of $Fe_3(CO)_{12}$ and $Fe(CO)_5$, or $Fe_2(CO)_9$ irradiated by UV light under pressure of TFE. However, $Fe(CO)_5$ is an extremely toxic and highly flammable volatile liquid, therefore $Fe_2(CO)_9$ is a safer alternative. $Fe_2(CO)_9$ breaks up into $Fe(CO)_5$ and the coordinately unsaturated $Fe(CO)_4$, allowing a vacant

site for the coordination of TFE. UV irradiation of the $Fe(CO)_5$ in solution will also form $Fe(CO)_4$ which will further react with the fluoroolefin (Scheme 2.1).

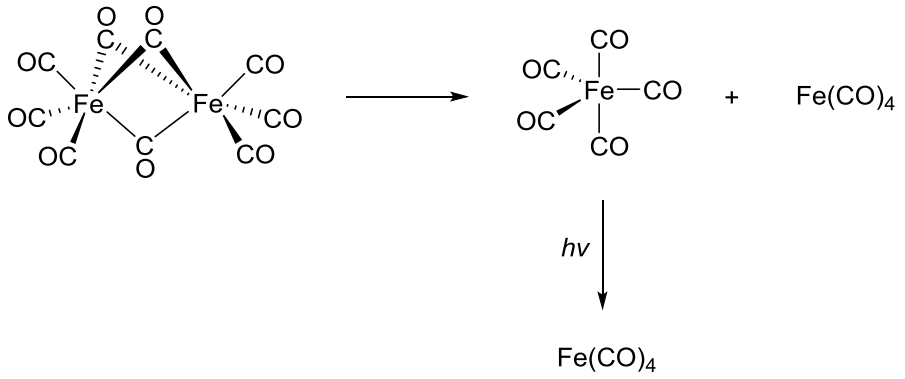

Scheme 2.1. Behavior of $Fe_2(CO)_9$ in solution and under UV light.

The reaction must be stirred vigorously while being irradiated under TFE in order to dissolve all the $Fe_2(CO)_9$ which is poorly soluble in hexanes. The original procedure suggested a reaction time of 20 hours, resulting in a 54% yield; of **2-1**. However, in our case conducting the reaction over 48 hours gave a 79% yield.

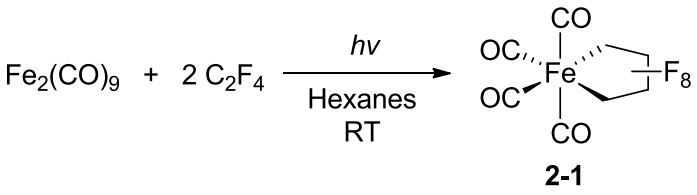

Scheme 2.2. Synthesis of **2-1** from $Fe_2(CO)_9$.

Ligand substitution must be performed after metallacyclopentane formation as it has been shown that replacing CO groups by phosphine ligands prior to addition of TFE leads to a mixture of three-membered (olefin-type) and five-membered metallacycles (Scheme 2.3).[9]

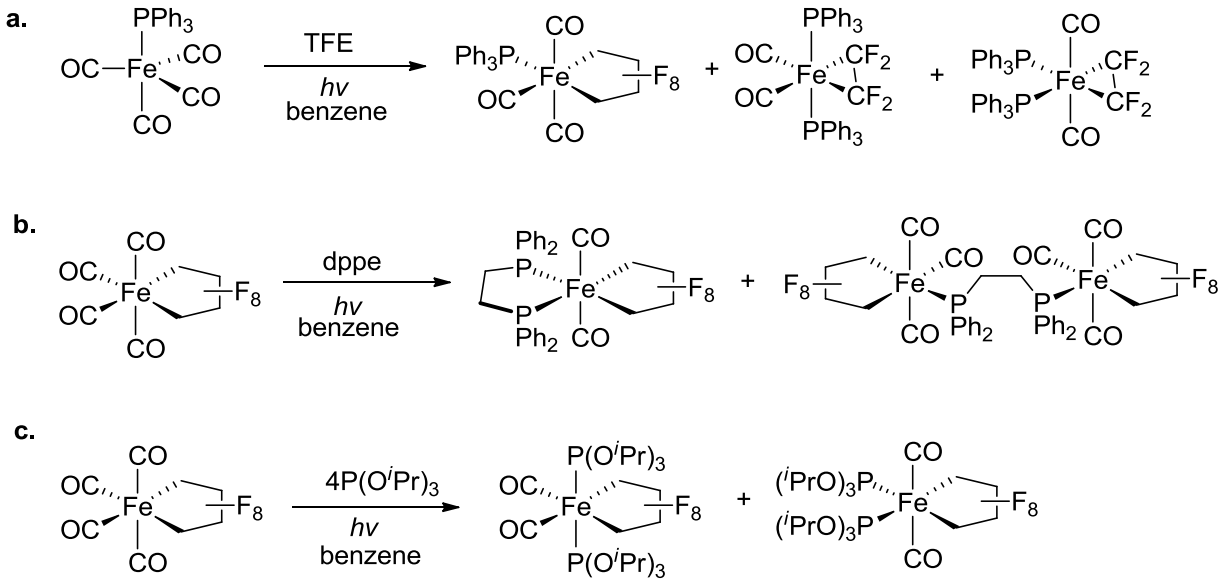

Scheme 2.3. Examples of lack of selectivity when conducting (a) substitution reaction before metallacycle formation and (b) and (c) substitution reactions on **2-1**.

To avoid the mixture of isomers obtained previously (Scheme 2.3) using some monodentate and bidentate ligands and to gain more insight into the reactivity of **2-1**, we investigated the reactivity of $Fe(CO)_4(1,4\text{-}C_4F_8)$ with a series of tridentate ligands, as well as new bidentate and monodentate ligands. These studies afforded new Fe(II) metallacyclopentanes and the first examples of first-row transition metal perfluoro-metallacyclocarbenes synthesized through C–F bond activation.

2.2.1 Formation of $Fe(IMes)(CO)_3(1,4\text{-}C_4F_8)$, 2-2a,b

When substitution of CO groups in **2-1** by the N-heterocyclic carbene ligands IMes was attempted at 60°C in a sealed reactor, a mixture of isomers was obtained after 24 hours (Scheme 2.4). For the complex with the axial IMes (**2-2a**), the fluorine atoms of each CF_2 group are non-equivalent, giving rise to four resonances (Figure 2.2) with a large geminal coupling constant at -134.4 and -133.5 ppm ($C_\beta F$, $^2J_{FF}$ = 244 Hz) and -90 and -70.6 ppm ($C_\alpha F$, $^2J_{FF}$ = 256 Hz). The

complex featuring an equatorial IMes (**2-2b**) has equivalent germinal fluorines, but four chemically different CF_2 groups at -137.7 and -136.8 ppm ($C_\beta F_2$) and -79.2 and -71.2 ppm ($C_\alpha F_2$). Interestingly, after 3 days, complex **2-2a** was gone and only **2-2b** was observed along with a minor unknown isomer (Figure 2.2). Further analysis based on a DEPT-135 experiment suggests modification to the N-heterocyclic carbene ligand by showing CH_2 resonances that were not present in the starting material, possibly explaining the additional resonances in the ^{19}F NMR spectrum.

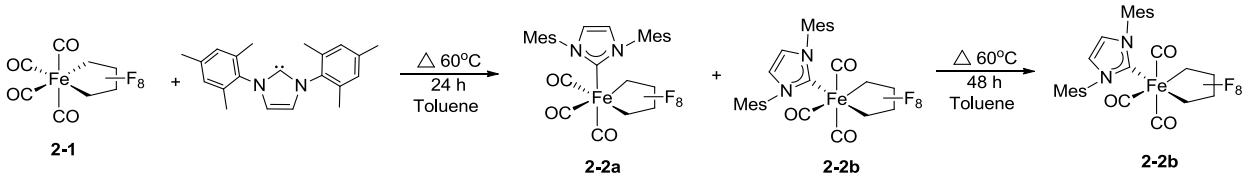

Scheme 2.4. Synthesis of $Fe(IMes)(CO)_3(1,4\text{-}C_4F_8)$, **2-2a, 2-2b**.

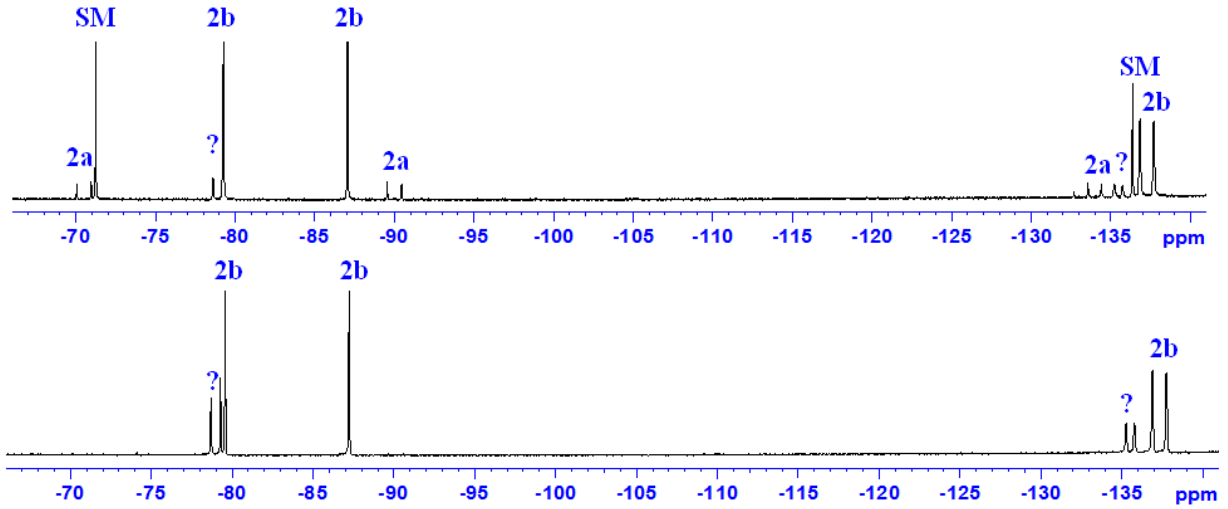

Figure 2.2. ^{19}F NMR spectra of $Fe(IMes)(CO)_3(1,4\text{-}C_4F_8)$ formation. Top spectrum was taken after an overnight reaction. Bottom spectrum was obtained after heating the reaction for 2 d.

The IR spectrum of the final product (Figure A.24) shows CO stretching frequencies slightly lower than the starting material $Fe(CO)_4(1,4\text{-}C_4F_8)$, **2-1**, (2100 cm^{-1}, 2020 cm^{-1}), which

are the highest frequencies of substituted complexes reported in this work. Despite NHCs being known to be strong donors, it is shown here that the electron density of the metal center depends more on the number of substituted CO ligands, than the donor strength of the L ligand.

2.2.2 Formation of Fe(dibpe)$(CO)_2$(1,4-C_4F_8), 2-3

An iron complex featuring a bulky, electron-rich bidentate phosphine ligand was synthesized for future reactivity studies. UV irradiation of **2-1** in the presence of 1,2-bis(diisobutylphosphino)ethane (dibpe) gave one isomer of Fe(dibpe)$(CO)_2$(1,4-C_4F_8) (**2-3**; Scheme 2.5). Ligand substitution with dibpe was significantly faster than with the tripodal phosphine ligand, possibly because it is more electron-rich. Moreover, this complex features *trans*-CO groups with C_{2v} symmetry.

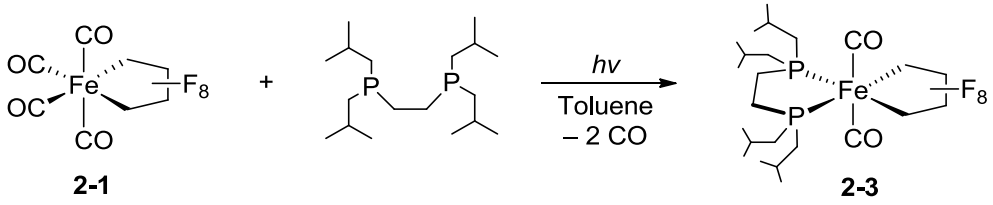

Scheme 2.5. Synthesis of Fe(dibpe)(1,4-C_4F_8), **2-3.**

Indeed, the $^{31}P\{^1H\}$ NMR spectrum (Figure A.5) shows a single resonance for the two equivalent phosphines at 56.7 ppm, and the ^{19}F NMR spectrum displays two distinct signals; one for the all the α-Fs at -76.2 ppm ($^3J_{FP}$ = 10 Hz, $^3J_{FF}$ = 6.5 Hz) and one for all the β-Fs at -137.5 ppm (Figure A.4). An increase of electron density at the metal center in **2-3** can be confirmed by its IR spectrum (ν_{CO} = 1970 cm^{-1}; Figure A.22).

2.2.3 Formation of Fe(κ^2-tripod)$(CO)_2$(1,4-C_4F_8), 2-4

Irradiation of **2-1** in the presence of one equivalent of the tridentate tripodal phosphine, 1,1,1-tris(diphenylphosphinomethyl)ethane (tripod) gave a single isomer of an 18-electron

complex Fe(κ^2-tripod)$(CO)_2$(1,4-C_4F_8), **2-4**, featuring an uncoordinated phosphine arm (Scheme 2.6). Indeed, the $^{31}P\{^1H\}$NMR spectrum (Figure A.3) displayed one signal for two equivalent phosphorus donors at 27.9 ppm coupled to fluorines, and a singlet at -31.1 ppm assigned to the uncoordinated arm. The proposed structure with *trans*-CO groups leads to a single ^{19}F NMR resonance for all four α-Fs at -76.1 ppm (dt, 4F, $^3J_{FP}$ = 14 Hz, $^3J_{FF}$ = 13 Hz) and one broad singlet at -136.7 ppm for all the β-Fs, indicating that the source of axial asymmetry caused by the dangling arm is too far away to generate distinct chemical shifts for the formally inequivalent geminal fluorines (Figure A.2).

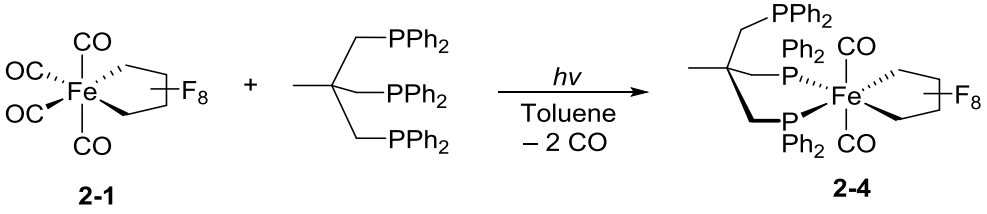

Scheme 2.6. Synthesis of Fe(κ^2-tripod)(1,4-C_4F_8), **2-4.**

A decrease in the carbonyl stretching frequency in the IR spectrum of **2-4** (1980 cm^{-1}) was observed when compared to **2-1** (2170 and 2130 cm^{-1}) (Figure A.20). As the electron density on the iron center increases due to the phosphine substitution, more π-backbonding takes place, weakening the C–O bond as more electron density is pushed into the empty π^* anti-bonding CO orbital. Moreover, the identity of **2-4** was confirmed by ESI-MS; $C_{47}H_{40}F_8FeO_2P_3^+$ 937.6, found 937.6.

Unfortunately, attempts at coordinating the third arm, by forcing the dissociation of one of the carbonyl groups, were unsuccessful. Neither days of exposure to UV light, nor heating in the solid state to 200°C, which converted the white powder into a brown oil, led to any changes in the NMR spectra. Treatment of **2-4** with excess trimethylamine *N*-oxide (TMNO) at 65°C was

expected to attack the carbonyl to release CO_2, coordinate trimethylamine to the metal, and have the free phosphine replace it. Instead a number of resonances corresponding to uncoordinated free arms and perhaps even P=O bonds were observed. Therefore, the free phosphine arm was protonated before addition of TMNO to protect it from oxidation. However, upon addition of TMNO, the arm was deprotonated and the $^{31}P\{^{1}H\}$ NMR spectrum showed mostly starting material. The CO ligand's ability to be displaced by TMNO has been shown to depend on its stretching frequency,[10] e.g. 2010 cm^{-1}. Lastly, the idea was to make the iron complex electron deficient by oxidizing it, therefore making it more likely to dissociate a CO ligand and coordinate the third P donor. Finally, reducing it back to Fe(II) couold afford the diamagnetic ferracyclopentane. Unfortunately, oxidation with $[Cp_2Fe]BF_4$ was not successful and the use of tris(4-bromophenyl)ammoniumyl hexachloroantimonate seemed to react with the free arm and not oxidize the metal.

In summary, one isomer of the stable Fe(κ^2-tripod)$(CO)_2$(1,4-C_4F_8), **2-4**, was synthesized, and all efforts to coordinate the third arm were unsuccessful.

2.2.4 Formation of FeF(triphos)(1,4-C_4F_7), 2-6

Irradiation of **2-1** with bis(2-diphenylphosphinoethyl)phenylphosphine (triphos), a linear tridentate phosphine ligand, yielded the highly stable 18-electron neutral iron(II) fluoride metallacyclocarbene product **2-6** (Scheme 2.7). Interestingly, the intermediate Fe(κ^3-triphos)(CO)(1,4-C_4F_8), **2-5**, was observed while the reaction was monitored by NMR spectroscopy (Figure A.6). The IR spectrum of **2-5** contains a major CO stretch at 1990 cm^{-1}, thus confirming more π-backbonding than **2-1**.

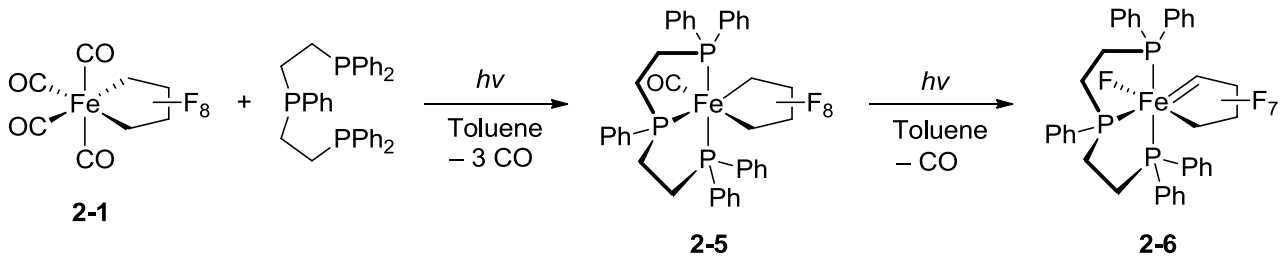

Scheme 2.7. Synthesis of FeF(triphos)(1,4-C_4F_7), **2-6**.

The ^{19}F NMR spectrum of the final product displays the characteristic F–carbene signal at 111 ppm and the fluoride ligand signal upfield at -400 ppm (Figure 2.3). Indeed, the ^{19}F NMR spectra of metal fluorocarbenes typically feature a positive chemical shift. In general, lower metal oxidation state and better electron-donating ability of the ancillary ligands cause an upfield shift, whereas high metal oxidation state, cationic complexes, and electron-accepting ligands lead to a downfield shift.[11] Metal–fluoride bonds also exhibit characteristic chemical shifts in the ^{19}F NMR spectra which are shifted upfield dramatically.

The ^{19}F NMR spectrum confirms the meridional coordination of the triphos ligand as the geminal fluorines are equivalent as a consequence of the mirror plane that includes the metallacycle ring. In fact, the ^{19}F NMR spectrum features a broad singlet at -134.1 ppm for the $C_\beta F_2$ between the $C_\alpha F_2$ and the second $C_\beta F_2$ group, a multiplet at -124.4 ppm ($^3J_{FF}$ = 11.5 Hz) for the $C_\beta F_2$ adjacent to the carbene moiety, and a singlet at -85.1 ppm for the $C_\alpha F_2$ group. An ^{19}F-^{19}F COSY experiment confirmed all these correlations (Figure A.9). No coupling was seen for the fluoride ligand even when a long range coupling experiment was performed. However, assuming the Fe–F is formed via α-F elimination, the fluoride ligand would be placed *cis* to the fluorocarbene. This symmetry is also seen by the $^{31}P\{^1H\}$ NMR spectrum, in which two broad

signals, integrating 2:1, are assigned to the tridentate phosphine ligand at 63.9 and 83.7 ppm, respectively (Figure A.8).

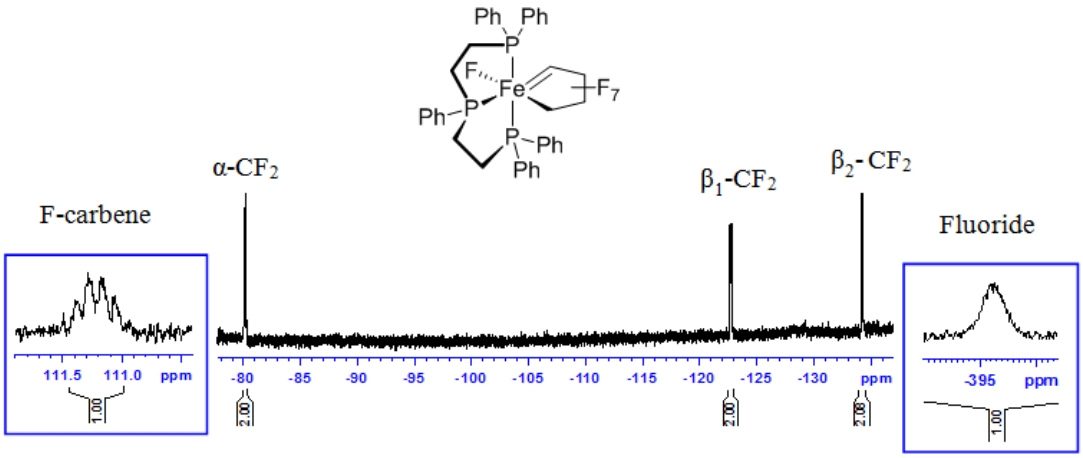

Figure 2.3. ^{19}F NMR spectrum of FeF(triphos)(1,4-C_4F_7), **2-6**.

The formula for **2-6** was confirmed by MALDI-TOF: mass calculated for $C_{38}H_{33}F_8FeP_3$ 790.1, found 790.9, as well as ESI-MS: mass calculated for $C_{38}H_{33}F_7FeP_3^+$ 771.1, found 771.0.

In summary, we report the first iron perfluorometallacycle from $Fe(CO)_4$(1,4-C_4F_8) with three CO groups substituted by phosphines, and one CO by a fluoride ligand coming from a fluorocyclocarbene formed *in situ*, presumably via α-F elimination.

2.2.5 Formation of [Fe(triphos)(1,4-C_4F_7)(NCMe)]$^+BPh_4^-$, 2-7

As the oily nature of **2-6** made it hard to grow good quality crystals for X-ray diffraction, we treated it with $NaBPh_4$ in acetonitrile to yield an 18-electron cationic species, [Fe(triphos)(1,4-C_4F_7)(NCMe)]$^+BPh_4^-$, **2-7** (Scheme 2.8).

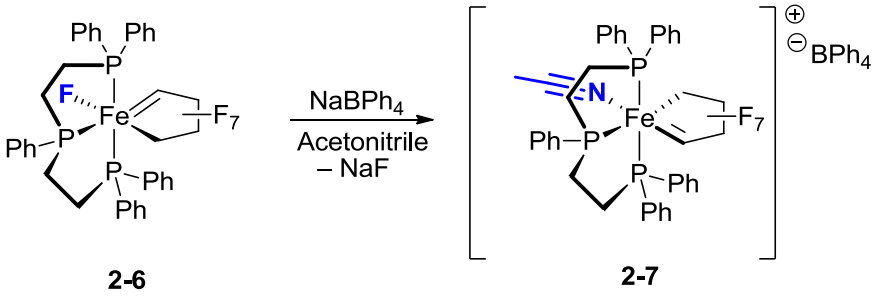

2-6 **2-7**

Scheme 2.8. Synthesis of $[Fe(triphos)(1,4\text{-}C_4F_7)(NCMe)]^+BPh_4^-$, **2-7.**

Few significant changes were observed in the ^{19}F NMR spectra (Figure A.10); only slight shifts of the signals and the disappearance of the fluoride resonance as expected. The most important shift involves the carbene-F resonance that shifted downfield from 108.3 ppm to 126.9 ppm due to the new cationic nature of the compound and the different *trans* ligand donor atom (see below). Small shifts of the two broad singlets in the $^{31}P\{^1H\}$ NMR spectrum were also observed (Figure A.11).

The molecular structure of **2-7**, determined by X-ray diffraction, is consistent with the NMR data reported (Figure 2.4). Note however that reaction of acetonitrile with the presumed 5-coordinate cationic intermediate gave the isomer with the N-donor *trans* to the carbene moiety whereas the fluoride was presumably *cis* to the carbene. The pseudo-octahedral structure features an $Fe=C^F$ bond length of 1.745(3) Å, which is shorter than its $Fe–CF_2$ bond of 2.011(3) Å, an average distance seen in other iron carbonyl perfluorometallacycle complexes.[9] Moreover, the bond distances between αC4–F6 and αC4–F7 are 1.377(4) Å and 1.403(4) Å, respectively. This complex features longer αC–F bond distances than βC–F, where βC2–F2 1.356(4) Å, βC2–F3 1.361(4) Å, βC3–F4 1.361(3) Å and βC3–F5 1.359(4) Å. The F–carbene bond of 1.364(4) Å is slightly shorter than the αC–Fs in this structure, consistent with the C_{sp2}–F bonds typically being shorter than C_{sp3}–F (1.340 vs 1.428 Å).[12]

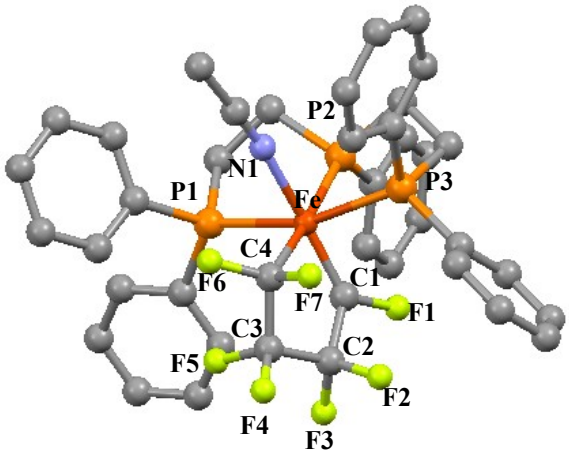

Figure 2.4. ORTEP representation of the molecular structure of [Fe(triphos)(1,4-C_4F_7)(NCMe)]$^+$$BPh_4^-$, **2-7**.Thermal ellipsoids are set at the 40% probability level. Hydrogen atoms and $^-BPh_4$ counterion are omitted for clarity. Selected bond lengths (Å) and angles (deg): Fe–C1 1.745(3), Fe−C4 2.011(3), C1–F1 1.364(4), C4–F6 1.377(4), C4–F7 1.403(4), C2–F2 1.356(4), C2–F3 1.361(4), C3–F4 1.361(3), C3–F5 1.359(4). C4–Fe–C1 81.1(1), C4–Fe–P3 98.2(1), C4–Fe–P1 95.9(1), C4–Fe–N1 86.5(1), C1–Fe–P1 104.7(1), C1–Fe–P2 101.7(1), C1–Fe–P3 89.0(1), P2–Fe–P1 81.99(4), P2–Fe–P3 83.29(4), N1–Fe–P1 82.49(9), N1–Fe–P2, 83.29(4), N1–Fe–P3 86.57(9).

2.2.6 Formation of Fe(OTf)(triphos)(1,4-C_4F_7), 2-8

For future reactivity studies (see Chapter 3), another complex was derived from FeF(triphos)(1,4-C_4F_8), **2-6**. Addition of 1 equivalent of TMS-OTf to **2-6** gave the neutral 18-electron compound Fe(OTf)(triphos)(1,4-C_4F_8) (**2-8**; Scheme 2.9).

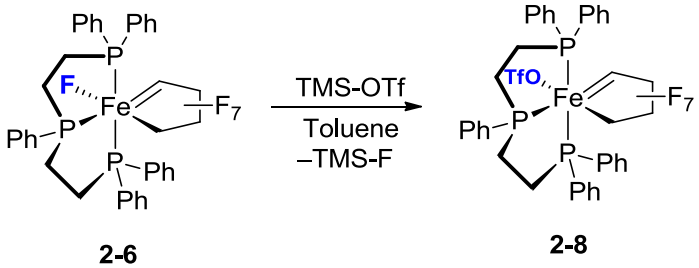

Scheme 2.9. Synthesis of Fe(OTf)(triphos)(1,4-C_4F_7), **2-8**.

The reaction was accompanied by an immediate colour change from brown to bright orange. Once again, the fluoride signal in the ^{19}F NMR disappears and the carbene signal shifted

downfield to 122.5 ppm (Figure A.12). As for the remaining metallacycle resonances and the ^{31}P NMR signals, minor shifts are observed due to replacement of the fluoride ligand by the triflate (Figure A.13) Note, however, that in the absence of an X-ray diffraction study we are unable to determine whether the triflate ligand is *cis* or *trans* to the carbene moiety.

Interestingly, when **2-8** was dissolved in a more coordinating solvent than toluene such as THF, a color change from orange to green was observed, presumably due to formation of a cationic THF-ligated species with an outer sphere triflate. This obvious lability of the triflate group will be exploited in future reactivity studies (Chapter 3).

2.2.7 Formation of Fe(terpy')(CO)(1,4-C_4F_8), 2-9

In order to expand the reactivity of **2-1** to include 'hard' ligands, we investigated the reaction of a linear tridentate nitrogen ligand. UV irradiation of a mixture of **2-1** and 4′-(4-methylphenyl)-2,2′:6′,2″-terpyridine gave Fe(terpy')(CO)(1,4-C_4F_8) (**2-9**; Scheme 2.10). Interestingly, the reaction stops at the monocarbonyl stage and no carbene formation was observed upon extended irradiation.

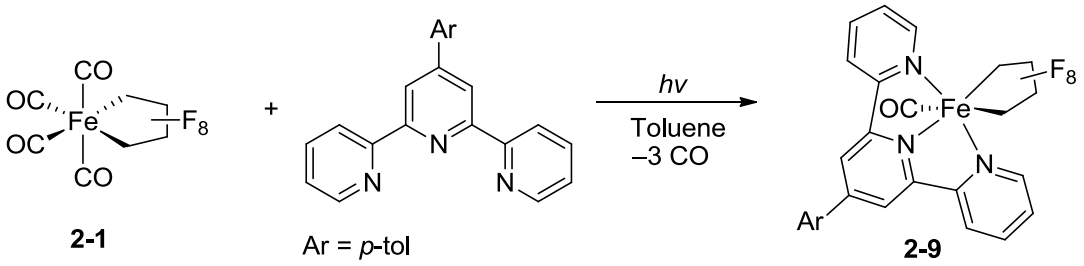

Scheme 2.10. Synthesis of Fe(terpy')CO(1,4-C_4F_8), **2-9**.

The IR spectrum exhibited the lowest CO stretching frequency reported in this work (1960 cm^{-1}) (Figure A.21), meaning this complex has the most π-backbonding. The increase of electron density at the metal center can be explained by the substitution of three CO ligands as well as by

the nature of the terpy' ligand. Even though the triphos ligand is only a weak π-acceptor, the CO stretching frequency of analogous complex Fe(triphos)CO(1,4-C_4F_8), **2-5**, is 1990 cm^{-1}. Thus we can assume that the terpy' π* acceptor orbitals are likely too high in energy to allow for efficient Fe back-bonding in complex **2-9.**

The ^{19}F NMR spectrum of **2-9** shows a distinct signal for each pair of geminal fluorines at -138.1 ($C_\beta F_2$), -137.6 ($C_\beta F_2$), -126.1 ($C_\alpha F_2$) and -98.2 ppm ($C_\alpha F_2$), suggesting mirror symmetry that includes the metallacycle plane (Figure A.14). The two pairs of β-F_2 have similar shifts since they are far from the rest of the molecule; however, the two sets of α-F_2 have a significant difference in shifts. The more downfield signal could be related to CF_2 group *trans* to the CO which might be more deshielded due to the π-backbonding, and the more upfield signal could be associated to the CF_2 *trans* to the nitrogen ligand which should be more shielded due to the electron-donating ability of the nitrogen-based ligand.

The X-ray structure obtained (Figure 2.5) is consistent with the ^{19}F NMR spectrum, and confirms that all three nitrogen atoms are coordinated to the iron center. The pseudo-octahedral complex features bond distances of 1.992(3) Å for Fe–C1 and 2.023(3) Å for Fe–C4. The αC–F bonds of the metallacycle, C1–F1 1.401(5) Å, C1–F2 1.411(3) Å, C4–F7 1.396(3) Å and C4–F8 1.402(5) Å, are longer than the βC–F bonds, C2–F3 1.368(4), C2–F4 1.362(4), C3–F5 1.360(4) and C3–F6 1.364(4).

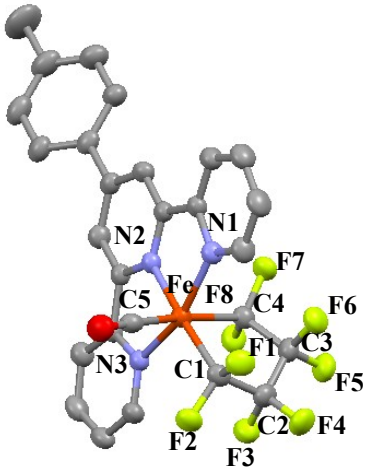

Figure 2.5. ORTEP representation of the molecular structure of Fe(terpy')CO(1,4-C_4F_8), **2-9**. Thermal ellipsoids are set at the 40% probability level. Hydrogen atoms are omitted for clarity. Selected bond lengths (Å) and angles (deg): Fe–C1 1.992(3), Fe−C4 2.023(3), C1–F1 1.401(5), C1–F2 1.411(3), C4–F7 1.396(3), C4–F8 1.402(5), C2–F3 1.368(4), C2–F4 1.362(4), C3–F5 1.360(4), C3–F6 1.364(4). C1–Fe1–C4 84.7(1), C1–Fe–N3 98.5(1), C1–Fe–N1 102.0(1), C1–Fe–C5 87.6(1), C4–Fe–N1 88.6(1), C4–Fe–N2 88.0(1), C4–Fe–N3 91.0(1), N1–Fe–N2 79.8(1), N2–Fe–N3 79.6(1), C5–Fe–N1 91.6(1), C5–Fe–N2 99.7(7), C5–Fe–N3 91.5(1).

2.2.8 Formation of [Fe(terpy')(CO)(1,4-C_4F_7)]$^+$OTf$^-$, 2-10

Intrigued by the idea of carbene formation, we treated complex **2-9** with excess TMS-OTf (reaction was too slow with 1 equivalent) which afforded an 18-electron Fe(II) cationic carbene-containing species, [Fe(terpy')(CO)(1,4-C_4F_7)]$^+$OTf$^-$ (**2-10**; Scheme 2.11). Carbene formation is hypothesized to occur *trans* to the nitrogen, because this C–F bond seems the most activated since it features the longest bond distance in complex **2-10**.

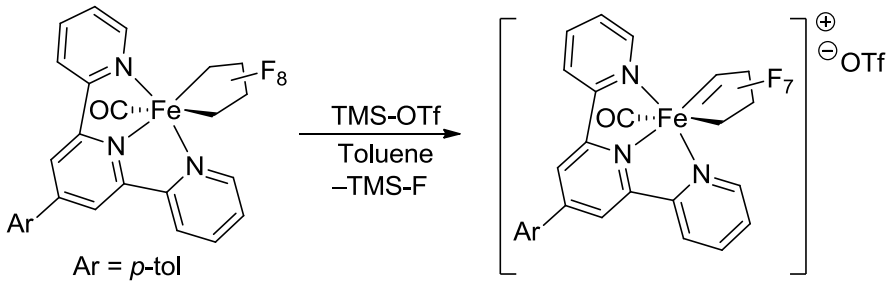

Scheme 2.11. Synthesis of $[Fe(terpy')(CO)(1,4\text{-}C_4F_7)]^+OTf^-$, **2-10**.

The ^{19}F NMR spectrum (Figure 2.6) of **2-10** displays the characteristic carbene-F signal, a triplet at 115 ppm with a coupling constant $^3J_{FF}$ of 33 Hz to the adjacent β-F_2. The sharp singlet at -80.5 ppm is assigned to the CF_3 group of the triflate counterion. The only $C_\alpha F_2$ gives rise to a triplet at -109.4 ppm with a coupling of 8.1 Hz to its neighbouring $C_\beta F_2$. The doublet of triplets at -131.5 ppm is due to the $C_\beta F_2$ group next to the carbene, where the fluorines are coupled to the carbene-F, as well as to the other $C_\beta F_2$ with a coupling constant of 12.5 Hz. Lastly, the $C_\beta F_2$ next to the $C_\alpha F_2$ appears at -136.9 ppm as a broad multiplet.

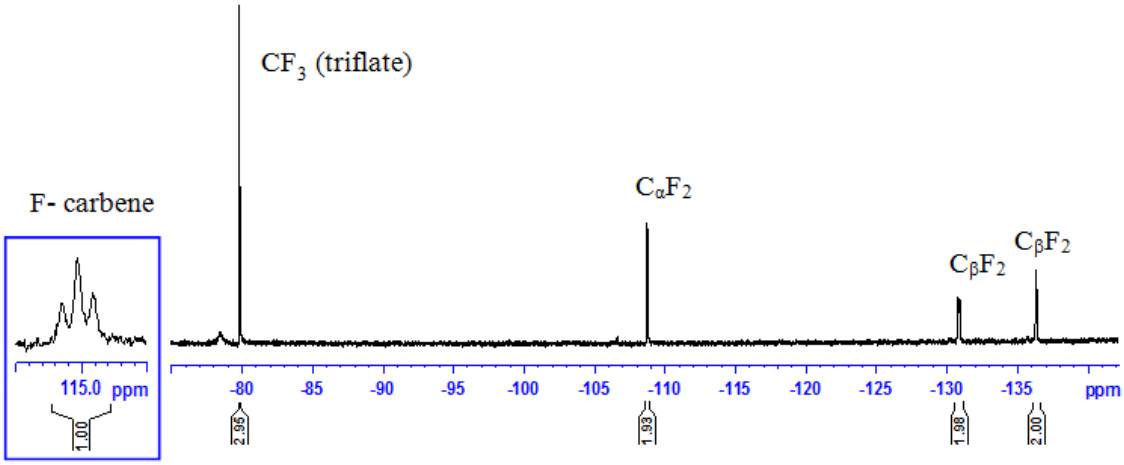

Figure 2.6. ^{19}F NMR spectrum of $[Fe(terpy')(CO)(1,4\text{-}C_4F_7)]^+OTf^-$, **2-10**.

The IR spectrum of **2-10** exhibits a CO stretching frequency of 1990 cm^{-1} (Figure A.23) which when compared to the frequency of its precursor (1960 cm^{-1}), is consistent with a cationic complex with reduced back-bonding.

2.3 Conclusions

In conclusion, a series of new iron perfluorometallacycle complexes have been synthesized and characterized by CO substitutions in $Fe(CO)_4(1,4\text{-}C_4F_8)$, **2-1.** It has been shown that substitution by the N-heterocyclic ligand, IMes, first affords the monosubstituted axial complex **2-2a** as the kinetic product, then converts to the equatorial structure **2-2b** assigned as the thermodynamic product when heated longer. Interestingly, the substitution by electron-rich chelating phosphine ligand, dibpe, only takes place under light irradiation, giving a single isomer **2-3** and no bridged-complex as previously reported with dppe. It has been also shown that phosphorus- and nitrogen-based linear tridentate ligands can substitute three COs to afford $Fe(L_3)(CO)(1,4\text{-}C_4F_8)$, **2-5**, **2-9**; however, the triphos complex undergoes C_α–F bond activation *in situ* to afford $FeF(P_3)(1,4\text{-}C_4F_7)$, **2-6**, the first example of a fluorinated metallacyclocarbene. Abstraction of the Fe-fluoride ligand with TMS-OTf affords the more labile triflate analog **2-8** while $NaBPh_4$ gives the cationic acetonitrile complex **2-7**. In contrast, C_α–F abstraction from the terpy' complex gave the cationic iron monocarbonyl carbene complex **2-10**. Furthermore, the tripodal tridentate phosphine ligand can only substitute two COs, but gives only one isomer **2-4**. It is also interesting to note that substitution attempts with anionic tris(pyrazolyl)borate (Tp) and P,N,S ligands were unsuccessful. Studies on the reactivity of these new compounds are discussed in Chapter 3.

2.4 Experimental Section

2.4.1 General Considerations

Experiments were conducted under nitrogen, using Schlenk techniques or an MBraun glove box. All solvents were deoxygenated by purging with nitrogen. Toluene, hexanes, diethyl ether and tetrahydrofuran (THF) were dried on columns of activated alumina using a J. C. Meyer solvent purification system. Benzene-d_6 (C_6D_6) was dried by stirring over activated alumina (ca. 10 wt.%) overnight, followed by filtration. Acetonitrile (CH_3CN), acetonitrile-d_3 (CD_3CN), and dichloromethane (DCM) were dried by refluxing over calcium hydride under nitrogen. After distillation, they were dried further by stirring over activated alumina (ca. 5 wt.%) overnight, followed by filtration. All solvents were stored over activated (heated at ca. 250^{o}C for >10 h under vacuum) 4 Å molecular sieves. Glassware was oven-dried at 150^{o}C for >2 h. The following chemicals were obtained commercially, as indicated: trimethylsilyl trifluoromethanesulfonate (Me_3SiOTf, Aldrich, 99%), diironnonacarbonyl ($Fe_2(CO)_9$, Aldrich) bis(2-diphenylphosphinoethyl)phenylphosphine (Triphos, Strem, 97%), 1,1,1-tris(diphenylphosphinomethyl)ethane (tripod, Strem, 97%), 1,2-bis(diisobutylphosphino)ethane (dibpe, Cytec-Solvay), 4′-(4-Methylphenyl)-2,2′:6′,2″-terpyridine (terpy', Aldrich, 98.5%). 1,3-dimesitylimidazolium tetrafluoroborate ($IMes{\cdot}HBF_4$) was prepared following a literature procedure[13] and deprotonated using KHMDS to obtain the free carbene. Tetrafluoroethylene was made by pyrolysis of polytetrafluoroethylene (Scientific Polymer Products, powdered) under vacuum, using a slightly modified literature procedure [10-20 mTorr, 650^{o}C, 15 g scale, product stabilized with R(+)-limonene (Aldrich, 97%), giving TFE of *ca.* 97% purity].[14] Compound $Fe(CO_4)(1,4\text{-}C_4F_8)$ was made by oxidative addition of tetrafluoroethylene to Fe_2CO_9 using a slightly modified literature procedure.[1] ^1H, ^{19}F, $^{31}P\{^1H\}$ and $^{13}C\{^1H\}$ NMR spectra were recorded on a 300 MHz Bruker Avance instrument at room-temperature (21-23^{o}C). ^1H NMR

spectra were referenced to the residual proton peaks associated with the deuterated solvents (C_6D_6: 7.16 ppm; CD_3CN: 1.94 ppm). ^1H NMR spectra werereferenced to the residual proton peaks associated with the deuterated solvents (C_6D_6: 7.16 ppm; CD_3CN: 1.94 ppm; THF-d_8: 1.73, 3.58 ppm). $^{31}P\{^1H\}$ NMR data were referenced to external H_3PO_4 (85 % aqueous solution), set to 0.0 ppm. Irradiation was performed using a Reptile UV lamp, high UVB mercury vapor flood lamp, UVB output 150μW/cm^2 at 4ft. Electrospray ionization mass spectral data were collected using an Applied Biosystem API2000 triple quadrupole mass spectrometer. MALDI spectra were recorded on Bruker UltrafleXtreme MALDI-TOF/TOF mass spectrometer interfaced to a glovebox. IR spectra were recorded on a Nexus 670 FT-IR, using KBr salt plates, and compounds were dissolved in DCM beforehand. UV-vis spectra were recorded on a Cary 100 instrument, using sealable quartz cuvettes (1.0 cm pathlength). X-ray crystallography samples were mounted on thin glass fibers using paraffin oil. Data were collected on a Bruker AXS KAPPA single crystal diffractometer equipped with a sealed Mo tube source (wavelength 0.71073Å) APEX II CCD detector. Raw data collection and processing were performed with APEX II software package from BRUKER AXS.

2.4.2 Synthesis and Characterization

Synthesis of $Fe(CO)_4(1,4\text{-}C_4F_8)$, 2-1. $Fe_2(CO)_9$ (2g, 5.5 mmol) was placed in a 350 ml Schlenk tube with a stir bar and 60 ml of hexanes. The solution turned green with a gold precipitate. On a Schlenk line, the flask was degassed with three freeze-pump-thaw cycles. The TFE gas was then added to a pressure of 8 psig (set on a gas regulator fitted to the cylinder) and the flask was sealed under pressure. The solution was stirred for 48 hours under UV light or until the solution became colourless. The solution was filtered through Celite to remove some brown insolubles, concentrated in vacuo and stored at -32^{o}C for 24 hours. The crystalline precipitate

obtained was filtered through a glass frit and washed with cold hexanes until the crystals became white. The final product was dried to afford a crystalline white powder. Yield: 1.6g, 79%. ^{19}F NMR (282 MHz, C_6D_6) δ -136.3 (s, 4F, $2C_\beta F_2$), -71.3 (s, 4F, $4C_\alpha F_2$). UV-vis (Cary 100, toluene); 280 nm. IR (FT-IR, cm^{-1}) 2170, 2130 (CO).

Synthesis of Fe(IMes)(CO)$_4$(1,4-C$_4$F$_8$), 2-2a,b. $Fe(CO)_4(1,4\text{-}C_4F_8)$ (40 mg, 0.11 mmol) and 1,3-dimesitylimidazol-2-ylidene (100 mg, 0.33 mmol) were dissolved in ca. 15 ml of toluene in a 100 ml Schlenk tube with a stir bar to give a yellow heterogeneous mixture and put under static vacuum. The solution was heated at 60^{o}C for 3 days. Upon heating the solution became homogeneous and changed from yellow to brown over time. The reaction mixture was concentrated in vacuo and stored at -32^{o}C in order to precipitate the excess IMes. The reaction was filtered through Celite pipette and the solution was dried in vacuo to afford a light brown powder. Yield: 49 mg, 69%. ^{19}F NMR (282 MHz, C_6D_6) δ -137.7 (s, 2F, $C_\beta F_2$), -136.9 (s, 2F, $C_\beta F_2$), -87.2 (s, 2F, $C_\alpha F_2$), -79.6 (quint, 2F, $^3J_{FF}$ = 4 Hz, $C_\alpha F_2$). IR (FT-IR, cm^{-1}) 2100, 2020 (CO).

Synthesis of Fe(dibpe)(CO)$_2$(1,4-C$_4$F$_8$), 2-3. $Fe(CO)_4(1,4\text{-}C_4F_8)$ (25 mg, 0.07 mmol) and 1,2-bis(diisobutylphosphino)ethane (18 mg, 0.07 mmol) were dissolved in ca. 5 ml of toluene in a 25 ml Schlenk tube with a stir bar to give a colourless solution and put under static vacuum. The reaction mixture was stirred and irradiated under the UV lamp for 18 hours to yield an orange solution. The solution was filtered through Celite and dried to yield a light yellow powder. Yield: 34.8 mg, 78.9%. ^{19}F NMR (282 MHz, C_6D_6) δ -137.5 (s, 4F, $C_\beta F_2$), -76.2 (dt, 4F, $^3J_{FP}$ = 10 Hz, $^3J_{FF}$ = 6.5 Hz, $C_\alpha F_2$). $^{31}P\{^1H\}$ (121 MHz, C_6D_6) δ 56.7 (m, $^3J_{PF}$ = 10 Hz, Fe–P). IR (FT-IR, cm^{-1}) 1970, 1950 (CO).

Synthesis of Fe(κ^2-tripod)(CO)$_2$(1,4-C$_4$F$_8$), 2-4. Fe(CO)$_4$(1,4-C$_4$F$_8$) (300 mg, 0.82 mmol) and 1,1,1-Tris(diphenylphosphinomethyl)ethane (509.4 mg, 0.82 mmol) were dissolved in ca. 15 ml of toluene in a 100 ml Schlenk tube with a stir bar to give a colourless solution and put under static vacuum. The reaction mixture was stirred and irradiated under the UV lamp for 24 hours to yield a yellow solution. The resulting solution was filtered through Celite and dried in vacuo. The yellow powder was washed with ether until the product turned white. The white powder was dried under vacuum. Yield: 395 mg, 78.1%. ^{19}F NMR (282 MHz, C_6D_6) δ -136.7 (br s, 4F, 2 $C_\beta F_2$), -76.1 (dt, 4F, $^3J_{FP}$ = 14.0 Hz, $^3J_{FF}$ = 13 Hz, 2 $C_\alpha F_2$). ^{31}P{^{1}H} (121 MHz, C_6D_6) δ -31.1 (s, 1P, uncoordinated arm), 27.9 (quint, 2P, $^3J_{PF}$ = 14.0 Hz, Fe–P). Electrospray Ionisation, solvent: CH_3CN; mass calculated for $C_{47}H_{40}F_8FeO_2P_3^+$ 937.6, found 937.6. IR (FT-IR, cm^{-1}) 2060, 1980, 1960 (CO).

Synthesis of FeF(triphos)(1,4-C$_4$F$_8$), 2-6. Fe(CO)$_4$(1,4-C$_4$F$_8$) (200 mg, 0.54 mmol) and bis(diphenylphosphinoethyl)phenylphosphine (291 mg, 0.54 mmol) were dissolved in ca. 30 ml of toluene in a 100 ml Schlenk tube with a stir bar to give a colourless solution and put under static vacuum. The reaction mixture started turning yellow after a few minutes of irradiation. The solution was irradiated under the UV lamp for three days to yield a brown heterogeneous solution. The reaction mixture was filtered through Celite and dried in vacuo in a vial to give a dark orange oil. Yield: 272 mg, 63.7%. ^{19}F NMR (282 MHz, C_6D_6) δ -134.1 (br s, 2F, $C_\beta F_2$), -124.4 (m, 2F, $^3J_{FF}$ = 11.5 Hz, $C_\beta F_2$), -85.1 (br s, 2F, Fe–$C_\alpha F_2$), 108.3 (m, 1F, $^3J_{FF}$ = 31 Hz, Fe=CF), Fe=CF). ^{31}P{^{1}H} (121 MHz, C_6D_6) δ 63.9 (br s, 2P, Fe–P), 83.7 (br s, 1P, Fe–P). MALDI-TOF, solvent: C_6H_6, matrix (pyrene solution 100 mM) / analyte (5 mM) ratio: 125 µL / 5 µL; mass calculated for $C_{38}H_{33}F_8FeP_3$ 790.1, found 790.9. Electrospray Ionisation, solvent: CH_3CN; mass calculated for $C_{38}H_{33}F_7FeP_3^+$ 771.1, found 771.0.

Synthesis of [Fe(triphos)(1,4-C_4F_7)(NCMe)]$^+BPh_4^-$, 2.7. FeF(triphos)(1,4-C_4F_8) (129 mg, 0.163 mmol) was placed in a vial and dissolved in ca. 5 ml of acetonitrile. To this stirred solution was added an excess of $NaBPh_4$ (140 mg, 0.41 mmol), causing a slow colour change from dark orange to brown over 24h. The reaction mixture was dried in vacuo and extracted with DCM. The product was isolated by filtration through a glass frit and dried in vacuo to yield a brown powder. X-ray quality crystals were grown from a cooled saturated THF solution. Yield: 137 mg, 72.8%. ^{19}F NMR (282 MHz, THF) δ -133.5 (br s, 2F, $C_\beta F_2$), -121.9 (br s, 2F, $C_\beta F_2$), -79.1 (m, 2F, $^3J_{FF}$ = 10.5 Hz, $C_\alpha F_2$), 126.9 (br s, 1F, Fe=CF). $^{31}P\{^1H\}$ (121 MHz, THF) 61.9 (s, 2P, Fe–P), 87.2 (m, 1P, $^3J_{PF}$ = 23 Hz, Fe–P).

Synthesis of Fe(OTf)(triphos)(1,4-C_4F_7), 2-8. FeF(triphos)(1,4-C_4F_8) (63 mg, 0.080 mmol) was placed in a vial and dissolved in ca. 3 ml of toluene. To this stirred solution was added 1 equivalent of TMS-OTf (14.4 μL, 0.408 mmol), causing an instant colour change from dark orange to bright orange. After stirring for 30 minutes, the reaction mixture was dried in vacuo for 3 hours to remove TMS-F and any unreacted TMS-OTf. The product was isolated as an orange powder. Yield: 66 mg, 83.8%. ^{19}F NMR (282 MHz, toluene) δ -157.6 (m, 1F, TMS-F), -134.4 (br s, 2P, $C_\beta F_2$), -122.8 (br d, 2F, $^3J_{FP}$ = 30.5 Hz $C_\beta F_2$), -80.7 (sept, 2F, $^3J_{FF}$ = 10 Hz, $C_\alpha F_2$), -79.2 (s, 3F, OTf), 122.5 (br m, 1F, $^3J_{FP}$ = 15.5 Hz, Fe=CF). $^{31}P\{^1H\}$ (121 MHz, toluene) δ 63.2 (s, 2P, Fe–P), 87.84 (br m, 1P, Fe–P).

Synthesis of Fe(terpy')(CO)(1,4-C_4F_8), 2-9. $Fe(CO)_4$(1,4-C_4F_8) (186 mg, 0.51 mmol) and 4′-(4-Methylphenyl)-2,2′:6′,2″-terpyridine (271 mg, 0.51 mmol) were dissolved in ca. 20 ml of toluene in a 100 ml Schlenk tube with a stir bar to give an orange solution and put under static vacuum. The reaction mixture was stirred and irradiated under the UV lamp for 48 h to yield a dark purple solution. The product was dried and isolated as a purple powder. X-ray quality

crystals were grown from a cooled saturated toluene solution. Yield: 304 mg, 87.2 %. ^{19}F NMR (282 MHz, C_6D_6) δ -138.1 (br s, 2F, $C_\beta F_2$), -137.6 (br s, 2F, $C_\beta F_2$), -126.1 (s, 2F, $C_\alpha F_2$), -98.2 (s, 2F, $C_\alpha F_2$). IR (FT-IR, cm^{-1}) 1960, 1930 (CO).

Synthesis of [Fe(terpy')(CO)(1,4-C_4F_7)]$^+$OTf$^-$, 2-10. Fe(terpy')CO(1,4-C_4F_8) (70 mg, 0.10 mmol) was placed in a vial and dissolved in ca. 5 ml of toluene. To this stirred solution was added an excess of TMS-OTf (45.2 μL, 0.25 mmol). The solution was allowed to stir overnight at room temperature. The newly formed compound crashed out of solution as a dark red/purple solid. The yellow liquid was decanted and the purple powder dried to remove excess TMS-OTf. Yield: 56.9 mg, 63%. ^{19}F NMR (282 MHz, THF) δ -136.9 (br m, 2F, $C_\beta F_2$), -131.5 (dt, 2F, $^3J_{FF}$ = 33 Hz, $^3J_{FF}$ = 12.5 Hz, $C_\beta F_2$), -109.4 (t, 2F, $^3J_{FF}$ = 8 Hz, $C_\alpha F_2$), -80.5 (s, 3F, OTf), 114.5 (t, 1F, $^3J_{FF}$ = 33 Hz, Fe=C^F). IR (FT-IR, cm^{-1}) 1990 (CO). ^{1}H NMR (300 Hz, THF-d_8) δ 2.5 (s, 3H, CH_3), 7.4 (br t, 2H, $^3J_{HH}$ = 5.5 Hz, CH), 7.5 (br d, 2H, $^3J_{HH}$ = 7.5 Hz, CH), 8.1 (m, 4H, CH), 8.6 (m, 4H, CH), 9.1 (s, 2H, CH).

2.5 References

(1) Manuel, T. A.; Stafford, S. L.; Stone, F. G. A. *J. Am. Chem. Soc.* **1961**, *104* (2), 2–3.

(2) Hoehn, H. H.; Pratt, L.; Watterson, K. F.; G., W. *J. Chem. Soc.* **1960**, 0, 2738–2745.

(3) Zhang, H.; Ouyang, Z.; Liu, Y.; Zhang, Q.; Wang, L.; Deng, L. *Angew. Chem. Int. Ed.* **2014**, *53* (32), 8432–8436.

(4) English, A. D.; Ittel, S. D.; Tolman, C. A.; Meakin, P.; Jesson, J. P. *J. Am. Chem. Soc.* **1977**, *99* (1), 117–120.

(5) Rathke, J. W.; Muetterties, E. L. *J. Am. Chem. Soc.* **1975**, *97* (11), 3272–3273.

(6) Mukhopadhyay, T. K.; Feller, R. K.; Rein, F. N.; Henson, N. J.; Smythe, N. C.; Trovitch, R. J.; Gordon, J. C. *Chem. Commun.* **2012**, *48* (69), 8670–8672.

(7) Bart, S. C.; Lobkovsky, E.; Chirik, P. J. *J. Am. Chem. Soc.* **2004**, *126* (42), 13794–13807.

(8) Hermes, A. R.; Warren, T. H.; Girolami, G. S. *Dalton Trans.* **1995**, 2, 301–305.

(9) Granville, S. L. University of Ottawa MSc thesis, **2010**.

(10) Luh, T.-Y. *Coord. Chem. Rev.* **1984**, *60*, 255–276.

(11) Crespi, A. M.; Shriver, D. F. *Organometallics* **1985**, *4* (10), 1830–1835.

(12) Allen, F. H.; Kennard, O.; Watson, D. G.; Brammer, L.; Orpen, A. G. *J. Chem. Soc.* **1987**, No. 12, 1–19.

(13) Hans, M.; Lorkowski, J.; Demonceau, A.; Delaude, L. *Beilstein J. Org. Chem. 2015* **2015**, No. 11, 2318–2325.

(14) Hunadi, R. J.; Baum, K. *Synthesis,* **1982**, *39*, 454.

Chapter 3

Reactivity of Iron Perfluorometallacycles

3.1 Introduction

The importance of fluorocarbons and their derivatives can be seen through their use as refrigerants, insecticides, solvents, and pharmaceutical compounds.[1] However, their syntheses are energy-intensive and environmentally problematic processes,[2] and development of more sustainable and energy efficient syntheses are desired.

$Fe(CO)_4(1,4\text{-}C_4F_8)$ is known to be highly stable, but the substitution of CO ligands by phosphine- or nitrogen-based groups can affect the reactivity of the metallacycle. Chemical modification of the metallacycle is often facilitated by activated C–F bonds and ring strain, oferring a potential method for the synthesis of small fluorocarbons. Baker *et al.* reported that hydrogenolysis of $Fe(CO)_4(1,4\text{-}C_4F_8)$, at elevated temperatures and H_2 pressure, gave two different hydrofluorocarbons: HFC-338pcc and HFC-347pcc (Scheme 3.1). HFC-347pcc was proposed to be formed through a carbene intermediate, and when triphenylphosphine was added to the reaction mixture, the conversion increased significantly.[3]

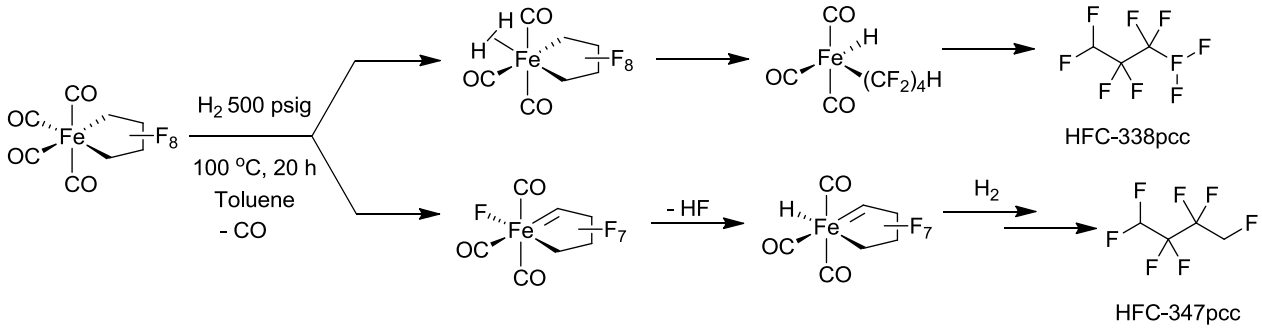

Scheme 3.1. Proposed mechanisms for the hydrogenolysis of $Fe(CO)_4(1,4\text{-}C_4F_8)$.

Moreover, Baker and coworkers developed a catalytic method for the hydrodimerization of TFE with perfluoronickelacyclopentane and NiL_4 intermediates.[4] The hydrogenolysis of the robust Ni–R^F bond required high temperatures and pressures and was only observed when π-acidic phosphite ligands were employed.[5] More recently, our group showed that the rate of Ni–C^F bond hydrogenolysis is greatly increased in the low-coordinate nickel NHC metallacycle (7 psig and 25°C vs. 700 psig and 100°C in the phosphite Ni metallacycle).[6]

Hydrogenolysis of the perfluorometallacycle is not the only modification possible. Indeed, selective carbon–fluorine bond activation of perfluoroorganometal complexes can provide novel synthetic routes to fluorinated organic molecules. For instance, α-F abstraction by an acid was demonstrated to give ligand migration to the α-C,[7] ring contraction M–cyclobutyl[6] or formation of carbene[8] or alkenyl products,[9,10] depending on the nature of the complex.

Further reactivity can be investigated once the metallacycle is modified. For example, the carbene formed can be nucleophilic or electrophilic. Electrophilic difluorocarbenes are known to be very sensitive to moisture, affording two equivalents of HF and a metal-coordinated CO group,[11] whereas nucleophlic carbenes tend to be unreactive towards moisture. Our group recently published several cobalt fluorocarbene complexes featuring some characteristics of Fischer carbenes, but with unusual nucleophilic reactivity.[12] Moreover, these transition metal carbenes undergo reactions with different olefins,[10] acetylenes,[13] silanes, etc. In this chapter, we discuss and compare the reactivity of our new d^6 perfluoroferraacycles and the Fe(II) perfluorometallacyclocarbene complexes presented in Chapter 2.

3.2 Reactivity of Iron Perfluorometallacycles with Lewis acids

In order to extend the selective activation of the C_α–F bond previously reported for fluoroalkyls of Mo,[8] Pt,[9,14] Co,[15] and Ni,[6,7,16] to iron complexes, each complex presented in Chapter 2 was treated with Lewis acids. When Fe(IMes)$(CO)_3$(1,4-C_4F_8), **2-2b,** was exposed to 1 equivalent, then excess of TMS-OTf, no reaction was observed for many days. Upon heating, resonances in the ^{19}F NMR spectrum, assigned to one of the equatorial isomers, started to slowly disappear giving multiple signals in the baseline, leaving the set of resonances assigned to the unidentified isomer unchanged (Figure A.25). The characteristic resonance for carbene-F was not observed and no reaction was observed also when complex, **2-2b**, was treated with $BF_3{\cdot}Et_2O$. Moreover, no C_α–F bond activation was revealed when Fe(κ^2-tripod)$(CO)_2$(1,4-C_4F_8), **2-4**, or Fe(dibpe)$(CO)_2$(1,4-C_4F_8), **2-3**, was treated with TMS-OTf and $BF_3{\cdot}Et_2O$. Indeed, the ^{19}F NMR spectra of these reactions showed no change in the metallacycle even upon addition of excess acid and heating; however, according to the $^{31}P\{^1H\}$ NMR spectrum the phosphine dangling arm of **2-4** reacted with the BF_3 group. In contrast, as detailed in Chapter 2, addition of TMS-OTf to Fe(terpy')(CO)(1,4-C_4F_8), **2-9**, afforded one isomer of the carbene-containing cationic species, [Fe(terpy')(CO)(1,4-C_4F_7)]$^+$OTf$^-$, **2-10**, showing facile activation of one of the C_α–F bonds.

These results show that C_α–F activation depends on the number of CO groups on the metal center and less on the donor strength of the L ligand. Indeed, NHCs are known to be strong donors; however, having only one IMes on the iron was not enough for selective C_α–F activation. Moreover, Fe(κ^2-tripod)$(CO)_2$(1,4-C_4F_8), **2-4**, did not display any C_α–F activation, nor did its more electron-rich counterpart, Fe(dibpe)$(CO)_2$(1,4-C_4F_8), **2-3**, as the π-acceptor capabilities of phosphines compete with the π-backbonding into the C_α–F anti-bonding orbital. The IR spectrum (Table 1.3) of Fe(terpy')(CO)(1,4-C_4F_8), **2-9**, confirmed more π-backbonding into the CO ligand, indicating additional electron density available because the terpy' π^* acceptor

orbitals are likely too high in energy to allow for efficient Fe back-bonding. The nature of this ligand then facilitates C_α–F activation as π-donation from Fe to the αC-F anti-bonding orbital now competes with a single CO ligand.

Table 3.1. CO stretching frequencies (cm^{-1}) for selected Fe complexes.

Complexes	**CO stretching frequencies (cm^{-1})**
Fe(IMes)$(CO)_3(1,4\text{-}C_4F_8)$	2100 (s), 2020 (s)
Fe(κ^2-tripod)$(CO)_2(1,4\text{-}C_4F_8)$	2060 (w), 1980 (s), 1960 (w)
Fe(dibpe)$(CO)_2(1,4\text{-}C_4F_8)$	1970 (s), 1950 (w)
Fe(triphos)$CO(1,4\text{-}C_4F_8)$	2030 (w), 1990 (s), 1960 (w)
Fe(terpy')$(CO)(1,4\text{-}C_4F_8)$	1960 (s), 1930 (w)
$[Fe(terpy')(CO)(1,4\text{-}C_4F_7)]^+OTf^-$	1990

*s = strong signal, w = weak signal

It was reported previously that photolysis of $[(\eta^5\text{-}C_5H_5)Mo(CF_3)(CO)_3]$ gave *trans*-$[(\eta^5\text{-}C_5H_5)Mo{=}CF_2(F)(CO)_2]$ via α-F elimination and rapid isomerisation of the *cis*-product.[17] The metal center acting like an internal Lewis acid was also observed during the transformation of intermediate Fe(triphos)$CO(1,4\text{-}C_4F_8)$, **2-5**, as it undergoes C_α–F elimination *in situ* to give FeF(triphos)$(1,4\text{-}C_4F_7)$, **2-6**, during the substitution reaction. The same phenomenon was not observed for Fe(terpy')$(CO)(1,4\text{-}C_4F_8)$, **2-9**, because the metal is less Lewis acidic due to the lack of π-back-donation to the nitrogen ligand.

3.3 Nucleophilic vs Electrophilic Character of the $Fe{=}C^F$ bonds

As mentioned previously, electrophilic difluorocarbenes are known to be very sensitive to moisture, whereas nucleophlic carbenes tend to be unreactive towards it. Interestingly, no reaction was observed, according to the ^{19}F and $^{31}P\{^1H\}$ NMR spectra, when FeF(triphos)(1,4-

C_4F_7), **2-6**, was exposed to water, suggesting a nucleophilic carbene. Moreover, the lack of electrophilic character of this carbene was supported by its unreactive nature towards nucleophiles such as pyridine, and morpholine which only seemed to displace the triphos ligand.

In contrast, treatment of the cationic analogue, $[Fe(triphos)(1,4\text{-}C_4F_7)(NCMe)]^+BPh_4^-$ **2-7**, with water caused the disappearance of the carbene resonance in the ^{19}F NMR spectrum (Figure A.26), suggesting an electrophilic carbene. The resonance at -183.9 ppm confirms the release of HF. However, analysis of the remaining resonances did not help with the identification of the product. Under the same conditions, the disappearance of the carbene resonance was also observed by ^{19}F NMR spectroscopy (Figure A.27) for $[Fe(OTf)(triphos)(1,4\text{-}C_4F_7)$, **2-8**. Reaction of $[Fe(terpy')(CO)(1,4\text{-}C_4F_7)]^+OTf^-$, **2-10**, with water led to an unknown hydrolysis product (Figure A.28), which is obviously not the same organic compound, (E)-1,2,3,3,4,4-hexafluoro-1-butene, obtained previously in our group when some perfluorometallacycles were exposed to water.[18] Reaction of pyridine with the cationic carbene-containing complexes gave paramagnetic products that were not characterized further.

3.4 Reactivity with Dihydrogen

When the metallacyclocarbene-containing complex, $FeF(triphos)(1,4\text{-}C_4F_7)$, **2-6**, was put under a dihydrogen atmosphere no reaction was observed. However, hydrofluoroalkane production was observed upon addition of H_2 to its analogues without a fluoride ligand, $[Fe(triphos)(1,4\text{-}C_4F_7)(NCMe)]^+BPh_4^-$, **2-7**, and $Fe(OTf)(triphos)(1,4\text{-}C_4F_7)$, **2-8**. Reactivity towards dihydrogen was also demonstrated with the terpy' carbene-containing complex, $[Fe(terpy')(CO)(1,4\text{-}C_4F_7)]^+OTf^-$, **2-10**, to give a different product than that obtained with the triphos complexes. Moreover, our iron perfluorometallacycles were shown to be unreactive towards dihydrogen gas when put under the same conditions as their carbene equivalents.

3.4.1 HFC-347pcc Production

Addition of dihydrogen to [Fe(triphos)(1,4-C_4F_7)(NCMe)]$^+BPh_4^-$, **2-7**, and Fe(OTf)(triphos)(1,4-C_4F_7), **2-8**, gave exclusively the HFC-347pcc product (Scheme 3.2), confirming Baker *et al.*'s hypothesis of a carbene intermediate for the hydrogenolysis of $Fe(CO)_4$(1,4-C_4F_8), **2-1**.[3] Indeed, our results demonstrated that HFC-347pcc is generated from an iron metallacyclocarbene intermediate.

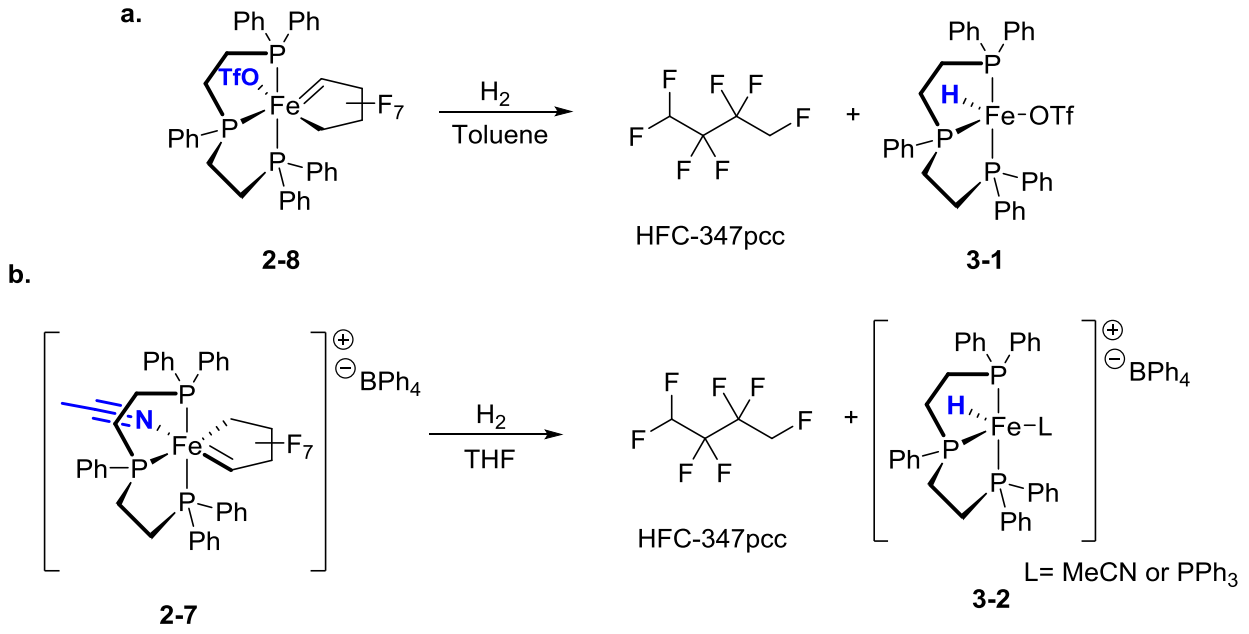

Scheme 3.2. Synthesis of HFC-347pcc from (a) Fe(OTf)(triphos)(1,4-C_4F_7), **2-8** (b) [Fe(triphos)(1,4-C_4F_7)(NCMe)]$^+BPh_4^-$, **2-7**.

The organic product formed was characterized by ^{19}F and $^{19}F\{^1H\}$ NMR spectra (Figure 3.1 and A.29). Typically, CH_2F and CF_2H groups adjacent to a CF_2 moiety display signals between -235 and -244 ppm and -134 and -144 ppm, respectively. Resonances of CF_2 groups usually are in the range of -105 to -132 ppm.[19] These data are consistent with the signals assigned to HFC-347pcc (Figure 3.1); the resonance at -242.1 ppm for the CH_2F coupled to two protons ($^2J_{FH}$ = 44.5 Hz), and the doublet at -137.3 ppm for CF_2H coupled to one proton ($^2J_{FH}$ =

52 Hz). The singlet at -125.3 ppm, revealed as a doublet of triplets ($^{3}J_{FF}$ = 15.5 Hz and 7.5 Hz) in the $^{19}F\{^{1}H\}$ NMR spectrum, is assigned to the CF_2 group next to the CH_2F moiety. Lastly, the multiplet at -132.8 ppm is assigned to the CF_2 beside the CF_2H fragment. The gaseous nature of the product was further confirmed by drying the sample and recording a ^{19}F NMR spectrum to confirm the absence of resonances due to HFC-347pcc.

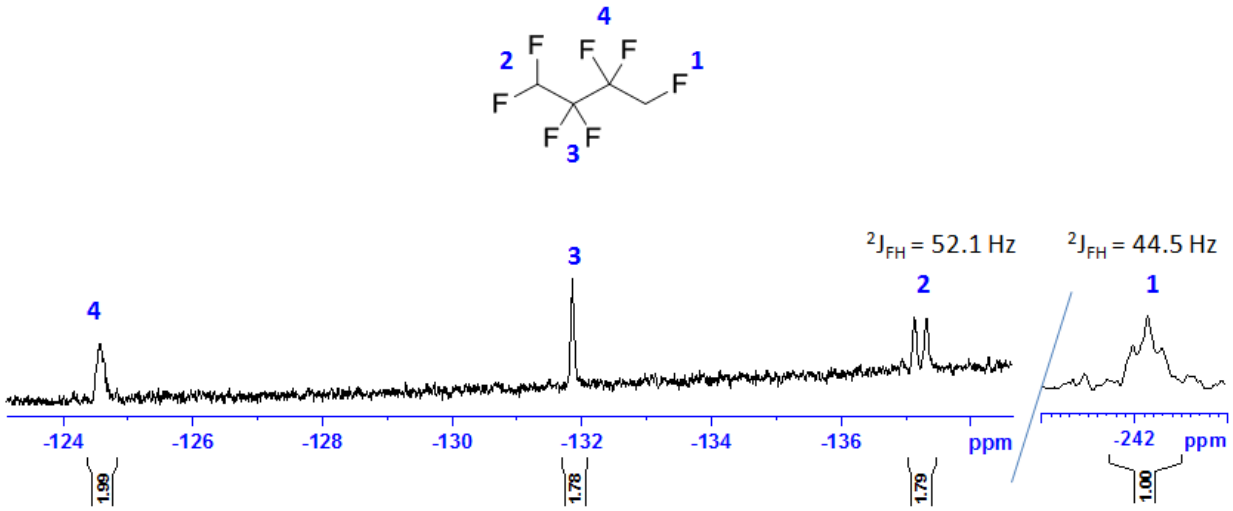

Figure 3.1. ^{19}F NMR spectrum of HFC-347pcc.

Interestingly, Fe(triphos)(1,4-C_4F_7)OTf, **2-8**, led to a significantly faster conversion than [Fe(triphos)(1,4-C_4F_7)(NCMe)]$^{+}BPh_4^{-}$, **2-7**, probably due to the lability of the triflate group, more easily creating an empty coordination site to form the dihydrogen complex. While presumed iron hydride formed after the release of the hydrofluoroalkane chain, FeH(triphos)(OTf), **3-1**, was not sufficiently stable for characterization, the structure of more stable [FeH(triphos)(NCMe)]$^{+}BPh_4^{-}$, **3-2**, was confirmed by NMR spectroscopy. Indeed, the hydride gave rise to a doublet at -22.2 ppm ($^{2}J_{HP}$ = 52 Hz) in the ^{1}H NMR spectrum (Figure A.31), and the triphos ligand to a doublet and a triplet ($^{2}J_{PP}$ = 28 Hz) in the $^{31}P\{^{1}H\}$ NMR spectrum (Figure A.30). In hopes of making a more stable and labile complex for future

catalysis, triphenylphosphine (PPh_3) was added to the solution prior to H_2 addition. As expected, the reaction gave HFC-347pcc; however, a mixture of iron hydride complexes, $[FeH(triphos)(NCMe)]^+BPh_4^-$ and $[FeH(triphos)(PPh_3)]^+BPh_4^-$ was detected by ^1H and $^{31}P\{^1H\}$ NMR spectra (Figure A.31 and A.32).

The proposed mechanism for the hydrogenolysis of $[Fe(triphos)(1,4\text{-}C_4F_7)(NCMe)]^+BPh_4^-$, **2-8**, (Scheme 3.3) or $Fe(triphos)(1,4\text{-}C_4F_7)OTf$ **2-7** first starts with the loss of a ligand (OTf or NCMe) to generate a vacant coordination site to allow formation of the dihydrogen intermediate. From there, the dihydrogen intermediate can protonate the α-carbons to form the iron carbene hydride complex. Another H_2 molecule then adds to Fe–H and Fe–C to generate the saturated Fe dihydrogen alkyl complex, which after α-carbon protonation, gives HFC-347pcc and the 16-electron cationic FeH complex.

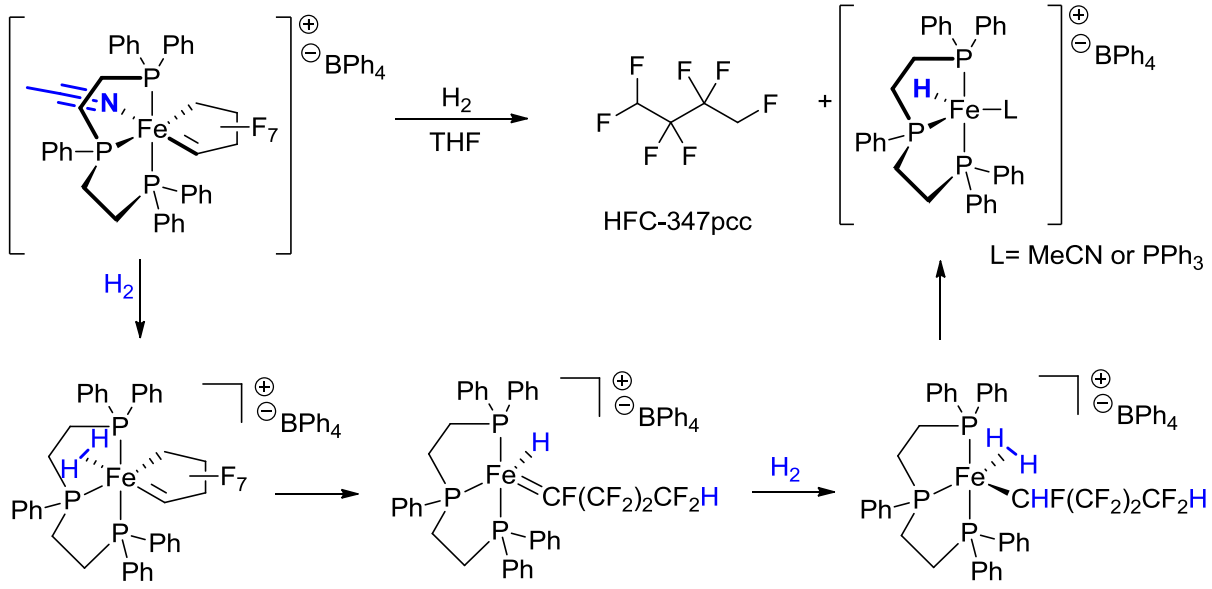

Scheme 3.3. Proposed mechanism for HFC-347pcc formation.

These iron carbene complexes exhibit higher reactivity toward H_2 (room temperature, low pressure), than the original hydrogenolysis of $Fe(CO)_4(1,4\text{-}C_4F_8)$ (500 psig, 100°C), presumably due to the more labile ligands and the more electron-rich iron center.

3.4.1.1 Preliminary Attempts at Catalysis

The proposed catalytic cycle of the hydrogenolysis of iron triphos perfluorometallacycle complex (Scheme 3.4) was targeted, but not accomplished. Ideally, starting with a 16-elctron Fe(0) complex, stabilized with a labile ligand such as PPh_3, would lead to oxidative coupling of TFE to form the metallacycle **(1)**. Next, as demonstrated in the triphos substitution reaction, C_α–F elimination would give the carbene **(2)**. A strong coordinating solvent would displace the fluoride ligand to the outer coordination sphere, allowing different isomers of the dihydrogen cationic complex **(3)**. The αCF_2 would then get protonated to give the carbene hydride complex **(4)**. Another H_2 molecule then adds to Fe–H and Fe–C to generate the saturated Fe dihydrogen alkyl complex **(5)**, which after α-carbon protonation, gives HFC-347pcc and the 16-electron FeH complex **(6)**. In order to restart the cycle, a base would be needed to trap HF, regenerating the initial neutral Fe(0) complex.

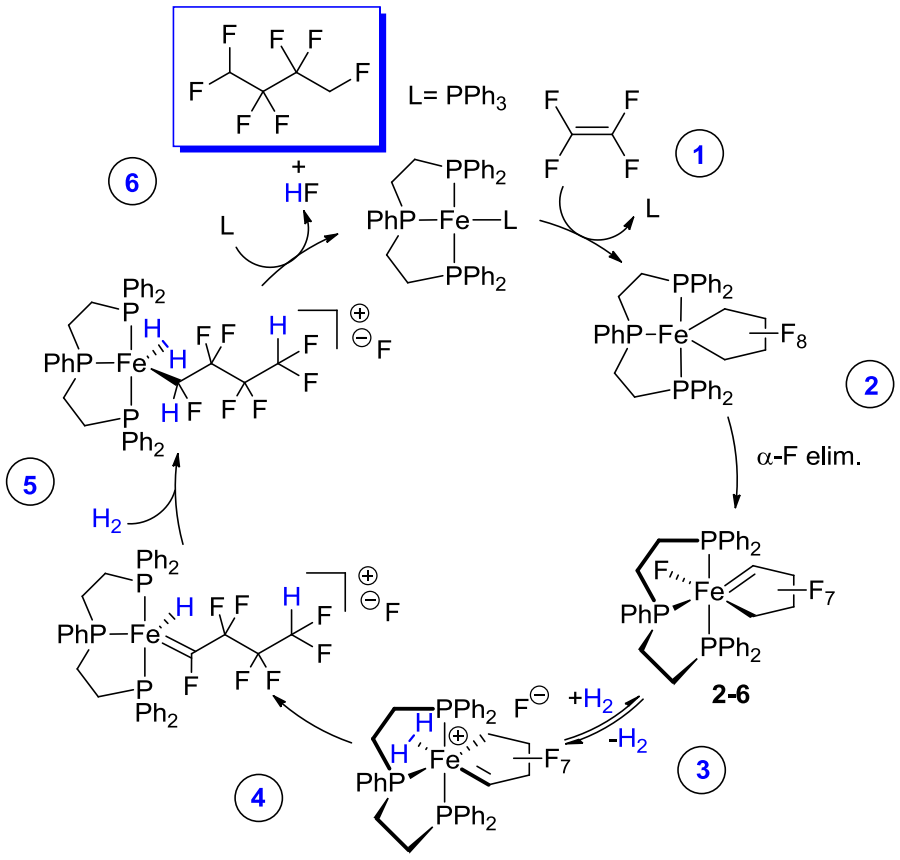

Scheme 3.4. Proposed catalytic cycle for the hydrogenolysis of iron perfluorometallacycle complexes.

Different steps in this proposed catalytic cycle were tested separately. For instance, starting with complex **2-6** and adding H_2 in the presence of a coordinating solvent such as DMF or CH_3CN showed that the fluoride complex remains unreactive towards H_2, and the ligand could not be displaced. Consequently, different bases were added in attempt to trap the fluoride such as CsF, DMAP (4-(Dimethylamino)pyridine) and DBU (1,8-Diazabicyclo[5.4.0]undec-7-ene), leaving a vacant coordination site. Unfortunately, no reaction was observed. Furthermore, addition of TFE to the $[FeH(triphos)(NCMe)]^+BPh_4^-$, $[FeH(triphos)(PPh_3)]^+BPh_4^-$ and FeH(triphos)(OTf) complexes did not result in the formation of metallacycle by insertion into the hydride.

3.4.2 Hydrogenolysis of [Fe(terpy')(CO)(1,4-C_4F_7)]$^+$OTf$^-$, 2-10

In contrast, addition of dihydrogen gas to [Fe(terpy')(CO)(1,4-C_4F_7)]$^+$OTf$^-$, **2-10**, did not release HFC-347pcc or any hydrofluoroalkane according to ^{19}F NMR spectroscopy. After one day, the ^{19}F NMR spectrum displayed three resonances (Figure A.33), related to a non-volatile compound, showing evident formation of a CF_2H group by a doublet at 139.2 ppm with a coupling to proton of 50 Hz. After two days, HF was detected as a doublet with a coupling constant of 446 Hz at -196.2 ppm and a shift in the previous resonances was observed along with a change in the integrations (Figure A.33). Interestingly, when the reaction was performed in THF-d_8 instead of THF, it was signicantly slower and did not form the same product as with THF (Figure A.33); however, HF and DF were formed according to the ^{19}F NMR spectrum, providing evidence for the involvement of the THF solvent. In addition, the IR spectrum confirms the absence of a CO stretching frequency in the final product.

In order to gain more insight into this unusual reaction pathway, the hydrogenation was conducted in acetonitrile. However, no reaction took place in this coordinating solvent; the ^{19}F NMR spectrum remained unchanged (except slight shifts), but the ^{1}H NMR seemed different from the starting material (Figures A.16 and A.17), suggesting coordination of an acetonitrile molecule. This result suggests plugging the open coordination site derived from CO loss prevents the hydrogenolysis reaction to proceed. The high solubility of the final product in benzene is strong evidence of the formation of a neutral species, as opposed to the starting material.

3.5 Attempted Reactions

Further investigation was conducted on the reactivity of some of the iron perfluorometallacycles. FeF(triphos)(1,4-C_4F_7), **2-6**, was treated with different silanes.

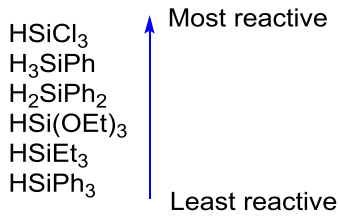

Figure 3.2. Silane reactivity.

Upon addition of the most reactive silane, $HSiCl_3$, a white precipitate instantly appeared; however, no significant change was noticed by NMR spectroscopy. After 4 days, the resonances in the ^{19}F NMR spectrum suggested the formation of unknown new products, but the carbene-F signal was still present. Complex **2-6** was unreactive towards $HSiEt_3$ under different conditions. Treatment with H_2SiPh_2 and H_3SiPh led to a slow reaction, resulting in the disappearance of the carbene-F resonance in the ^{19}F NMR spectrum, but also the appearance of multiple signals which could not be assigned to any product. Its cationic analogue, $[Fe(triphos)(1,4\text{-}C_4F_7)(NCMe)]^+BPh_4^-$, **2-7**, showed some different reactivity towards silanes, but products were still unidentified. The metallacycles that did not contain a carbene were unreactive towards silanes.

Previous studies in our group showed that a cobalt fluorocarbene complex, displaying nucleophilic reactivity, undergoes cyclization with phenylacetylenes.[15] For this reason reactions with acetylenes such as 2-butyne and phenylacetylene were attempted, but no change was observed in the structure according to NMR spectra for complex **2-6**. $[Fe(triphos)(1,4\text{-}C_4F_7)(NCMe)]^+BPh_4^-$, **2-7**, and $[Fe(terpy')(CO)(1,4\text{-}C_4F_7)]^+OTf^-$, **2-8**, were also treated with acetylenes, giving an unidentified mixture of compounds.

Based on published results from our group in which nickel perfluorometallacycle complexes were reacted with Brønsted acids,[6] the new iron perfluorometallacycle complexes

were treated with trifluoroacetic acid and acetic acid. Addition of trifluoroacetic acid to the Ni complex gave HF and a trifluoroacetate-substituted metallacycle whereas reaction with less acidic trimethylbenzoic acid gave primarily the Ni–C^F bond cleavage product. However, similar reactivity with iron was not observed, and when these acids were added to the carbene-containing compounds, no protonation of the carbene was observed.

Lastly, iron perfluorometallacyclocarbene complexes were unreactive toward an electrophilic olefin such as TFE, and when exposed to a more electron-rich olefin such as ethylene; the complexes seemed to decompose and release HF when heated.

3.6 Conclusions

In conclusion, this chapter explored the reactivity of the complexes presented in Chapter 2 by establishing the nature of the carbenes, investigating selective C_α–F bond activation and hydrogenolysis of the metallacycles. The lack of reactivity of Fe(IMes)$(CO)_3$(1,4-C_4F_8), **2-2b**, Fe(dibpe)$(CO)_2$(1,4-C_4F_8), **2-3**, and Fe(κ^2-tripod)$(CO)_2$(1,4-C_4F_8), **2-4**, towards Lewis acids revealed that C_α–F bond activation in these iron metallaycles only occurs when there is enough π-backbonding into the αC–F anti-bonding orbital, as π-acceptor phosphines and carbonyl ligands can compete for the metal back-bonding. Indeed, C_α–F abstraction is only observed with Fe(terpy')(CO)(1,4-C_4F_8), **2-9**, due to the poor acceptor ability of the nitrogen ligand. On the other hand, the lack of electron density on the metal center can cause the Fe center to act as an internal Lewis acid, promoting C_α–F migration as observed *in situ* during the substitution reaction of the linear triphos to afford FeF(triphos)(1,4-C_4F_7), **2-6**. α-F elimination seems to be a characteristic reaction of less electron-rich metals as it was not observed in d^8 [Ni] perfluorometallacycles.[6] **2-6** exhibited no sensitivity to moisture, suggesting a nucleophilic carbene, while the Fe(OTf)(triphos)(1,4-C_4F_7), **2-8**, [Fe(terpy')(CO)(1,4-C_4F_7)]$^+$OTf$^-$, **2-10**, and

[Fe(triphos)(1,4-C_4F_7)(NCMe)]$^+BPh_4^-$, **2-7**, complexes displayed electrophilic carbene character. Furthermore, addition of H_2 to complex **2-7** and **2-8** gave HCF-347pcc, confirming the hypothesis that this hydrofluoroalkane was generated from an Fe carbene intermediate. Hydrogenolysis of **2-1** required high pressures and temperatures, whereas the combination of a stronger donor and a labile ligand such as OTf or CH_3CN in complex **2-7** or **2-8**, allowed for facile hydrogenolysis at room temperature and low pressures. Iron perfluorometallacycle complexes (**2-2**, **2-3**, **2-4**, **2-6**, **2-9**) were unreactive towards H_2 under the same conditions. In contrast, [Fe(terpy')(CO)(1,4-C_4F_7)]$^+OTf^-$, **2-10**, reacted with H_2 to yield an unidentified iron complex and HF, showing that the nature of the ancillary ligand influences the reactivity.

3.7 Experimental Section

3.7.1 General Considerations

Experiments were conducted under nitrogen, using Schlenk techniques or an MBraun glove box. All solvents were deoxygenated by purging with nitrogen. Toluene, hexanes, diethyl ether and tetrahydrofuran (THF) were dried on columns of activated alumina using a J. C. Meyer solvent purification system. Benzene-d_6 (C_6D_6) was dried by stirring over activated alumina (ca. 10 wt.%) overnight, followed by filtration. Acetonitrile (CH_3CN), acetonitrile-d_3 (CD_3CN), and dichloromethane (DCM) were dried by refluxing over calcium hydride under nitrogen. After distillation, they were dried further by stirring over activated alumina (ca. 5 wt.%) overnight, followed by filtration. All solvents were stored over activated (heated at ca. 250^{o}C for >10 h under vacuum) 4 Å molecular sieves. Glassware was oven-dried at 150^{o}C for >2 h. The following chemicals were obtained commercially, as indicated: dihydrogen gas (H_2, Linde, grade 5.5), trimethylsilyl trifluoromethanesulfonate (Me_3SiOTf, Aldrich, 99%), all Fe complexes were prepared according to Chapter 2, and. ^1H, ^{19}F, $^{31}P\{^1H\}$ and $^{13}C\{^1H\}$ NMR spectra were recorded

on a 300 MHz Bruker Avance instrument at room-temperature (21-23^{o}C). ^{1}H NMR spectra were referenced to the residual proton peaks associated with the deuterated solvents (C_6D_6: 7.16 ppm; CD_3CN: 1.94 ppm). $^{31}P\{^{1}H\}$ NMR data were referenced to external H_3PO_4 (85 % aqueous solution), set to 0.0 ppm.

3.7.2 Synthesis and Characterization

Hydrogenolysis of Fe(triphos) perfluorometallacyclocarbenes with H_2. In a typical reaction 10 mg of the iron complex was dissolved in ca. 0.5 ml of THF in an NMR tube fitted with a septum cap. Excess H_2 gas was added via a 3 ml syringe through the septum cap of the NMR tube. The NMR spectra were then recorded after a colour change was observed. Resonances for HFC-347pcc: ^{19}F NMR (282 MHz, THF) δ -242.1 (t, 1F, $^{2}J_{FH}$ = 45.5 Hz, CH_2F), -137.3 (d, 2F, $^{2}J_{FH}$ = 45.5 Hz, CF_2H), -132 (s, 2F, CF_2), -124.6 (s, 2F, CF_2). $^{19}F\{^{1}H\}$ NMR (282 MHz, THF) δ -244.5 (s, 1F, CH_2F), -139.2 (s, 2F, CF_2H), -132.8 (m, $^{3}J_{FF}$ = 5.8 Hz, CF_2), -125.3 (dt, 2F, $^{3}J_{FF}$ = 15.5 Hz and 7.5 Hz, CF_2).

[Fe(triphos)(1,4-C_4F_7)(NCMe)]$^{+}$$BPh_4^{-}$ + H_2. The reaction colour changed from dark brown to a lighter brown overnight. The [FeH(triphos)(NCMe)]BPh_4 complex was characterized by NMR spectroscopy techniques. $^{31}P\{^{1}H\}$ (121 MHz, THF) δ 89.2 (d, 2P $^{2}J_{PP}$ = 28 Hz, Fe–P), 131.8 (t, 1P, $^{2}J_{PP}$ = 28 Hz, Fe–P). ^{1}H (300 MHz, THF) δ -22.2 (quartet, 1H, $^{2}J_{HP}$ = 52 Hz, Fe–H).

[Fe(triphos)(1,4-C_4F_7)(NCMe)]$^{+}$$BPh_4^{-}$ + PPh_3 + H_2. The reaction colour changed from dark brown to a lighter brown overnight. A mixture of iron hydride complexes was formed: [FeH(triphos)(PPh_3)]BPh_4 and [FeH(triphos)(NCMe)]BPh_4, and characterized by NMR spectroscopy techniques. Resonances of [FeH(triphos)(NCMe)]BPh_4 were identified above.

$^{31}P\{^{1}H\}$ (121 MHz, THF) δ 59.6 (m, 1P, Fe–PPh_3), 74.8 (t, 2P, $^{2}J_{PP}$ = 35 Hz, Fe–P), 130.6 (dt, 1P, $^{2}J_{PP}$ = 81 Hz and 31 Hz, Fe–P), ^{1}H (300 MHz, THF) δ -21.6 (m, 1H, Fe–H).

Fe(OTf)(triphos)(1,4-C_4F_7) + H_2. The colour changed from orange to yellow instantly, leaving a brown precipitated. The volatile product was characterized by NMR spectroscopy techniques (see above). The FeH(OTf)(triphos) complex formed could not be characterized due to its low stability.

Reaction of [Fe(terpy')(CO)(1,4-C_4F_7)]$^{+}$OTf^{-} + H_2. [Fe(terpy')(CO)(1,4-C_4F_7)]$^{+}$OTf^{-} (10 mg, 0.01 mmol) was dissolved in ca. 0.5 ml of THF in an NMR tube fitted with a septum cap. Excess H_2 gas was added via a 3 ml syringe through the septum cap of the NMR tube. The reaction colour changed from red/brown to purple over 24 hours. The reaction mixture was characterized by NMR spectroscopy. ^{19}F NMR (282 MHz, THF) δ -196.2 (d, 1F, J_{HF} = 446 Hz, HF), -139.2 (d, 2F, $^{2}J_{FH}$ = 49 Hz, CF_2H), -125.5 (s, 1F), -112.9 (s, 2F), -79.1 (br m). $^{19}F\{^{1}H\}$ NMR (282 MHz, THF) δ -196.1 (s, 1F, HF), -139.2 (s, 2F, CF_2H), -125.5 (s, 1F), -112.9 (s, 2F), -79.1 (br m). ^{19}F NMR (282 MHz, THF-d_8) δ -196.5 (d, 1F, J_{HF} = 446 Hz, HF), -198.6 (t, J_{DF} = 76 Hz, DF), -121.1 (s), -113.0 (s), -77.0 (s). *Warning: Hydrofluoric acid (HF) is highly corrosive and hazardous to handle. Consult MSDS sheet before use and obtain the proper first aid kit containing tubes of 2.5% calcium gluconate.*

3.8 References

(1) Chambers, R. D. 2nd ed.; Fluorine in Organic Chemistry, Blackwell: Oxford, **2004**.

(2) Kitazume, T. *J. Fluor. Chem.* **2000**, *105* (2), 265–278.

(3) Baker, R. T.; Beatty, P. R.; Farnham, B. W.; Wallace, L. R. US patent 5,545,769, **1996**.

(4) Baker, R. T.; Beatty, R. P.; Farnham, W. B.; Robert, D.; Wallace, L. US patent *5670,679*, **1997.**

(5) Gasafi-Martin, W.; Oberendfellner, G.; Werner, K. Von. *Can. J. Chem.* **1996**, *74* (11), 1922–1924.

(6) Andrella, N. O.; Sicard, A. J.; Gorelsky, S. I.; Korobkov, I.; Baker, R. T. *Chem. Sci.* **2015**, *6* (11), 6392–6397.

(7) Giffin, K. A.; Korobkov, I.; Baker, R. T. *Dalton Trans.* **2015**, *44* (45), 19587–19596.

(8) Reger, D. L.; Dukes, M. D. *J. Organomet. Chem.* **1978**, *153* (1), 67–72.

(9) Ohashi, M.; Shibata, M.; Ogoshi, S. *Angew. Chem. Int. Ed.* **2014**, *53* (49), 13578–13582.

(10) Harrison, D. J.; Lee, G. M.; Leclerc, M. C.; Korobkov, I.; Baker, R. T. *J. Am. Chem. Soc.* **2013**, *135* (49), 18296–18299.

(11) Brothers, P. J.; Roper, W. R. *Chem. Rev.* **1988**, *88* (7), 1293–1326.

(12) Harrison, D. J.; Gorelsky, S. I.; Lee, G. M.; Korobkov, I.; Baker, R. T. *Organometallics* **2013**, *32* (1), 12–15.

(13) Giffin, K. A.; Pua, L. A.; Piotrkowski, S.; Gabidullin, B. M.; Korobkov, I.; Hughes, R. P.; Baker, R. T. *J. Am. Chem. Soc.* **2017**, *139* (11), 4075–4086.

(14) Xu, W.; Sun, H.; Xiong, Z.; Li, X. *Organometallics* **2013**, *32* (23), 7122–7132.

(15) Lee, G. M.; Leung, A. S. C.; Harrison, D. J.; Korobkov, I.; Hughes, R. P.; Baker, R. T. *Organometallics* **2017**, *36* (15), 2853–2860.

(16) Burch, R. R.; Calabrese, J. C.; Ittel, S. D. *Organometallics* **1988**, *7* (7), 1642–1648.

(17) Campen, A. K.; Mahmoud, K. A.; Rest, A. J.; Willis, P. A. *J. Chem. Soc. Dalt. Trans.* **1990**, No. 9, 2817–2823.

(18) Giffin, K. A.; Harrison, D. J.; Korobkov, I.; Baker, R. T. *Organometallics* **2013**, *32* (24), 7424–7430.

(19) Burdon, J.; Ezmirly, S. T.; Huckerby, T. N. *J. Fluor. Chem.* **1988**, *40*, 283–318.

Chapter 4

Reactivity of Cobalt Carbonyl Hydride Complexes with Tetrafluoroethylene

4.1 Introduction

In Chapters 2 and 3, we expanded the known chemistry of d^6 fluorometallacycles in our study of Fe(II) complexes derived from zerovalent precursors. Parallel to the iron perfluorometallacycle project, attempts at studying Co(III) perfluorometallacycles were made as they have not been extensively studied since the preparation of $CpCo(CO)(1,4\text{-}C_4F_8)$ by Stone in 1961 (Scheme 4.1).[1]

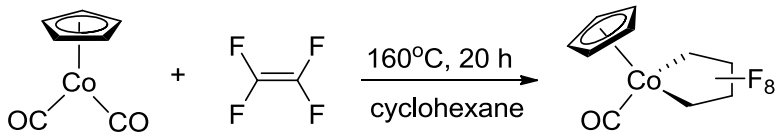

Scheme 4.1. Synthesis of $CpCoCO(1,4\text{-}C_4F_8)$.

A series of known (η^3-cyclooctenyl)Co(I) complexes (Figure 4.1) were initially synthesized[2] from the 1,5-cyclooctadiene complex for reactivity studies with TFE. These compounds were selected due to electron density provided from the phosphine ligands, which can encourage the coordination of an electrophilic olefin like TFE, and their ability to form labile adducts with olefins such as ethylene. However, these cobalt complexes were unreactive towards VDF, and did not form the desired metallacycle when exposed to TFE.

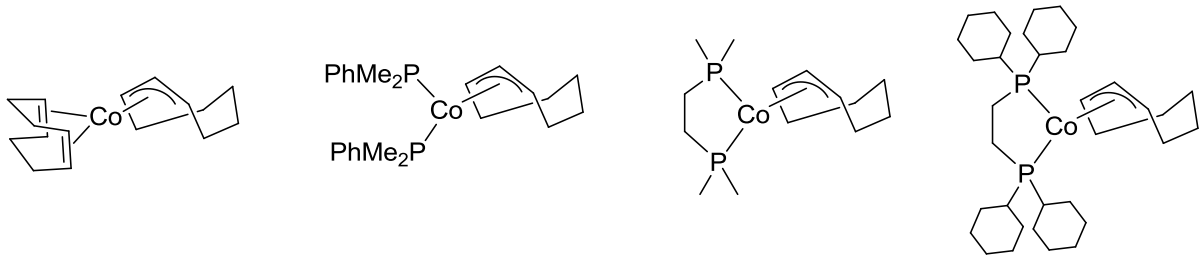

Figure 4.1. Selected (η^3-cyclooctenyl)Co(I) complexes synthesized.

Tetrahedral Co(I) complexes, $CoCl(PPh_3)_3$ and $CoI(PPh_3)_3$, were next prepared following a known procedure,[3] but also did not effect oxidative coupling of TFE. Even changing the PPh_3 ligand for the more electron donating $P(^nPr)_3$ group did not result in the desired reactivity. In contrast, addition of TFE to the zerovalent $Co(PMe_3)_4$ complex displaced PMe_3, forming a mixture of the diamagnetic olefin and metallacycle complexes (likely by electron transfer to a 'sacrificial' TFE) as evidenced by ^{19}F and ^{31}P NMR spectroscopy (Figure 4.35, A.36); however, yields were poor and further analysis was not pursued.

Instead our focus shifted towards the reactivity of zinc tetracarbonylcobaltate (Scheme 4.2) reported previously by our group.[4] The latter was treated with MeI in solvent to give solid ZnI_2 precipitate and the known methylcobalt(I) complex, $CoMe(CO)_4$. The latter complex did not react with TFE and attempts at substituting the carbonyl groups for different phosphine ligands, to make the metal center more electron-rich were unsuccessful

$$Co_2(CO)_8 + \text{excess Zn} \longrightarrow Zn[Co(CO)_4]_2$$

Scheme 4.2. Synthesis of zinc tetracarbonylcobaltate.

4.2 Synthesis of Cobalt Carbonyl Hydride Complexes

Our attention then shifted towards cobalt carbonyl hydride complexes. As described in Chapter 3, the reactivity of the iron hydride formed after HFC-347pcc formation could not be studied either due to its lack of stability or its lack of reactivity towards TFE. For this reason, we investigated the reactivity of cobalt carbonyl hydrides towards fluoroolefins since Co(I) is more prone to react with electrophilic olefins than Fe(II) due to the former's more electron-rich metal center.

The cobalt hydride complex was prepared following a modified literature procedure,[5] using zinc tetracarbonylcobaltate and dried acid (H_3PO_4, *p*-toluenesulfonic acid or $HBF_4 \cdot Et_2O$) as precursors. The parent cobalt carbonyl hydride, $CoH(CO)_4$ decomposes rapidly in the liquid phase (Scheme 4.3), and must be prepared and kept at low temperatures (-78°C). In contrast to the methyl complex, however, the Co–H complex underwent facile ligand substitution.

$$2\ HCo(CO)_4 \longrightarrow H_2 + [Co(CO)_4]_2$$

$$2\ [Co(CO)_4]_2 \rightleftharpoons [Co(CO)_3]_4 + 4\ CO$$

Scheme 4.3. Decomposition of $CoH(CO)_4$.

4.2.1 Synthesis of Substituted Cobalt Carbonyl Hydride Complexes

Dicarbonylbis(triphenylphosphine)cobalt hydride $[CoH(CO)_2(PPh_3)_2]$ has previously been prepared from the reaction of $CoH(CO)_4$ with PPh_3 to give a mixture of the mono- and disubstituted cobalt carbonyl hydride complexes. Recrystallization of the final product confirmed the structure of both trigonal bipyramidal (TBP) and square-pyramidal (SP) geometries for the disubstituted complex (Scheme 4.4).[6] Authors of this publication noted the establishment of rapid equilibrium in solution between various TBP and SP geometries by NMR spectroscopy.

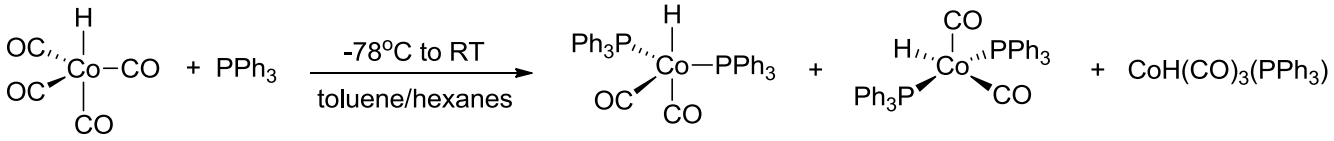

Scheme 4.4. Reaction of $CoH(CO)_4$ with PPh_3.

Complexes of the type HML_4 (M = Co, Rh, Ir) have received much attention due to their role as catalysts in the hydroformylation reaction. A number of researchers have investigated the use of chelating diphosphine ligands in attempts to control the geometry of HML_4 complexes. Crystal structures of Ir and Rh complexes showed that in the solid state they adopt distorted TBP geometries, and that SP geometries are disfavored due to steric interactions of the chelated phosphine ligands.[6]

In order to form a stable cobalt hydride complex, CO ligands can be substituted by other ancillary ligands such as phosphines by addition to the cold reaction mixture. The substitution reaction starts once the flask is allowed to warm to room temperature (Scheme 4.5).

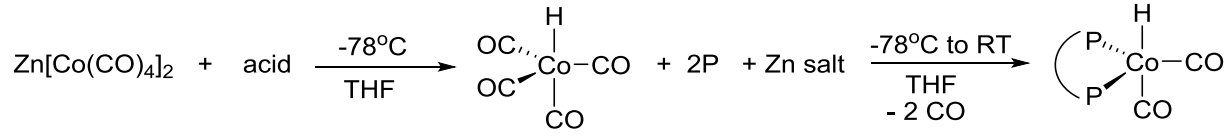

acid = H_3PO_4, $HBF_4{\cdot}Et_2O$, *p*-toluenesulfonic acid

Scheme 4.5. Synthesis of phosphine-substituted complexes cobalt carbonyl hydride.

Alternative procedures involve starting with the phosphine-substituted cobaltate salt, followed by the hydride formation.[7] However, this method was not convenient is our case due to our desire to try a number of different substitutions.

Substitution of CO groups in $CoH(CO)_4$ was attempted with a variety of mono-, bi-and tridentate phosphine ligands (Scheme 4.6). Reaction with 1,1,1-tris(diphenylphosphinomethyl)ethane (tripod) gave the 18-electron cobalt(I) complex, $CoH(\kappa^2$-tripod$)(CO)_2$, **4-1**. The hydride was confirmed by its characteristic shift in the ^{1}H NMR spectrum (Figure A.38) at -12.1 ppm. In the $^{31}P\{^1H\}$ NMR spectrum (Figure A.37), the two equivalent coordinated phosphines were assigned to a singlet at 34 ppm, and the uncoordinated arm gave rise to a singlet in the free phosphine region at -30 ppm. The free phosphine arm did not coordinate to the metal center upon UV irradiation.

Using the bidentate phosphine ligand, 1,2-bis(diphenylphosphino)ethane (dppe), gave the tricarbonyl Co(I) hydride, $Co(H)(dppe)(CO)_2$, **4-2**, confirmed by a triplet ($^2J_{HP}$ = 8 Hz) in the hydride region at -10.7 ppm in the ^{1}H NMR spectrum (Figure A.42), suggesting a hydride *cis* to two Ps. Although the $^{31}P\{^1H\}$ NMR spectrum (Figure A.43) indicated a mixture of products, extraction of the reaction residue into diethyl ether gave isolated **4-2** which gave rise to a singlet at 80.6 ppm. A more electron-rich bidentate ligand, 1,2-bis(dicyclopentylphosphino)ethane (dcppe), was also added to $CoH(CO)_4$ to yield **4-3**, an analogue of the dppe complex (Figures A.46 and A.47).

Lastly, one CO ligand was substituted by a monodentate ligand. Addition of tricyclopentylphosphine (Pcp_3) gave the monosubstituted Co(I) hydride complex $CoH(Pcp_3)(CO)_3$, **4-4**, featuring H *trans* to P, as evidenced by the doublet at -10.8 ppm in the ^{1}H NMR spectrum (Figure A.50) with a large coupling to P of 32.5 Hz. Similar results were obtained with the triisobutylphosphine (P^iBu_3) ligand based on the NMR spectra of **4-5** (Figure A.54 and A.54). In both structures, the phosphine ligand was assigned to a broad singlet in the $^{31}P\{^1H\}$ NMR spectra (Figure A.51 and A.55).

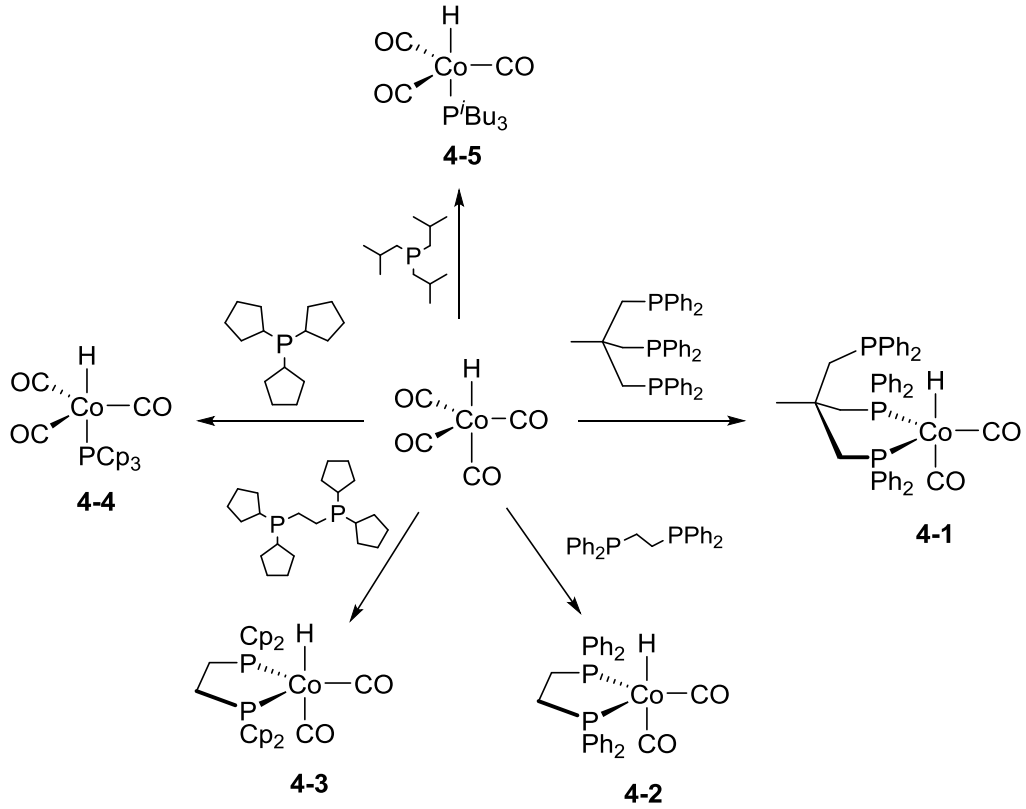

* Reaction conditions: -78^{o}C to RT, 2 h in THF

Scheme 4.6. Substitution reactions on $CoH(CO)_4$.

In contrast, substitution reactions with phenanthroline (phen), linear triphos, and IMes were unsuccessful (Scheme 4.7). Indeed, addition of phen to $CoH(CO)_4$ resulted in a complex that did not contain Co–H, whereas the IMes substituted product resulted in decomposition upon drying. Similarly to tripod, the third arm of the linear triphos did not initially coordinate to the metal center; however no hydride was detected by ^{1}H NMR spectroscopy. It was possible, however, to coordinate the third arm of this ligand by UV irradiation.

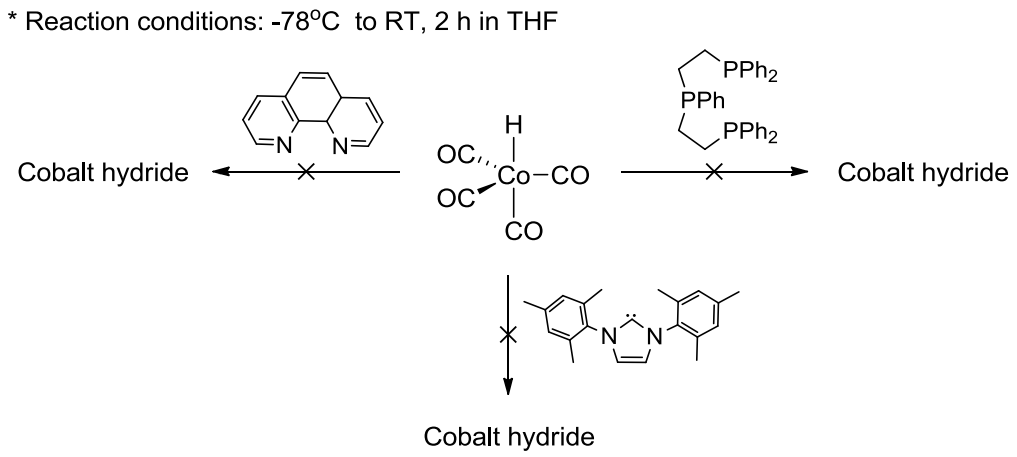

Scheme 4.7. Unsuccessful substitution reactions on $CoH(CO)_4$.

4.3 Reactivity with Fluoroolefins

The different phosphine-substituted cobalt(I) carbonyl hydride complexes synthesized were reacted with fluoroolefins. The section below discusses the different products formed as well as the effects of the ancillary ligands on the rate of metallacycle formation and product ratios.

4.3.1 Synthesis of Cobalt Hydride Perfluorometallacycle Complexes

Monitoring the addition of TFE to $CoH(\kappa^2\text{-tripod})(CO)_2$, **4-1**, by ^{19}F NMR spectroscopy indicated formation of three different products: the Co-tetrafluoroethyl complex, **4-6**, derived from insertion of TFE into Co-H, hydrogenated TFE (1,1,2,2,-tetrafluoroethane), and an apparent metallacycle hydride complex, **4-7** (Scheme 4.8).

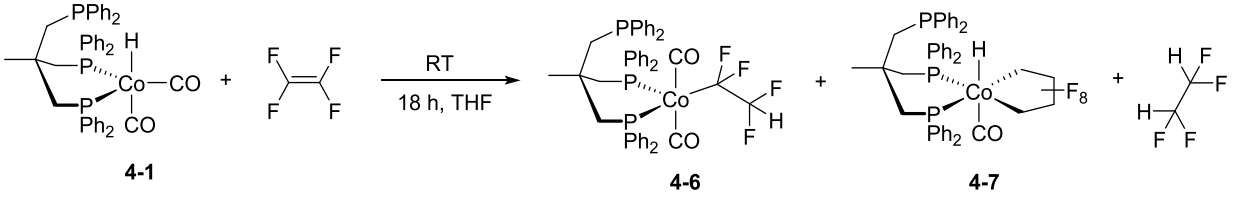

Scheme 4.8. Reaction of $CoH(\kappa^2\text{-tripod})(CO)_2$, **4-1**, with TFE.

The ^{19}F NMR spectrum of insertion product **4-6** (Figure 4.2) contained broad resonances at -65.8 (br s) and -127.4 ppm (br d, $^{2}J_{FH}$ = 52.5 Hz) while the hydrogenated TFE showed a sharp doublet resonance at -139.1 ppm ($^{2}J_{FH}$ = 57 Hz). The ^{19}F NMR spectrum of **4-7** appeared initially as an unsymmetrical metallacyclopentane with four different strongly coupled germinal CF_2 groups ($^{2}J_{FF} \approx 200$ Hz). Indeed, a ^{19}F-^{19}F COSY experiment (Figure A.40) confirmed all the expected correlations for the metallacycle. Interestingly, when a proton-decoupled ^{19}F NMR spectrum was recorded (Figure A.39), the βFs of the metallacycle showed obvious coupling to proton, with less evident coupling for the αFs, suggesting a hydride on the cobalt in a novel Co(III) hydride dialkyl complex. However, the Co–H was not readily observed at RT in the ^{1}H NMR spectrum and data from the MALDI and ESI mass spectra were similarly inclonclusive. Finally, on closer inspection of the crude reaction mixture, a minor fluorometallacycle product was also evident.

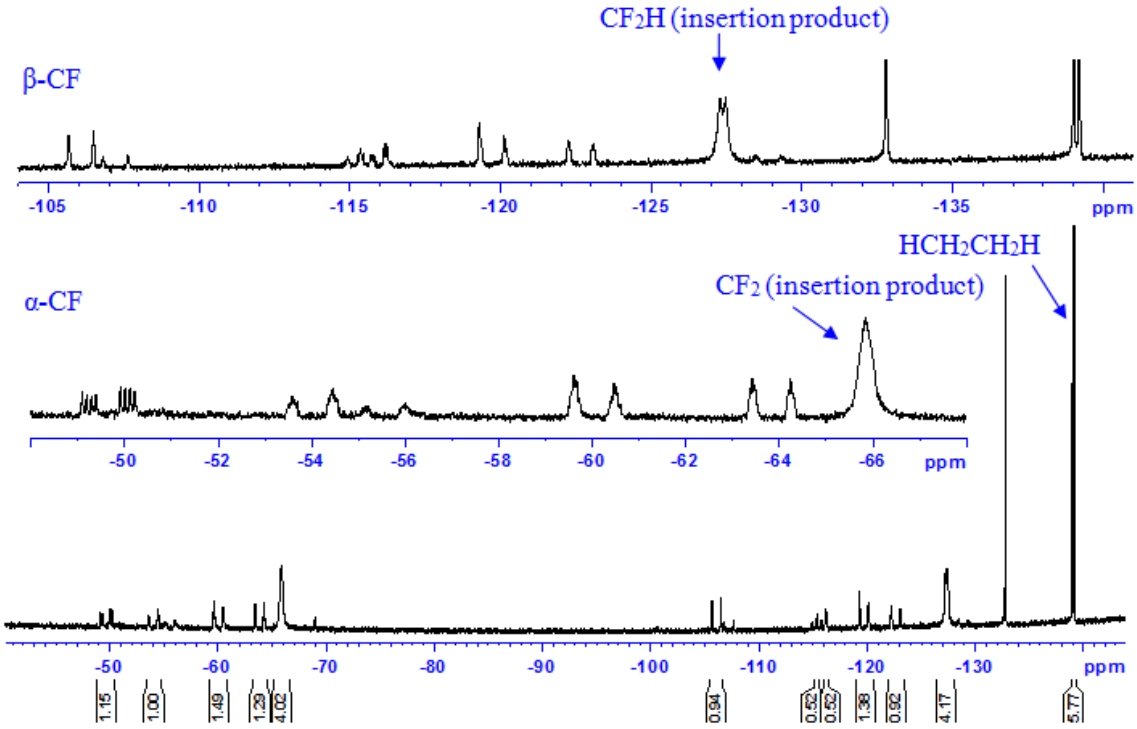

Figure 4.2. ^{19}F NMR spectrum of CoH(κ^{2}-tripod)(CO)(1,4-C_4F_8), **4-7**, after 2 d.

Addition of TFE to $CoH(dppe)(CO)_2$,**4-2**, also gave insertion (**4-8)**, hydrogenation and metallacycle (**4-9**) products (Scheme 4.9); however, the metallacycle now showed only 4 different ^{19}F NMR doublets due to an apparent mirror plane perpendicular to the P_2CoC_2 plane (Figure A.44). The sharper resonances for the insertion product allowed us to identify a triplet at -60.5 ppm due to coupling to the two Ps ($^3J_{FP}$ = 42 Hz).

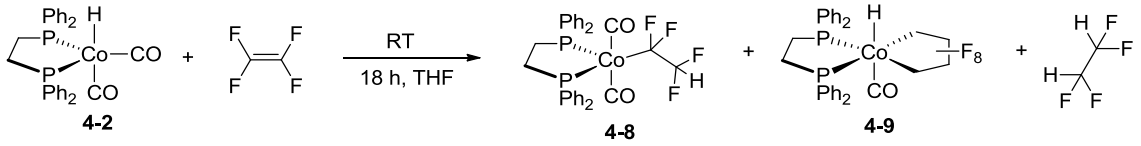

Scheme 4.9. Reaction of $CoH(dppe)(CO)_2$, **4-2**, with TFE

Interestingly, addition of TFE to $CoH(dcppe)(CO)_2$, **4-3**, and $HCo(Pcp_3)(CO)_3$, **4-4**, only gave the insertion products (**4-10**, **4-11**) and hydrogenated TFE (Scheme 4.10) (Figure A.48, A.49, A.52, A.53). The ligand's orientation or bulk could possibly hinder formation of the metallacycle. Furthermore, when the Co(triphos) carbonyl complex with three coordinated phosphines was exposed to TFE, a vinyl ligand with CF_3 groups was apparent by ^{19}F NMR spectroscopy. No further studies were conducted on this reaction.

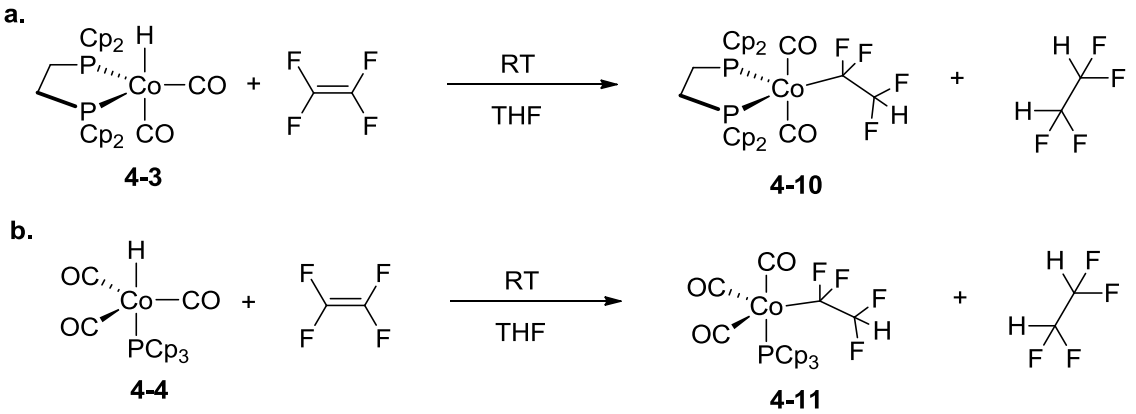

Scheme 4.10. Reaction of TFE with (a) $CoH(dcppe)(CO)_2$, **4-3** (b) $CoH(Pcp_3)(CO)_3$, **4-4**.

Lastly, reaction of $CoH(P^iBu_3)(CO)_3$, **4-5**, with TFE resulted in the cleanest reaction according to the ^{19}F and $^{19}F\{^1H\}$ NMR spectra (Scheme 4.11). Indeed, no additional

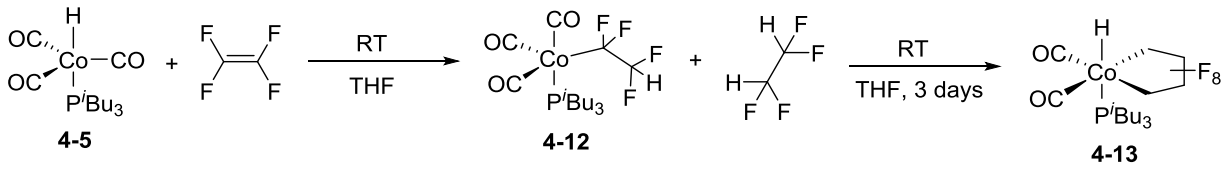

Scheme 4.11. Reaction of $CoH(P^iBu_3)(CO)_2$, **4-5**, with TFE.

metallacycle resonances were detected in the baseline, and well-defined coupling is observed between the geminal and vicinal fluorines for both the insertion product (**4-12**; Figure 4.3) and metallacycle (**4-13**; Figure 4.4). The data for the latter suggest P is *trans* to H because of symmetry on both sides of the metallacycle resulting in four sets of doublet with large geminal coupling constants.

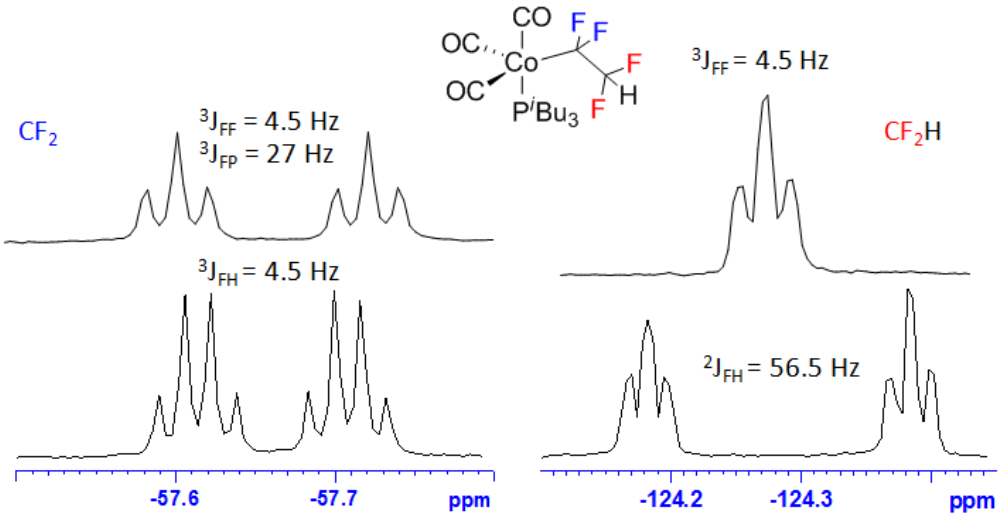

Figure 4.3. Selected insertion product resonances from ^{19}F NMR spectra for $Co(P^iBu_3)(CO)_3(CF_2CF_2H)$, **4-12**, after 7 d. (Bottom spectrum: ^{19}F NMR; top spectrum $^{19}F\{^1H\}$ NMR).

Upon addition of TFE to **4-5** the solution colour turned instantly to red and only the insertion product and hydrogenated TFE were detected by ^{19}F NMR. The insertion product then slowly decreased as the metallacycle resonances grew in over a several week period at ambient temperature.

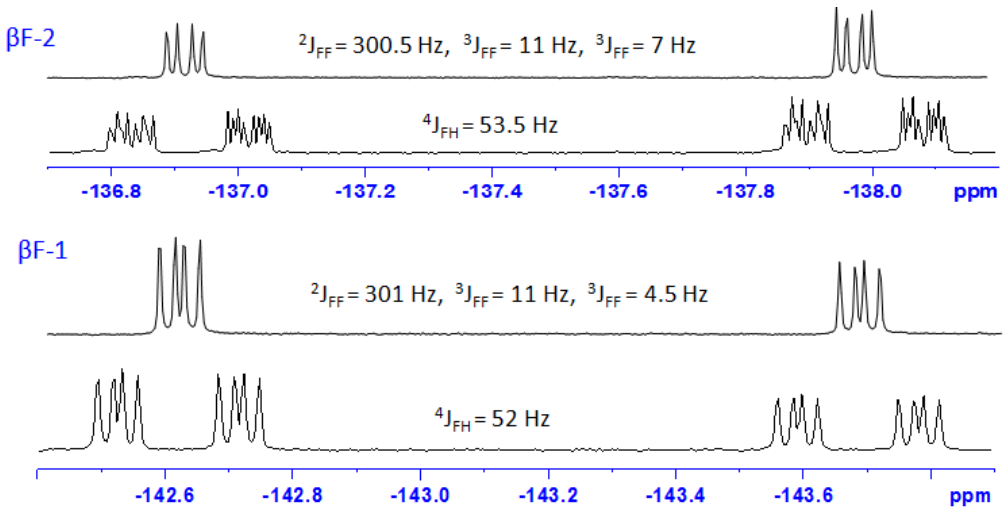

Figure 4.4. Selected metallacycle resonances from ^{19}F NMR spectra for $CoH(P^{i}Bu_3)(CO)_2(1,4\text{-}C_4F_8)$ for βFs, **4-13**. (Bottom spectrum: ^{19}F NMR; top spectrum $^{19}F\{1H\}$ NMR) after 7 d.

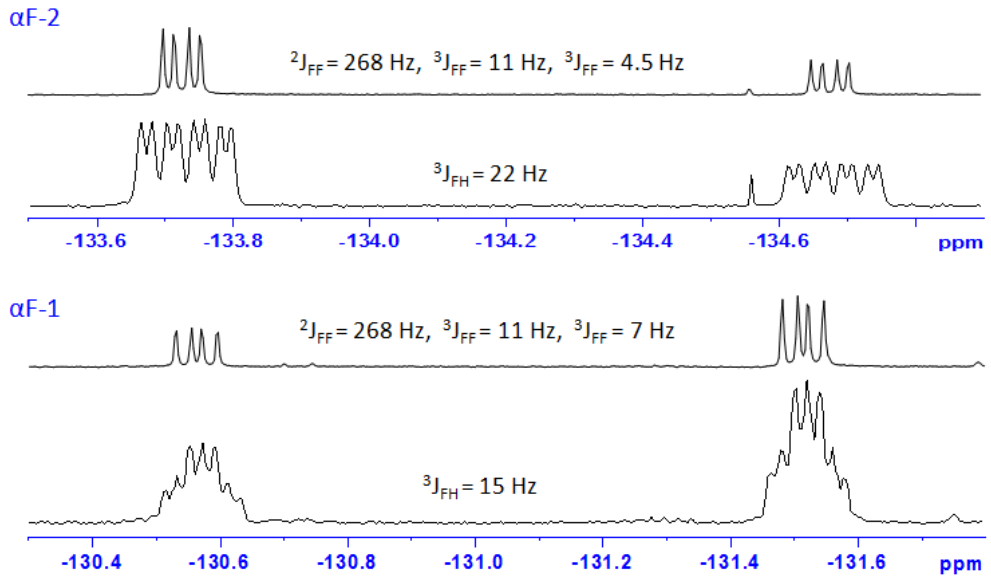

Figure 4.5. Selected metallacycle resonances from ^{19}F NMR spectra for $CoH(P^{i}Bu_3)(CO)_2(1,4\text{-}C_4F_8)$ for αFs, **4-13**. (Bottom spectrum: ^{19}F NMR; top spectrum $^{19}F\{^{1}H\}$ NMR) after 7 d.

The reaction products from **4-5** and TFE were elucidated further from their ^{1}H and ^{31}P NMR spectra. The Co–H resonance of **4-13** was observed as an incompletely resolved multiplet at -21 ppm (Figure A.57). The $^{31}P\{^{1}H\}$ NMR spectrum (Figure 4.6) was consistent with the data from the ^{19}F NMR spectrum, except for a singlet at 51.2 ppm that could not be assigned to any product described above. The triplet at 40.5 ppm ($^{3}J_{PF}$ = 27 Hz) can be attributed to the phosphine ligand of the insertion product **4-12** and the broad resonance at 42.1 ppm is due to the metallacycle product **4-13**. Further investigation demonstrated that the major peak at 51.2 ppm is due to the red zerovalent dimer, $(P^{i}Bu_3)(CO)_3Co–Co(CO)_3(P^{i}Bu_3)$, **4-14**, associated presumably with formation of the TFE hydrogenation product.[5]

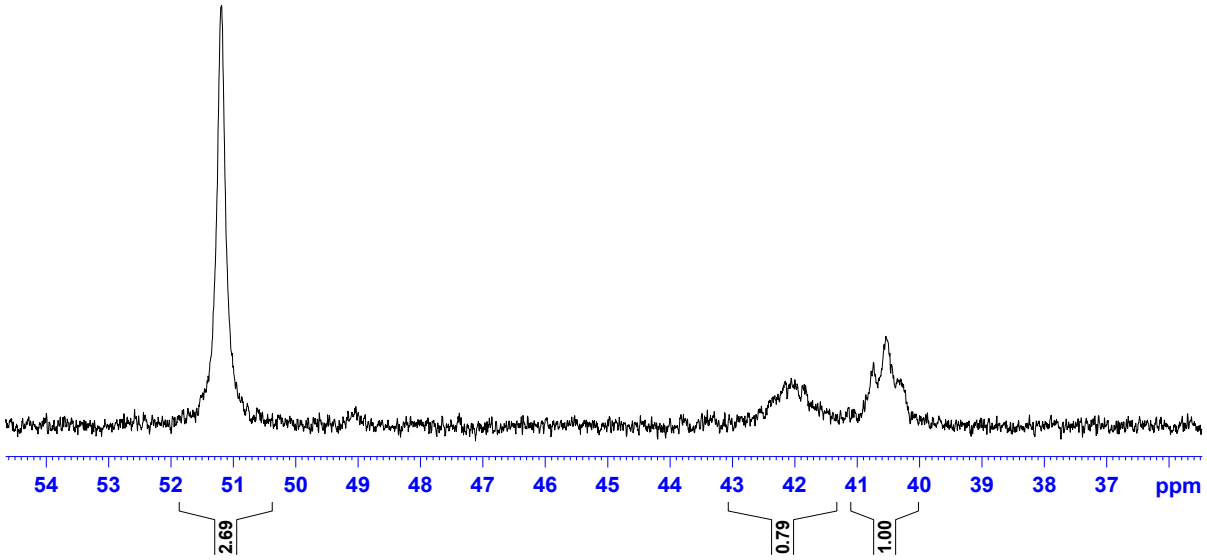

Figure 4.6. $^{31}P\{^{1}H\}$ NMR spectrum of the $CoH(P^{i}Bu_3)(CO)_3$ + TFE reaction after 7 d.

The molecular structure of dimer **4-14** consists of two trigonal bipyramidal Co centers and an unsupported Co-Co bond of 2.6513(3) Å (Figure 4.6).

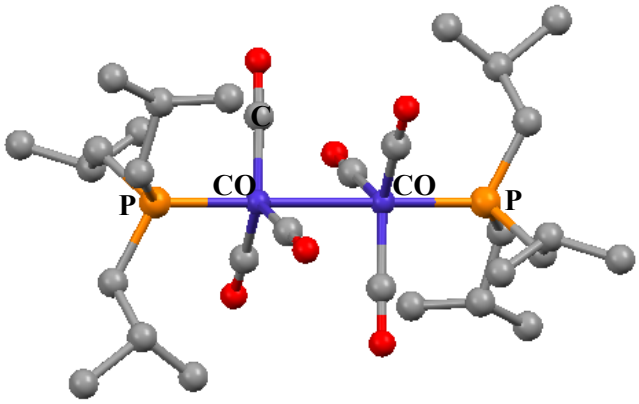

Figure 4.7. ORTEP representation of the molecular structure of $(P^iBu_3)(CO)_3Co–Co(CO)_3(P^iBu_3)$, **4-14**. Thermal ellipsoids are set at the 40% probability level. Hydrogen atoms are omitted for clarity. Selected bond lengths (Å) Co–Co 2.6513(3),Co–P 2.1796(3), Co–C 1.7738(2).

A similar singlet at 70.5 ppm in the $^{31}P\{^1H\}$ NMR spectrum of the $CoH(Pcp_3)(CO)_3$ reaction with TFE, **4-4**, is assigned to the zerovalent dimer, $(Pcp_3)(CO)_3Co–Co(CO)_3(Pcp_3)$. However, the disubstituted cobalt complexes seem to form a different structure of the dimer as the $^{31}P\{^1H\}$ NMR resonances associated to the latter are broad.

4.2.2 Reactions of Cobalt Hydrides with other Fluoroalkenes

The most reactive cobalt dppe hydride complex **4-2** reacted sluggishly with VDF; only small amounts of the hydrofluoroalkane and dimer product were formed after two weeks, and no metallacycle. These same products were also observed for both trifluoroethylene, and trifluoromethyl trifluorovinyl ether; however with the latter an additional product that is neither the insertion product nor the metallacycle was observed. Further analysis will be required for full characterization.

4.2.2 Suggested Mechanism

In order to gain more insight into the mechanism of TFE reactions with cobalt hydrides multiple experiments were conducted. Addition of 0.5 equivalent of TFE to $CoH(\kappa^2$-tripod$)(CO)_2$, **4-2**, gave only hydrogenated TFE and insertion product; metallacycle resonances were barely noticeable in the ^{19}F NMR after all TFE was consumed. This suggests the need for a second equivalent of fluoroolefin to react with the insertion product to form the metallacycle. When the reaction was performed in acetonitrile instead of THF, no major metallacycle species was observed, only $H(CF_2)_2H$ and $Co(CF_2CF_2H)(\kappa^2$-tripod$)(CO)_2$, **4-6**, suggesting the need for an open coordination site. Addition of TFE to $(P^iBu_3)(CO)_3Co–Co(CO)_3(P^iBu_3)$ did not show any reaction.

The mechanism below is proposed based on the data collected, using $CoH(P^iBu_3)(CO)_3$, **4-5**, as an example. Our hypothesis involves initial loss of CO ligand to generate a vacant site, forming a 16e- complex which can coordinate the fluoroolefin. Then, the olefin inserts into the Co–H bond, forming the 16e- insertion intermediate $Co(CF_2CF_2H)(P^iBu_3)(CO)_2$, **A**. From there the reaction can take two different routes; reaction of **A** with the liberated CO gives the 18e- insertion product or reaction of **A** with a second equivalent of Co–H affords hydrogenated TFE and the dimer $(P^iBu_3)(CO)_3Co–Co(CO)_3(P^iBu_3)$. Finally, loss of CO from the 18e- insertion product and reaction with a second equivalent of TFE yields, after deinsertion and oxidative coupling to yield the perfluorocobaltacyle hydride complex (Scheme 4.12).

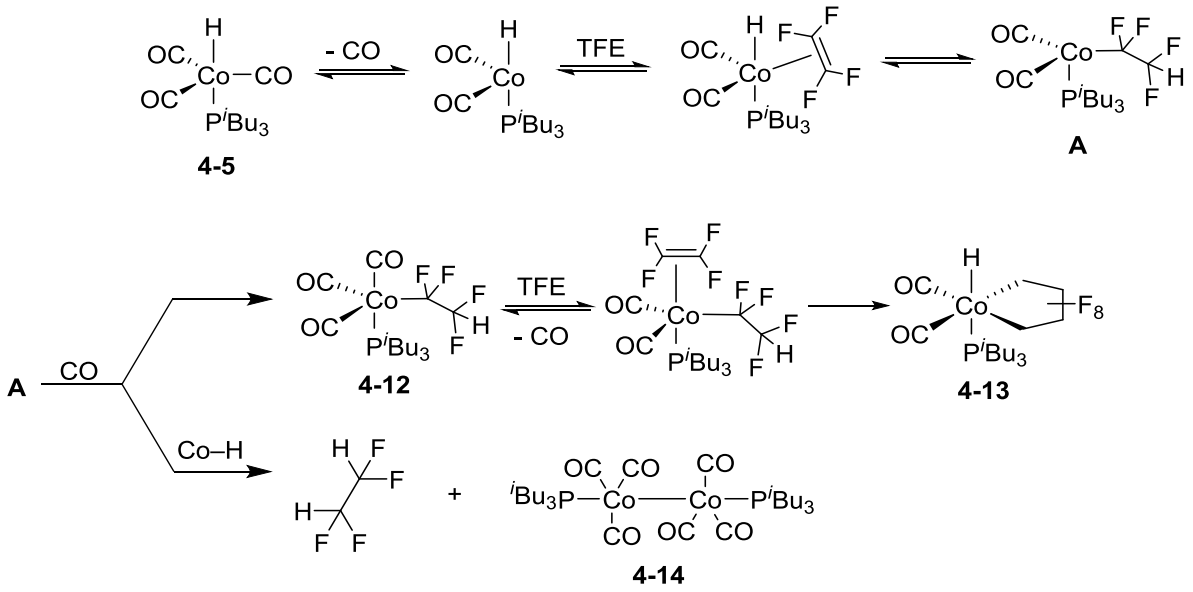

Scheme 4.12. Proposed mechanism for TFE reactions with cobalt hydride complexes.

4.3 Preliminary Reactivity Studies

In order to study the selective activation of the C_α–F bond on cobalt perfluorometallacycles, these compounds were treated with TMS-OTf. After a few hours, the ^{19}F NMR spectrum showed a resonance for TMS-F and OTf only, meaning either all fluorines were abstracted or the final product is paramagnetic. UV irradiation of the $CoH(P^iBu_3)(CO)_3$ and TFE reaction resulted in the slow disappearance of the insertion product resonances in the ^{19}F NMR spectrum, and in the production of hydrogenated TFE. Metallacycle photolysis was attempted to induce reductive elimination and form the fluoroalkyl chain. Further analysis will be needed.

4.4 Conclusions

In conclusion, a series of five stable Co(I) hydride complexes exhibited a range of reactivity with TFE. With the bulkiest ligands, $CoH(dcppe)(CO)_2$, **4-3**, and $CoH(Pcp_3)(CO)_3$, **4-4**, a mixture of the insertion product and the zerovalent dimer/hydrogenated TFE products was obtained in a ratio of 2:1 and 1:2, respectively. With the slightly less bulky P^iBu_3 ligand the ratio

was 4:3 and the insertion product eventually reacted further with TFE to give the cobalt hydride metallacycle **4-13**, although the reaction was incomplete after several weeks. In contrast, with the dppe and tripod cobalt carbonyl hydrides, metallacycle product formation was evident at short reaction times with insertion/hydrogenation ratios of 1:1 and 1:1. These results suggest that the most electron-rich ligands prevented metallacycle formation or slowed it down most likely due to strong π-backbonding into the CO ligands, making it harder to generate an open coordination site. On the other hand, less electron-rich, steric bulky ligands prevented the bimolecular Co dimer formation, but left enough room for binding a second equivalent of TFE for metallacycle formation. Also as all reactions were conducted in a closed system to contain the TFE gas, reversible CO coordination likely inhibits metallacycle formation from the insertion product. While preliminary experiments show promotion of this reaction by light, side reactions also become evident presumably from CO loss from the metallacycle product. Further experiments at specific wavelengths may prove fruitful here.

4.5 Experimental Section

4.5.1 General Considerations

Experiments were conducted under nitrogen, using Schlenk techniques or an MBraun glove box. All solvents were deoxygenated by purging with nitrogen. Toluene, hexanes, diethyl ether and tetrahydrofuran (THF) were dried on columns of activated alumina using a J. C. Meyer solvent purification system. Benzene-d_6 (C_6D_6) was dried by stirring over activated alumina (ca. 10 wt.%) overnight, followed by filtration. Acetonitrile (CH_3CN), acetonitrile-d_3 (CD_3CN), and dichloromethane (DCM) were dried by refluxing over calcium hydride under nitrogen. After distillation, they were dried further by stirring over activated alumina (ca. 5 wt.%) overnight,

followed by filtration. All solvents were stored over activated (heated at ca. 250°C for >10 h under vacuum) 4 Å molecular sieves. Glassware was oven-dried at 150°C for >2 h. The following chemicals were obtained commercially, as indicated: dicobalt octacarbonyl ($(Co)_2(CO)_8$, Aldrich, 90%), phosphoric acid (H_3PO_4, Aldrich, 99.99%), bis(2-diphenylphosphinoethyl)phenylphosphine (Triphos, Strem, 97%), tetrafluoroboric acid diethyl ether complex ($HBF_4{\cdot}Et_2O$, Aldrich), *p*-toluenesulfonic acid monohydrate (Aldrich, 99%), 1,1,1-tris(diphenylphosphinomethyl)ethane (tripod, Strem, 97%), 1,2-bis(diphenylphosphino)ethane (dppe, Aldrich, 99%), tricyclopentylphosphine (Pcp_3, Cytec-Solvay), triisobutylphosphine (P^iBu_3, Cytec-Solvay). $Zn[Co(CO)_4]_2$ was synthesized following a known procedure.[4] Tetrafluoroethylene was made by pyrolysis of polytetrafluoroethylene (Scientific Polymer Products, powdered) under vacuum, using a slightly modified literature procedure [10-20 mTorr, 650°C, 15 g scale, product stabilized with R(+)-limonene (Aldrich, 97%), giving TFE of *ca.* 97% purity].[8] H_3PO_4 was dried in vacuo over 2 hours. *p*-Toluenesulfonic acid monohydrate was dried by a toluene reflux overnight. ^1H, ^{19}F, $^{31}P\{^1H\}$ and $^{13}C\{^1H\}$ NMR spectra were recorded on a 300 MHz Bruker Avance instrument at room-temperature (21-23°C). ^1H NMR spectra were referenced to the residual proton peaks associated with the deuterated solvents (C_6D_6: 7.16 ppm; CD_3CN: 1.94 ppm). ^1H NMR spectra werereferenced to the residual proton peaks associated with the deuterated solvents (C_6D_6: 7.16 ppm; CD_3CN: 1.94 ppm; $CDCl_3$: 7.26 ppm; CD_2Cl_2: 5.32 ppm). $^{31}P\{^1H\}$ NMR data were referenced to external H_3PO_4 (85 % aqueous solution), set to 0.0 ppm. Irradiation was perfomred using a Reptile UV lamp, high UVB mercury vapor flood lamp, UVB output 150μW/cm^2 at 4ft. Electrospray ionization mass spectral data were collected using an Applied Biosystem API2000 triple quadrupole mass spectrometer. MALDI spectra were recorded on Bruker UltrafleXtreme MALDI-TOF/TOF mass spectrometer interfaced to a

glovebox. X-ray crystallography samples were mounted on thin glass fibers using paraffin oil. Data were collected on a Bruker AXS KAPPA single crystal diffractometer equipped with a sealed Mo tube source (wavelength 0.71073Å) APEX II CCD detector. Raw data collection and processing were performed with APEX II software package from BRUKER AXS.

4.5.2 Synthesis and Characterization

Synthesis of CoH(tripod)$(CO)_2$, 4-1. In a glove box, a 100 ml round-bottomed Schlenk flask was charged with $Zn[Co(CO)_4]_2$ (200 mg, 0.49 mmol) dissolved in THF (ca. 15 ml), affording a slightly green solution, and sealed with a septum cap. Dried H_3PO_4 (96.6 mg, 0.99 mmol) and 1,1,1-tris(diphenylphosphinomethyl)ethane (616 mg, 0.99 mmol) were dissolved in THF (ca. 4 ml) separately, and transferred to separate 10 ml syringes. On a Schlenk line the flask was put under a N_2 flow and cooled at -78^{o}C using an acetone/dry ice bath. The acid was then injected slowly over 20 minutes. The homogeneous green solution became a heterogeneous yellow mixture. After stirring for 20 minutes, the tripodal phosphine ligand solution was injected. The solution was stirred at low temperature for 10 minutes and then warmed to room temperature and stirred for an additional 2 hours, over which time a gradual colour change to bright yellow was observed. The resulting mixture was filtered through a glass frit to remove the zinc salt and the filtrate dried in vacuo to give a fluffy yellow powder. Yield: 464 mg, 60.7%. $^{31}P\{^1H\}$ (121 MHz, C_6D_6) δ -30.0 (s, 1P, free arm), -28.6 (br s, 3P, free ligand), 34.0 (s, 2P, Fe–P). ^1H (300 MHz, THF) δ -12.1 (br s, 1H, Co–H).

Synthesis of CoH(dppe)$(CO)_2$, 4-2. This complex was prepared as for **4-1** using 200 mg of $Zn[Co(CO)_4]_2$ (0.49 mmol) in 15 mL of THF and 96 mg of dried H_3PO_4 (0.99 mmol) and 394 mg of 1,2-bis(diphenylphosphino)ethane (0.99 mmol) each dissolved in 4 mL of THF. On warming to room temperature a gradual colour change to bright orange was observed. After 2

hours stirring, filtration and solvent removal the product was extracted into ether, dried and isolated as an orange powder. Yield: 278 mg, 51.2%. $^{31}P\{^{1}H\}$ (121 MHz, ether) δ 80.6 (s, 2P, Fe–P), ^{1}H (300 MHz, ether) δ -12.1 (t, 1H, $^{2}J_{HP}$ = 8 Hz, Co–H).

Synthesis of CoH(dcppe)(CO)$_2$, **4-3**. This complex was prepared as for **4-1** using 200 mg of $Zn[Co(CO)_4]_2$ (0.49 mmol) in 15 mL of THF and 97 mg of dried H_3PO_4 (0.99 mmol) and 362.8 mg of 1,2-bis(dicyclopentylphosphino)ethane (0.99 mmol) each dissolved in 4 mL of THF. . On warming to room temperature a gradual colour change to bright yellow was observed. After 2 hours stirring, filtration and solvent removal the product was isolated as a yellow oil. Yield: 296.4 mg, 58.2%. $^{31}P\{^{1}H\}$ (121 MHz, THF) δ 102.8 (br s, 2P, Fe–P), ^{1}H (300 MHz, THF) δ -11.1 (br s, 1H, Co–H).

Synthesis of CoH(Pcp$_3$)(CO)$_3$, **4-4**. This complex was prepared as for **4-1** using 200 mg of $Zn[Co(CO)_4]_2$ (0.49 mmol) in 15 mL of THF and 96 mg of dried H_3PO_4 (0.99 mmol) and 382.5 mg of tricyclopentylphosphine (0.99 mmol) each dissolved in 4 mL of THF. On warming to room temperature a gradual colour change to yellow was observed. After 2 hours stirring, filtration and solvent removal the product was isolated as an orange oil. Yield: 271.4 mg, 71.6% $^{31}P\{^{1}H\}$ (121 MHz, ether) δ 65.6 (br s, 1P, Fe–P), ^{1}H (300 MHz, Et_2O) δ -10.8 (d, 1H, $^{2}J_{HP}$ = 32.5 Hz, Co–H).

Synthesis of CoH(P^{i}Bu$_3$)(CO)$_3$, **4-5**. This complex was prepared as for **4-1** using 200 mg of $Zn[Co(CO)_4]_2$ (0.49 mmol) in 15 mL of THF and 96 mg of dried H_3PO_4 (0.99 mmol) and 0.35 mL of triisobutylphosphine (0.99 mmol) each dissolved in 4 mL of THF. On warming to room temperature a gradual colour change to yellow was observed. After 2 hours stirring, filtration and solvent removal the product was isolated as a red oil. Yield: 208.9 mg, 61.3%. $^{31}P\{^{1}H\}$ (121

MHz, THF) 40.1 ppm (br s, 1P, Fe–P), ^{1}H (300 MHz, THF) δ -10.6 (d, 1H, $^{2}J_{HP}$ = 48 Hz, Co–H).

Reactions of cobalt carbonyl hydrides with TFE. In a typical reaction 15 mg of the Co-H complex was dissolved in 0.5 mL of THF in an NMR tube fitted with a septum cap and TFE was added via a 3 ml syringe through the septum cap. The NMR spectra were then recorded over days to weeks.

CoH(tripod)(CO)$_2$ + TFE. The reaction mixture changed from yellow to orange overnight. NMR data after 2 d: ^{19}F NMR (282 MHz, THF) δ -139.1 (d, 4F, $^{2}J_{FH}$ = 57 Hz, H(C*F*$_2$)$_2$H), -127.4 (br d, 2F, $^{2}J_{FH}$ = 52 Hz, Co-CF$_2$C*F*$_2$H), -122.7 (br dt, 1F, $^{2}J_{FF}$ = 231 Hz, J_{FH} = 16.5 Hz, C$_\beta$F), -119.7 (br d, 1F, $^{2}J_{FF}$ = 234 Hz, C$_\beta$F), -115.7 (ddd, 1F, J_{FH} = 26 Hz, $^{3}J_{FF}$ = 6 Hz, $^{2}J_{FF}$ = 236.7 Hz, C$_\beta$F), -106.2 (dt, 1F, J_{FH} = 9.5 Hz, $^{2}J_{FF}$ = 233 Hz, C$_\beta$F), -65.8 (br s, 2F, Fe–CF$_2$), -63.8 (br d,1F, $^{2}J_{FF}$ = 232 Hz, C$_\alpha$F), -60.1 (br d, $^{2}J_{FF}$ = 246 Hz, C$_\alpha$F), -53.9 (br d, 1F, $^{2}J_{FF}$ = 245 Hz, C$_\alpha$F), -49.9 (ddd, 1F, $^{2}J_{FF}$ = 231.5 Hz, $^{3}J_{FF}$ = 28 Hz, $^{3}J_{FF}$ = 56.5 Hz, C$_\alpha$F). ^{19}F{^{1}H} NMR (282 MHz, THF) δ -139.1 (s, 4F, H(C*F*$_2$)$_2$H), -127.4 (br s, 2F, Co-CF$_2$C*F*$_2$H), -122.7 (br d, 1F, $^{2}J_{FF}$ = 231 Hz, C$_\beta$F), -119.7 (br d, 1F, $^{2}J_{FF}$ = 234 Hz, C$_\beta$F), -115.7 (dd, 1F, $^{3}J_{FF}$ = 15.5 Hz, $^{2}J_{FF}$ = 237 Hz, C$_\beta$F), -106.2 (d, 1F, $^{2}J_{FF}$ = 233 Hz, C$_\beta$F), -65.8 (br s, 2F, Co-C*F*$_2$CF$_2$H), -63.8 (br d, 1F, $^{2}J_{FF}$ = 232 Hz, C$_\alpha$F), -60.1 (br d, $^{2}J_{FF}$ = 246 Hz, C$_\alpha$F), -53.9 (br d, 1F, $^{2}J_{FF}$ = 245 Hz, C$_\alpha$F), -49.9 (ddd, 1F, $^{2}J_{FF}$ = 231.5 Hz, $^{3}J_{FF}$ = 28 Hz, $^{3}J_{FF}$ = 56.5 Hz, C$_\alpha$F). ^{31}P{^{1}H} NMR (121 MHz, THF) -27.6 (s, 1P, free arm), 37.2 (s, 2P, Co–P), 23.8 (s, 2P, Co dimer?), 14.5 (s, 1P, Co–P).

CoH(dppe)(CO)$_2$ + TFE. The reaction colour changed from yellow to orange overnight. NMR data after 2 d: ^{19}F NMR (282 MHz, Et$_2$O) δ -137.9 (d, 4F, $^{2}J_{FH}$ = 55.5 Hz, H(C*F*$_2$)$_2$H), -125.7 (d, 2F, $^{2}J_{FH}$ = 58 Hz, Co-CF$_2$C*F*$_2$H), -120.58 (d, 2F, $^{2}J_{FF}$ = 237.5 Hz, C$_\beta$F), -114.1 (d, 2F,

$^{2}J_{FF}$ = 237.5 Hz, $C_{\beta}F$), -60.5 (t, 2F, $^{3}J_{FP}$ = 41.76 Hz, Co–C*F*$_2$CF$_2$H), -59.6 (d, 2F, $^{2}J_{FF}$ = 243 Hz, $C_{\alpha}F$), -52.9 (d, 2F, $^{3}J_{FF}$ = 240 Hz, $C_{\alpha}F$). $^{19}F\{^{1}H\}$ NMR (282 MHz, Et_2O) δ -137.9 (s, 4F, H(C*F*$_2$)$_2$H), -125.7 (s, 2F, Co-CF$_2$C*F*$_2$H), -120.58 (d, 2F, $^{2}J_{FF}$ = 237.5 Hz, $C_{\beta}F$), -114.1 (dd, 2F, $^{2}J_{FF}$ = 237.5 Hz, $^{3}J_{FF}$ = 16.5 Hz, $C_{\beta}F$), -60.5 (t, 2F, $^{3}J_{FP}$ = 42 Hz, Co–C*F*$_2$CF$_2$H), -59.6 (d, 2F, $^{2}J_{FF}$ = 243 Hz, $C_{\alpha}F$), -52.9 (dt, 2F, $^{2}J_{FF}$ = 240 Hz, $^{3}J_{FP}$ = 29 Hz, $C_{\alpha}F$). $^{31}P\{^{1}H\}$ NMR (121 MHz, THF) -24.5 (d, 2P, $^{3}J_{PF}$ = 42 Hz, Co–P (insertion product)), 57.8 ppm (br s, 2P, Co–P).

CoH(dcppe)(CO)$_2$ + TFE. The reaction colour changed from yellow to orange overnight. NMR data after 7 d: ^{19}F NMR (282 MHz, THF) δ -139.3 (d, 4F, $^{2}J_{FH}$ = 56 Hz, H(C*F*$_2$)$_2$H), -124.9 (dt, 2F, $^{2}J_{FH}$ = 56 Hz, $^{3}J_{FF}$ = 4.5 Hz, Co–CF$_2$*CF*$_2$H), -59.8 (dq, 2F, $^{3}J_{FF}$ = 4.5 Hz, $^{3}J_{FH}$ = 4.5 Hz, Co–C*F*$_2$CF$_2$H). $^{19}F\{^{1}H\}$ NMR (282 MHz, THF) δ -139.3 (s, 4F, H(C*F*$_2$)$_2$H), -124.9 (t, 2F, $^{3}J_{FF}$ = 4.5 Hz, Co–CF$_2$*CF*$_2$H), -59.8 (dt, 2F, $^{3}J_{FF}$ = 4.5 Hz, Co–C*F*$_2$CF$_2$H). $^{31}P\{^{1}H\}$ NMR (121 MHz, THF) δ 68.7 (br s, 2P, Co–P), 86.1 (s, 4P, Co dimer).

CoH(Pcp$_3$)(CO)$_3$ + TFE. The reaction colour changed from yellow to orange. NMR data after 7 d: ^{19}F NMR (282 MHz, THF) δ -139.1 (d, 4F, $^{2}J_{FH}$ = 56 Hz, H(C*F*$_2$)$_2$H), -124.9 (dt, 2F, $^{2}J_{FH}$ = 56 Hz, $^{3}J_{FF}$ = 4.5 Hz, Co–CF$_2$*CF*$_2$H), -62.9 (t, 2F, $^{3}J_{FF}$ = 4.5 Hz, Co–C*F*$_2$CF$_2$H). $^{19}F\{^{1}H\}$ NMR (282 MHz, THF) δ -139.3 (s, 4F, H(C*F*$_2$)$_2$H), -127.7 (s, 2F, Co–CF$_2$*CF*$_2$H), -62.9 (dt, 2F, $^{3}J_{FP}$ = 2 5Hz, $^{3}J_{FF}$ = 4.5 Hz, Co–C*F*$_2$CF$_2$H). $^{31}P\{^{1}H\}$ NMR (121 MHz, THF) δ 57.5 (t, 2P, JPF = 25 Hz, Co–P insertion product), 70.5 (s, 4P, Co dimer).

CoH(P^{i}Bu$_3$)(CO)$_3$ + TFE. The reaction colour immediately changed to red and to orange over one week. NMR data after 7 d: ^{19}F NMR (282 MHz, THF-d_8) δ -144.9 (dddd, 2F, $^{4}J_{FH}$ = 53.5 Hz, $^{2}J_{FF}$ = 300.5 Hz, $^{3}J_{FF}$ = 11 Hz, $^{3}J_{FF}$ = 7 Hz, $C_{\beta}F$), -139.1 (d, 4F, $^{2}J_{FH}$ = 57 Hz, H(C*F*$_2$)$_2$H), -137.5 (dddd, 2F, $^{4}J_{FH}$ = 52 Hz, $^{2}J_{FF}$ = 301 Hz, $^{3}J_{FF}$ = 11 Hz, $^{3}J_{FF}$ = 4.5 Hz, $C_{\beta}F$), -

134.2 (dddd, 2F, $^{3}J_{FH}$ = 22 Hz, $^{2}J_{FF}$ = 268 Hz, $^{3}J_{FF}$ = 11 Hz, $^{3}J_{FF}$ = 4.5 Hz, $C_{\alpha}F$), (dddd, 2F, $^{3}J_{FH}$ = 15 Hz, $^{2}J_{FF}$ = 268 Hz, $^{3}J_{FF}$ = 11 Hz, $^{3}J_{FF}$ = 7 Hz, $C_{\alpha}F$), -124.3 (dt, 2F, $^{2}J_{FH}$ = 56.5 Hz, $^{3}J_{FF}$ = 4.5 Hz, Co–CF_2CF_2H), -57.6 (dq, 2F, $^{3}J_{FP}$ = 27 Hz, $^{3}J_{FF}$ = 4.5 Hz, $^{3}J_{FH}$ = 4.5 Hz, Co–CF_2CF_2H). $^{19}F\{^{1}H\}$ NMR (282 MHz, THF-d_8) δ -144.9 (ddd, 2F, $^{2}J_{FF}$ = 300.5 Hz, $^{3}J_{FF}$ = 11 Hz, $^{3}J_{FF}$ = 7 Hz, $C_{\beta}F$), -139.1 (d, 4F, $^{2}J_{FH}$ = 57 Hz, $H(CF_2)_2H$), -137.5 (ddd, 2F, $^{2}J_{FF}$ = 301 Hz, $^{3}J_{FF}$ = 11 Hz, $^{3}J_{FF}$ = 4.5 Hz, $C_{\beta}F$), -134.2 (ddd, 2F, $^{2}J_{FF}$ = 268 Hz, $^{3}J_{FF}$ = 11 Hz, $^{3}J_{FF}$ = 4.5 Hz, $C_{\alpha}F$), (ddd, 2F, $^{2}J_{FF}$ = 268 Hz, $^{3}J_{FF}$ = 11 Hz, $^{3}J_{FF}$ = 7 Hz, $C_{\alpha}F$), -124.3 (t, 2F, $^{3}J_{FF}$ = 4.5 Hz, Co–CF_2CF_2H), -57.6 (dt, 2F, $^{3}J_{FP}$ = 27 Hz, $^{3}J_{FF}$ = 4.5 Hz, Co–CF_2CF_2H). $^{31}P\{^{1}H\}$ (121 MHz, THF) 40.6 (t, 1P, $^{3}J_{PF}$ = 27 Hz, Fe–P insertion product), 42.1 (br s, 1P, Fe–P), 51.2 ppm (s, 2P, P–Co–Co–P). ^{1}H NMR (300 MHz, THF) δ -21.0 (m, 1H, Co–H).

4.6 References

(1) Coyle, T. D.; Kings, R. B.; Pitcher, E.; Stafford, S. L.; Teichel, P.; Stone, F. G. A. *J. Inorg. Nucl. Chem.* **1961**, *20* (1–2), 172–173.

(2) Groβheimann, G.; Jolly, P. W. *Inorg. Chim. Acta* **1998**, *270*, 60–67.

(3) Nobile, C. F.; Rossi, M.; Sacco, A. *Inorg. Chim. Acta* **1971**, *5*, 698–700.

(4) Harrison, D. J.; Daniels, A. L.; Korobkov, I.; Baker, R. T. *Organometallics* **2015**, *34* (18), 4598–4604.

(5) Sternberg, H. W.; Wender, I.; Friedel, R. A.; Orchin, M. *J. Am. Chem. Soc.* **1953**, *75* (11), 2717–2720.

(6) Zhao, D.; Brammer, L. *Inorg. Chem.* **1994**, *33* (25), 5897–5902.

(7) Moore, E. J.; Sullivan, J. M.; Norton, J. R. *J. Am. Chem. Soc.* **1986**, *108* (9), 2257–2263.

(8) Hunadi, R. J.; Baum, K. *Synthesis.* **1982**, *39*, 454.

Chapter 5

Conclusions and Future Outlook

This work explored further the reactivity of d^6 perfluorometallacycle complexes. Early work from Baker *et al*. showed that hydrogenolysis of $Fe(CO)_4(1,4\text{-}C_4F_8)$ under harsh conditions generates a variety of C_4 hydrofluorocarbons depending on different additives, showing a decrease of selectivity compared to Ni perfluorometallacycle complexes that afford exclusively $H(CF_2)_4H$. Increased conversion and decreased selectivity by the inclusion of more hydrogens on the terminal carbons were demonstrated in the presence of PPh_3, suggesting that phosphines stabilize an Fe carbene intermediate, leading to more C_α-F bond activations. In order to gain a deeper understanding of this process, Chapter 2 focused on the synthesis and characterization of a series of new NHC-, phosphine- and nitrogen-ligand-substituted Fe(II) perfluorometallacycles derived from the first one ever reported, $Fe(CO)_4(1,4\text{-}C_4F_8)$, **2-1**. This led to the discovery of the first examples of fluorinated metallacyclocarbenes. The *in situ* αF-migration to Fe during the substitution reaction using the linear triphos ligand is a rare example of metallacycle C_α–F bond activation without external additives. While Grushin and co-workers reported conversion of a (PNP)Rh–CF_3 complex to (PNP)Rh=CF_2(F),[1] C_α–F bond activation in perfluorometallacyclopentanes is usually induced by Lewis acids.[2,3,4,5] In contrast, reactions of low-valent Ni precursors with CH_2=CF_2 afford alkenyl complexes derived from β-F elimination[6] and similar reactions with CHF=CF_2 afford unsaturated hydrofluorocarbons derived from both C_α–F and C_β–F bond activation.[7] Although we did not investigate bulky phosphite ligands, it appears that some degree of π-acidity is required for substitution of the last CO ligand, as

evidenced by the stronger back-bonding in [Fe(terpy')CO(1,4-C_4F_8)] (ν_{CO} = 1960 cm^{-1}) vs. the triphos analog (ν_{CO} = 1990 cm^{-1}).

The reactivity of our new Fe(II) perfluorometallacycle complexes was further investigated in Chapter 3 initially by treatment with Lewis acids to study the selective activation of the C_α–F bonds. The lack of reactivity of the mono- and di-substituted Fe carbonyl perfluorometallacycles with Lewis acids and H_2 confirmed that C_α–F bond activation requires substantial back-bonding into the C_α–F anti-bonding orbital, which is difficult to achieve in the presence of multiple π -acceptors. Indeed, despite the presence of a CO ligand on Fe(terpy')(CO)(1,4-C_4F_8), the pure-donor nitrogen ligands allowed for C_α–F bond activation by Lewis acids, affording a cationic Fe carbene complex by fluoride abstraction. Furthermore, investigations into the nature of these newly formed perfluorometallacyclocarbenes suggest that the Fe=C bond in FeF(triphos)(1,4-C_4F_7) exhibits nucleophilic characteristics, whereas its cationic analogue [Fe(CNMe)(triphos)(1,4-C_4F_7)]BPh_4, Fe(OTf)(triphos)(1,4-C_4F_7), and nitrogen-substituted [Fe(terpy')(CO)(1,4-C_4F_7)]OTf all display electrophilic Fe=C reactivity. Interestingly, hydrogenolysis of [Fe(CNMe)(triphos)(1,4-C_4F_8)]BPh_4 and Fe(OTf)(triphos)(1,4-C_4F_8) under mild conditions gave exclusively $H(CF_2)_3CFH_2$ (HFC-347pcc) and iron hydrides, confirming Baker's previous hypothesis of this HFC being formed through a carbene intermediate. In contrast, reaction of the cationic terpy' Fe carbene complex with H_2 afforded a neutral unidentified Fe complex and HF, showing that the nature of the ancillary ligands greatly influences the reactivity.

Our work on d^6 perfluorometallacycle complexes was further expanded to Co(I) phosphine hydride complexes. A series of five stable phosphine-substituted Co(I) hydride complexes exhibited a range of reactivity with TFE, giving four different products: the Co-

tetrafluoroethyl complex, derived from insertion of TFE into Co–H, hydrogenated TFE (1,1,2,2,-tetrafluoroethane) along with the resulting zerovalent cobalt dimer, and an unusual metallacycle hydride complex. Formation of the TFE hydrogenation product and cobalt dimer is proposed to occur by reaction of the Co–H with the key 16e- $CoL_n(CO)_{3-n}(CF_2CF_2H)$ intermediate, whereas reaction of TFE with the latter gives the desired metallacycle hydride, $CoHL_n(CO)_{3-n}(1,4\text{-}C_4F_8)$. Our observations that the most electron-rich ligands prevented metallacycle formation or slowed it down can likely be attributed to strong π-backbonding into the CO ligands, making it harder to generate an open coordination site. Using less electron-rich, steric bulky ligands to prevent the bimolecular Co dimer formation, however, still needs to leave enough room for binding a second equivalent of TFE for metallacycle formation.

This work has led to multiple insights into the reactivity of d^6 perfluorometallacycles; however, much remains to be understood. Further characterization of $Fe(CO)_3(IMes)(1,4\text{-}C_4F_8)$, using mass spectroscopy, NMR techniques and X-ray diffraction will finally solve the mystery of the two similar isomers formed. Additional studies on the reactivity of these fluorocarbenes with water could lead to the discovery of new hydrolysis products. In keeping with our interest in generating hydrofluoroolefins (HFOs), this project would also benefit from furhter characterization of the $[Fe(terpy')(CO)(1,4\text{-}C_4F_7)]^+OTf^-$ and H_2 reaction product and a DFT study to more fully understand the difference in H_2 reactivity of $[Fe(terpy')(CO)(1,4\text{-}C_4F_8)]OTf$ vs $[Fe(CNMe)(triphos)(1,4\text{-}C_4F_8)]BPh_4$. There is also potential to exploit the reactivity of Fe(triphos) perfluorometallacycle derivatives towards H_2 for the catalytic formation of hydrofluorocarbons. As proposed in Chapter 3 (Scheme 3.4), in order to turn over the cycle a suitable base has to be selected to trap HF as it has been shown that TFE does not react with the iron hydrides formed. A route to the 16e- zerovalent $Fe(P_3)(L)$ complex (L being a labile ligand)

has to be established to enable continuous oxidative coupling of TFE. Preliminary attempts resulted in successful substitution by PPh_3, but deprotonation of the Fe–H bond was unsuccessful. Lastly, in order to get this catalytic cycle to work, we have to be able to displace the fluoride ligand formed via α-F elimination. However, once a new perfluorometallacycle is formed in the catalytic cycle, there are different possibilities for C_α–F bond activations, which could lead to a low selectivity by having multiple substitutions on the chain as demonstrated with the hydrogenolysis of $Fe(CO)_4(1,4\text{-}C_4F_8)$. The hydrogenolysis mechanism of these complexes in a catalytic system is still undetermined and could benefit from computational studies for a better understanding. For instance, lack of selectivity was observed for the hydrogenolysis of $Fe(CO)_4(1,4\text{-}C_4F_8)$, generating two Hs on both sides of the chain, leading us to question the metallacycle protonation mechanism. Many routes are possible (Scheme 5.1); **A** and **B** were explained in this Thesis, however route **C**, based on Hughes C–F bond hydrogenolysis work on iridium complexes,[8] suggests multiple hydrogenations and carbene formation at Cα–F on both sides to give HFC-356qcc.

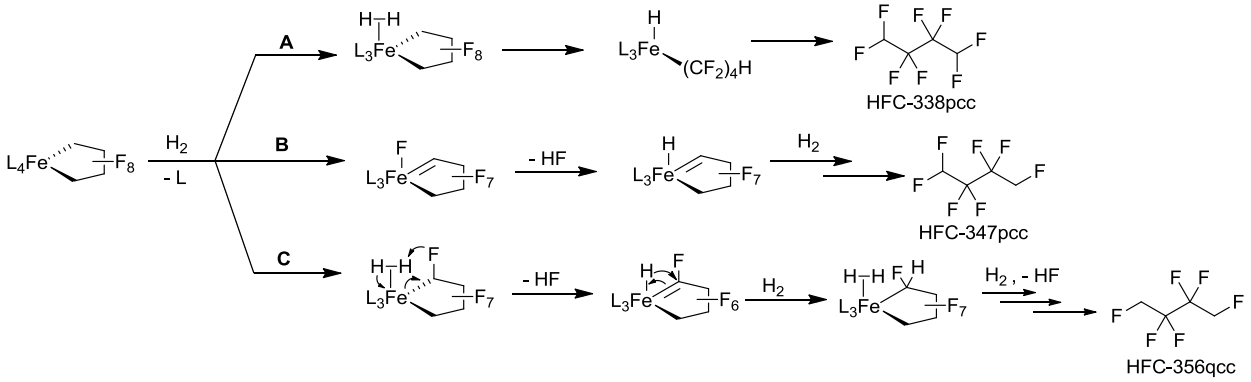

Scheme 5.1. Possible hydrogenolysis routes for Fe(II) perfluorometallacycles.

It would be interesting to expand the reactivity studies of these iron systems to other fluoroolefins such as trifluoroethylene (HTFE) and 1,1-difluoroethylene (VDF). Finally, it would

be important to successfully synthesize the ideal 16e- Fe(0) triphos-containing precursor for the projected catalytic cycle. Furthermore, to encourage TFE oxidative coupling, and stabilize the precursor to close the cycle once the HFC is released, we need a labile ligand which can be PPh_3. The proposed Fe(triphos)(PPh_3) could potentially be synthesized by the substitution of triphos on iron halide complexes, followed with Na^0 reduction in the presence of 1 equivalent of triphenylphosphine based on the modification of a known synthesis for the zerovalent 18e- Fe(triphos)(bpy).[9] However, the bulk of the ligand might prevent the five-membered ring formation and give the olefin complex instead, as previously reported when CO ligand substitution was achieved prior to TFE addition.[10] Solutions to this potential problem include increasing the TFE pressure or finding ligands or designing ligands with similar electronics to the linear triphos, but less bulky.

Further characterization of the new Co(III) perfluorometallacycle hydride complexes and the insertion product, synthesized in Chapter 4, will be valuable. UV irradiation seemed to reduce rapidly the amount of insertion product in solution. To investigate further the mechanism of these Co(I) carbonyl hydride reactions with TFE, and establish the role played by the labile CO, the reaction could be performed in an open system by bubbling TFE into the solution. Another point to be studied in the future is the selective C_α–F bond activation of these Co complexes by reacting them with H_2 and Lewis acids, which can eventually lead to the design of the catalytic cycle below (Scheme 5.2). Steps **1** and **2** were demonstrated in this Thesis, however step **3** involves the formation of a 16-electron intermediate by protonation of Cα, followed by β-F elimination (step **4**) to release the HFO and form a cobalt fluoride complex. In step **5**, the cobalt hydride is regenerated using a silane.

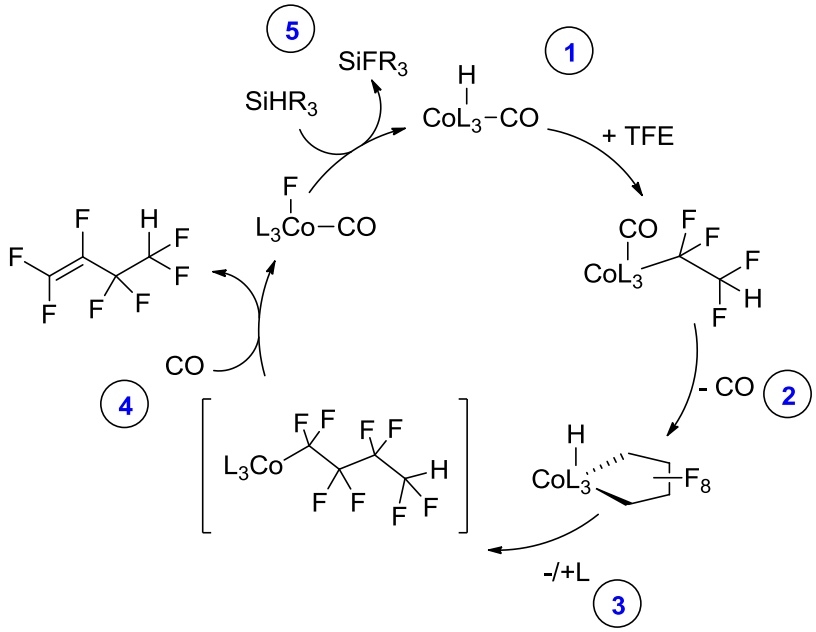

Scheme 5.2. Proposed catalytic cycle for HFO generation via cobalt perfluorometallacycle.

These findings have brought a better understanding of the reactivity of d^6 iron and cobalt perfluorometallacycle complexes; however this area still remains largely unexplored and has the potential to generate attractive additions to current catalytic fluoroalkene transformations utilizing nickel[11] and copper.[12]

5.1 References

(1) Pell, C. J.; Zhu, Y.; Huacuja, R.; Herbert, D. E.; Hughes, R. P.; Ozerov, O. V. *Chem. Sci.* **2017**, *8* (4), 3178–3186.

(2) Burch, R. R.; Calabrese, J. C.; Ittel, S. D. *Organometallics* **1988**, *7* (7), 1642–1648.

(3) Giffin, K. A.; Korobkov, I.; Baker, R. T. *Dalt. Trans.* **2015**, *44* (45), 19587–19596.

(4) Giffin, K. A.; Harrison, D. J.; Korobkov, I.; Baker, R. T. *Organometallics* **2013**, *32* (24), 7424–7430.

(5) Andrella, N. O.; Sicard, A. J.; Gorelsky, S. I.; Korobkov, I.; Baker, R. T. *Chem. Sci.* **2015**, *6* (11), 6392–6397.

(6) Sicard, A. J. University of Ottawa MSc thesis, **2016**.

(7) Giffin, K. A. University of Ottawa Ph.D thesis, **2017**.

(8) Hughes, R. P.; Willemsen, S.; Williamson, A.; Zhang, D. *Organometallics* **2002**, *21* (15), 3085–3087.

(9) Mukhopadhyay, T. K.; Feller, R. K.; Rein, F. N.; Henson, N. J.; Smythe, N. C.; Trovitch, R. J.; Gordon, J. C. *Chem. Commun.* **2012**, *48* (69), 8670–8672.

(10) Granville, S. L. University of Ottawa MSc thesis, **2010**.

(11) Sicard, A. J.; Baker, R. T., World patent WO 2018/039794, **2016**, University of Ottawa.

(12) Andrella, N. O.; Baker, R. T., World patent WO 2018/039795, **2017**, University of Ottawa.

Appendices

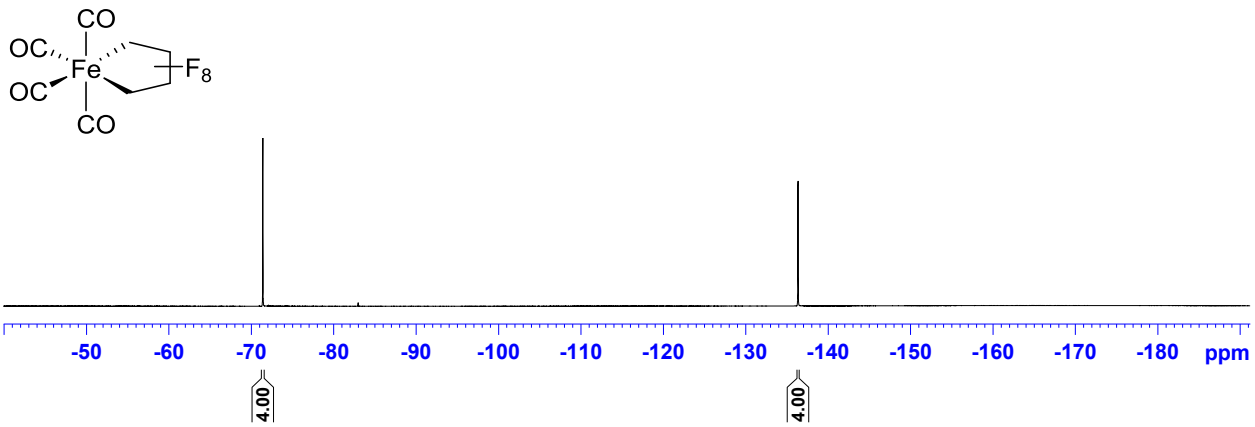

Figure A.1. ^{19}F NMR (282 MHz, C_6D_6) spectrum for $Fe(CO)_4(1,4\text{-}C_2F_8)$, **2-1**.

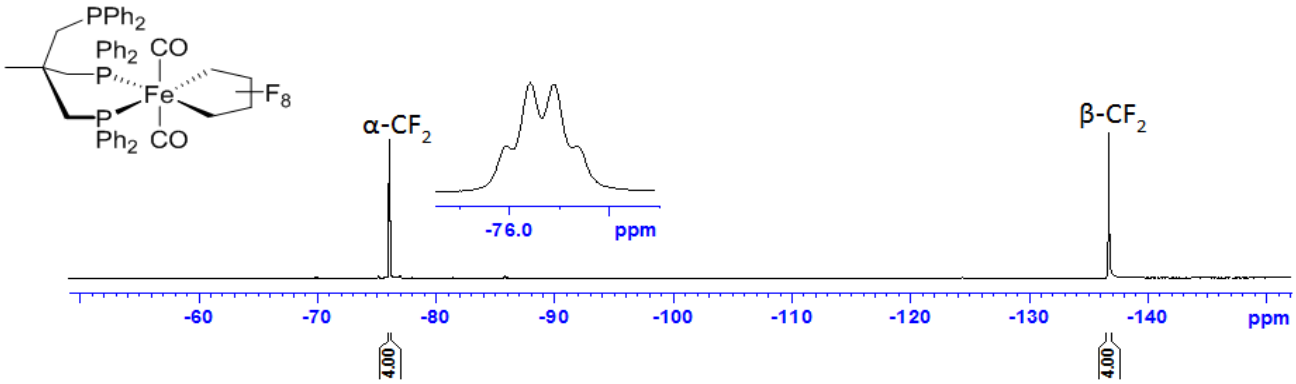

Figure A.2. ^{19}F NMR (282 MHz, C_6D_6) spectrum for complex $Fe(\kappa^2\text{-tripod})(CO)_2(1,4\text{-}C_4F_8)$, **2-4**.

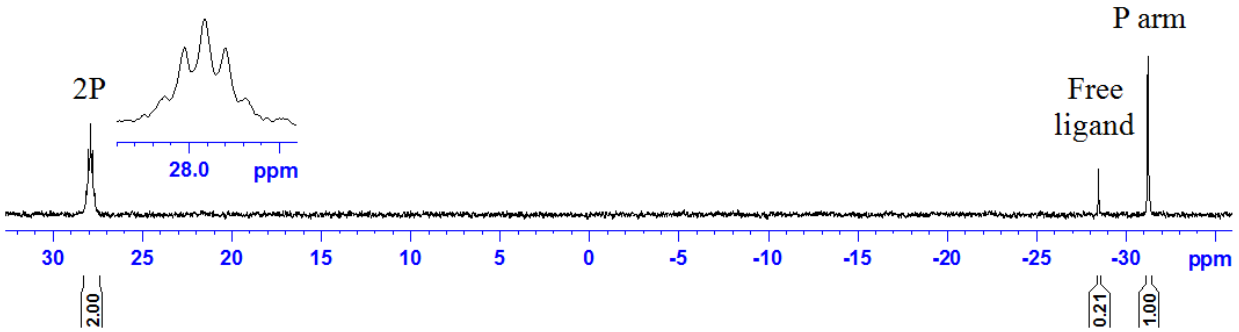

Figure A.3. $^{31}P\{^1H\}$ NMR (121 MHz, C_6D_6) spectrum of complex $Fe(\kappa^2\text{-tripod})(CO)_2(1,4\text{-}C_4F_8)$, **2-4**.

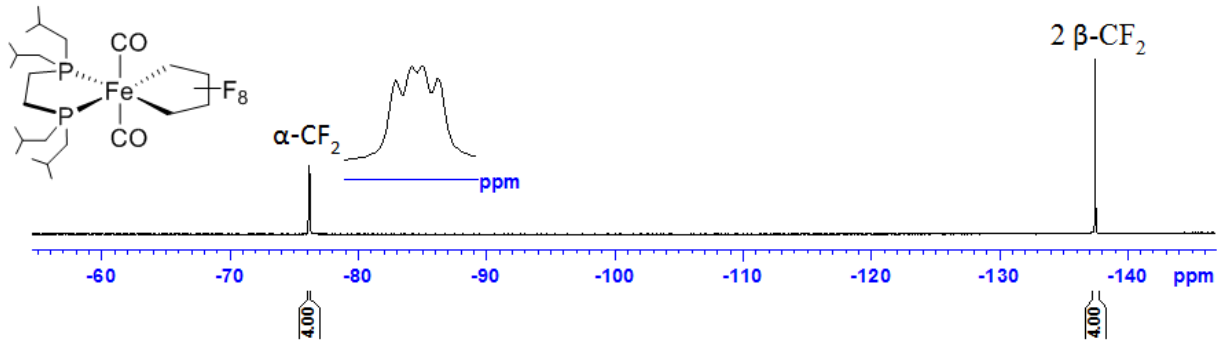

Figure A.4. ^{19}F NMR (282 MHz, C_6D_6) spectrum for complex Fe(dibpe)$(CO)_2$(1,4-C_4F_8), **2-3**.

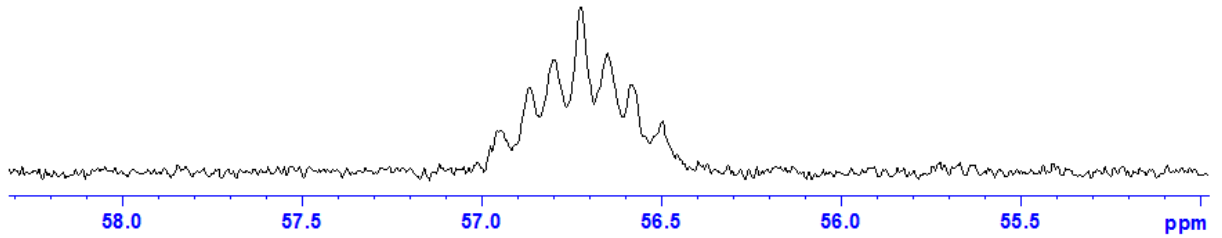

Figure A.5. $^{31}P\{^1H\}$ NMR (121 MHz, C_6D_6) spectrum of complex Fe(dibpe)$(CO)_2$(1,4-C_4F_8), **2-3**.

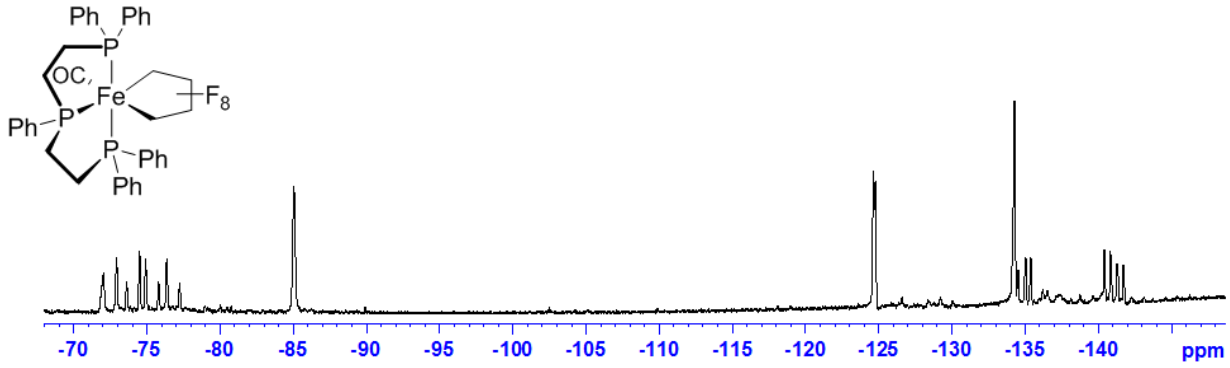

Figure A.6. ^{19}F NMR (282 MHz, toluene) spectrum for complex Fe(triphos)(CO)(1,4-C_4F_8), **2-5**.

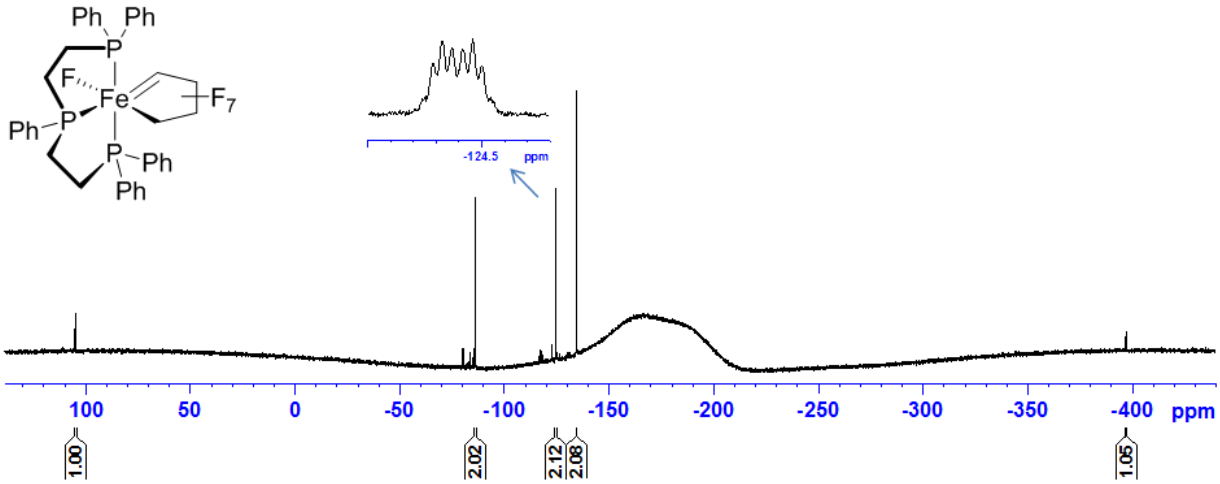

Figure A.7. ^{19}F NMR (282 MHz, C_6D_6) spectrum for complex FeF(triphos)(1,4-C_4F_7), **2-6**.

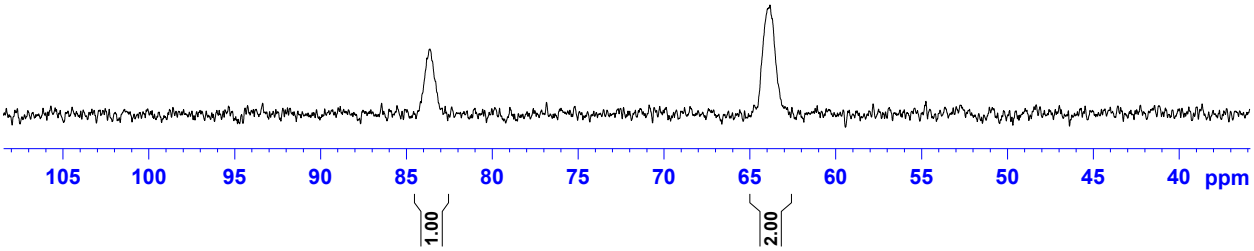

Figure A.8. $^{31}P\{^1H\}$ NMR (121 MHz, C_6D_6) spectrum of complex FeF(triphos)(1,4-C_4F_7), **2-6**.

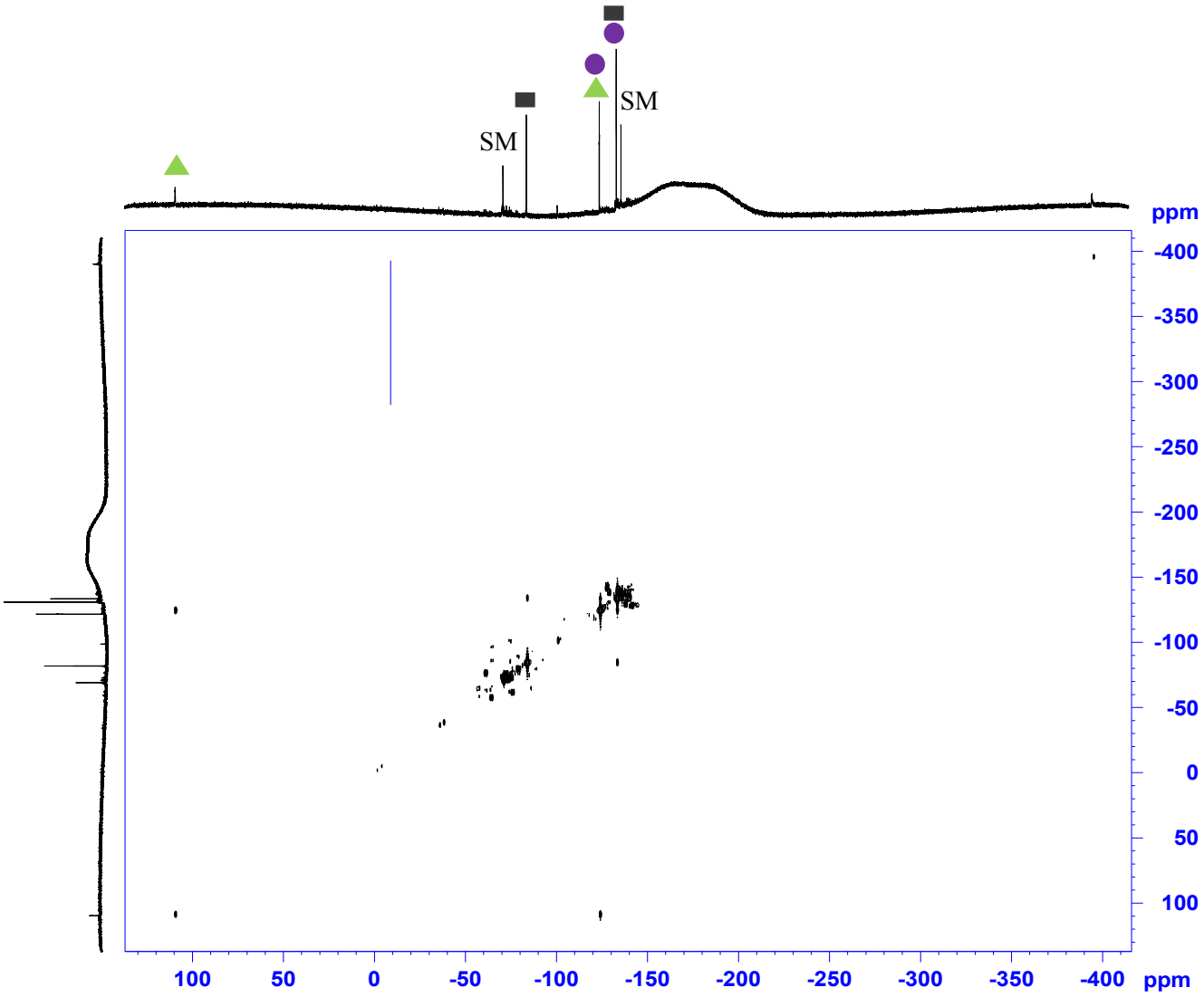

Figure A.9. ^{19}F-^{19}F COSY NMR (282 MHz, toluene) spectrum for complex FeF(triphos)(1,4-C_4F_7), **2-6**.

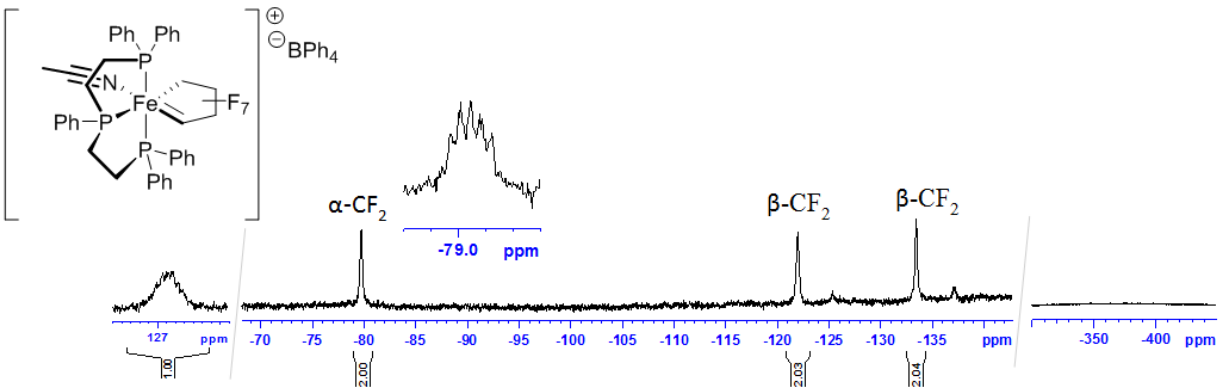

Figure A.10. ^{19}F NMR (282 MHz, THF) spectrum for complex [Fe(triphos)(1,4-C_4F_7)CH_3CN]$^+BPh_4^-$, **2-7**.

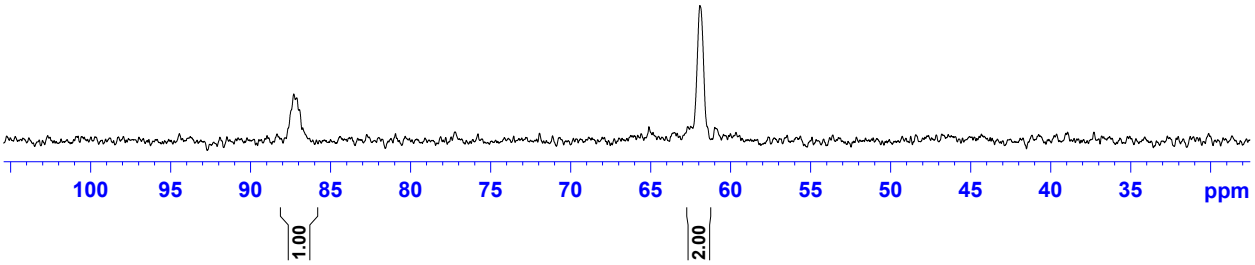

Figure A.11. $^{31}P\{^{1}H\}$ NMR (121 MHz, THF) spectrum of complex [Fe(triphos)(1,4-C_4F_7)(NCMe)]$^{+}BPh_4^{-}$, **2-7**.

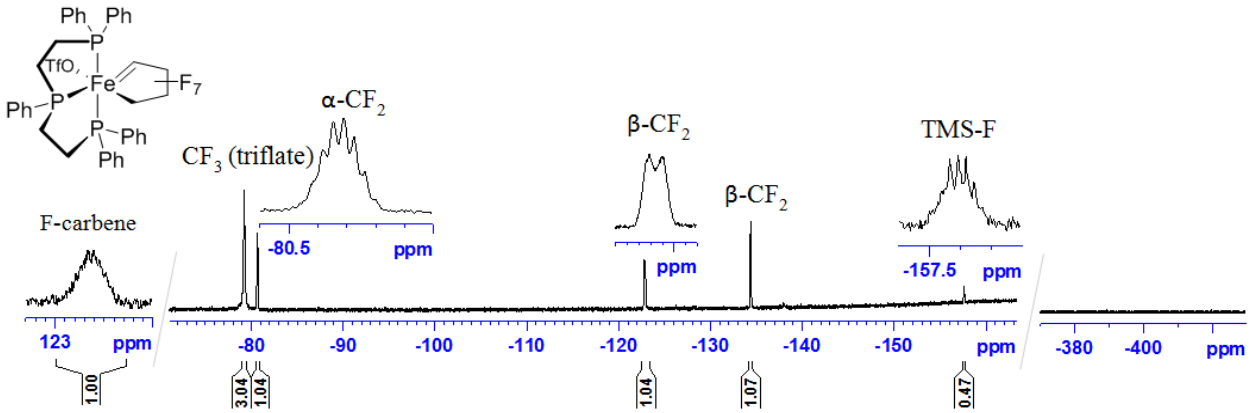

Figure A.12. ^{19}F NMR (282 MHz, toluene) spectrum for complex Fe(OTf)(triphos)(1,4-C_4F_7), **2-8**.

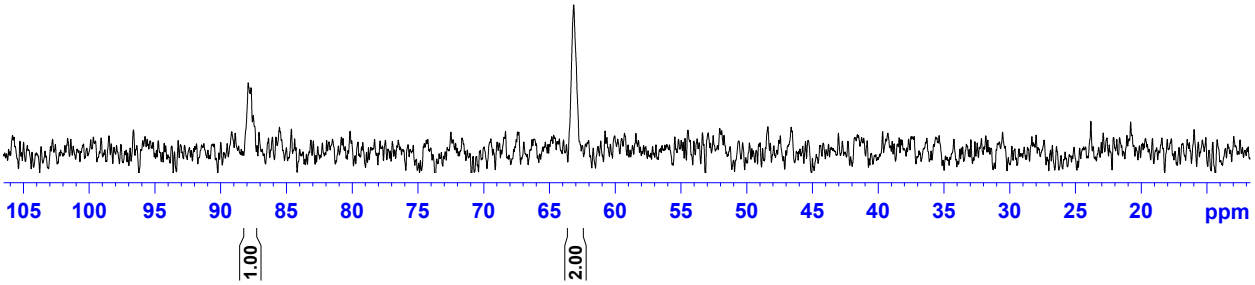

Figure A.13. $^{31}P\{^{1}H\}$ NMR (121 MHz, toluene) spectrum of complex Fe(OTf)(triphos)(1,4-C_4F_7), **2-8**.

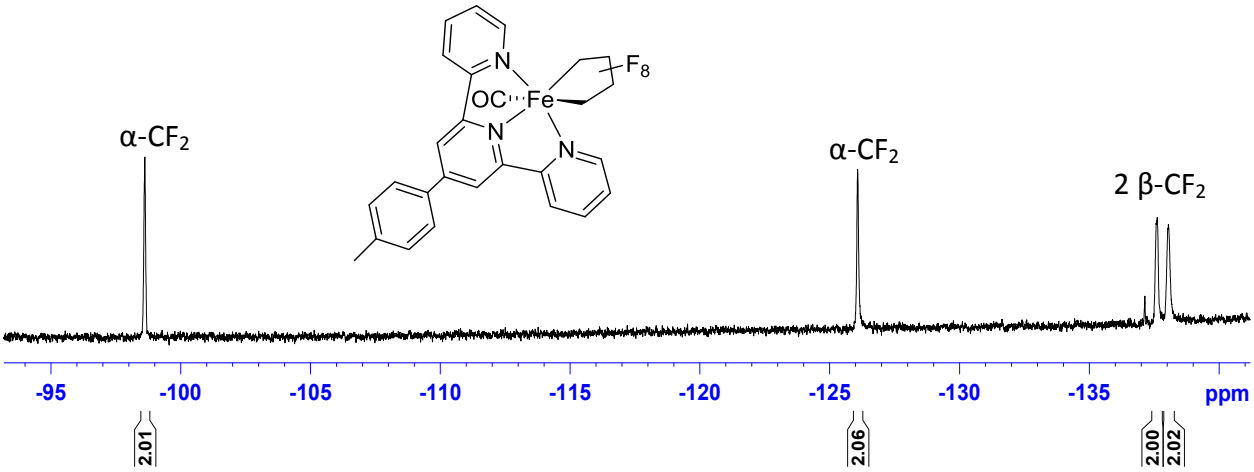

Figure A.14. ^{19}F NMR (282 MHz, toluene) spectrum for complex Fe(terpy')(CO)(1,4-C_4F_8), **2-9**.

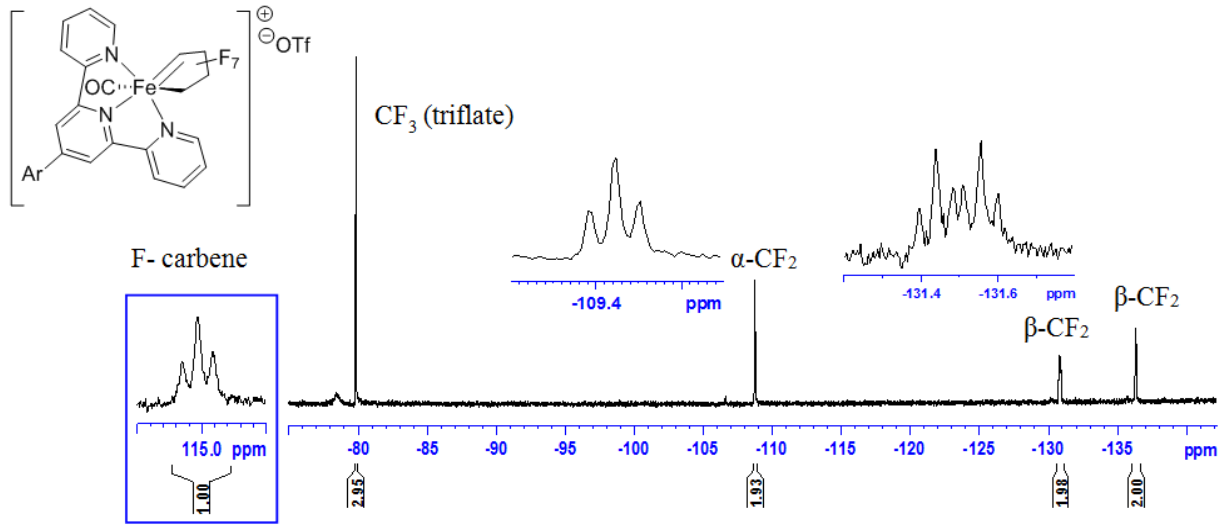

Figure A.15. ^{19}F NMR (282 MHz, THF) spectrum for complex [Fe(terpy')(CO)(1,4-C_4F_7)]$^+$OTf$^-$, **2-10**.

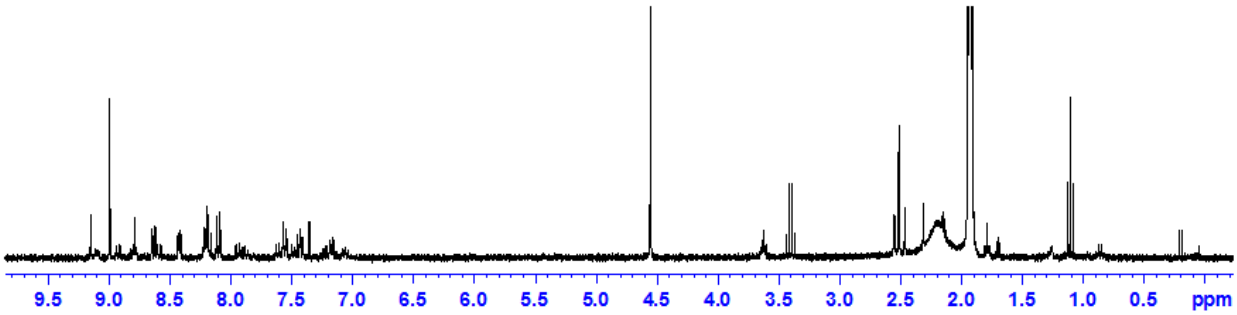

Figure A.16. ^{1}H NMR (300 MHz, THF-d_8; top, CD_3CN, bottom) spectrum of [Fe(terpy')(CO)(1,4-C_4F_7)]$^+$OTf$^-$, **2-10**.

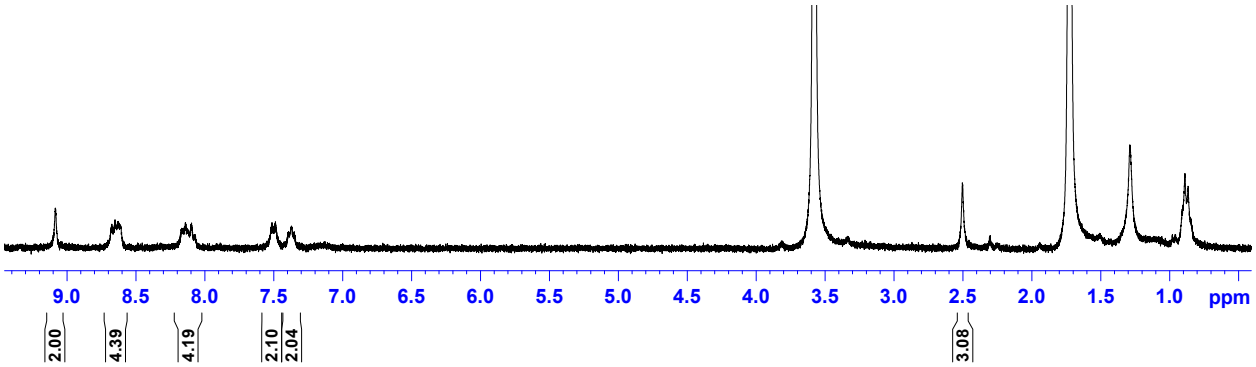

Figure A.17. ^{1}H NMR spectrum (300MHz, THF-d_8) of complex [Fe(terpy')(CO)(1,4-C_4F_7)]$^{+}$OTf^{-}, **2-10**.

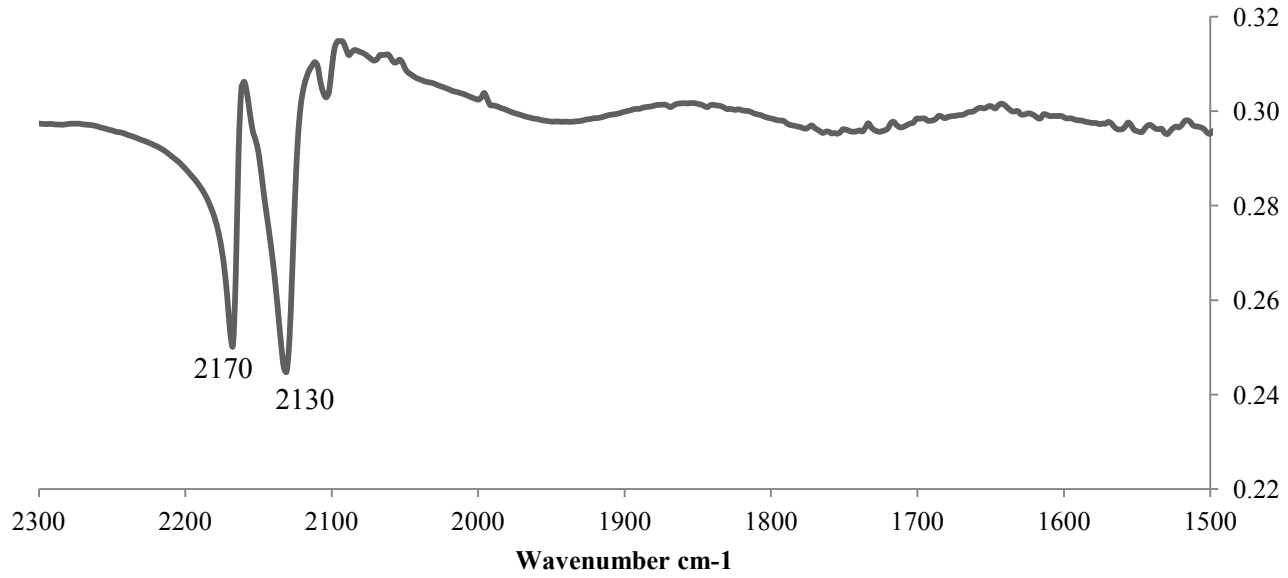

Figure A.18. IR spectrum of Fe(CO)$_4$(1,4-C_4F_8), **2-1**.

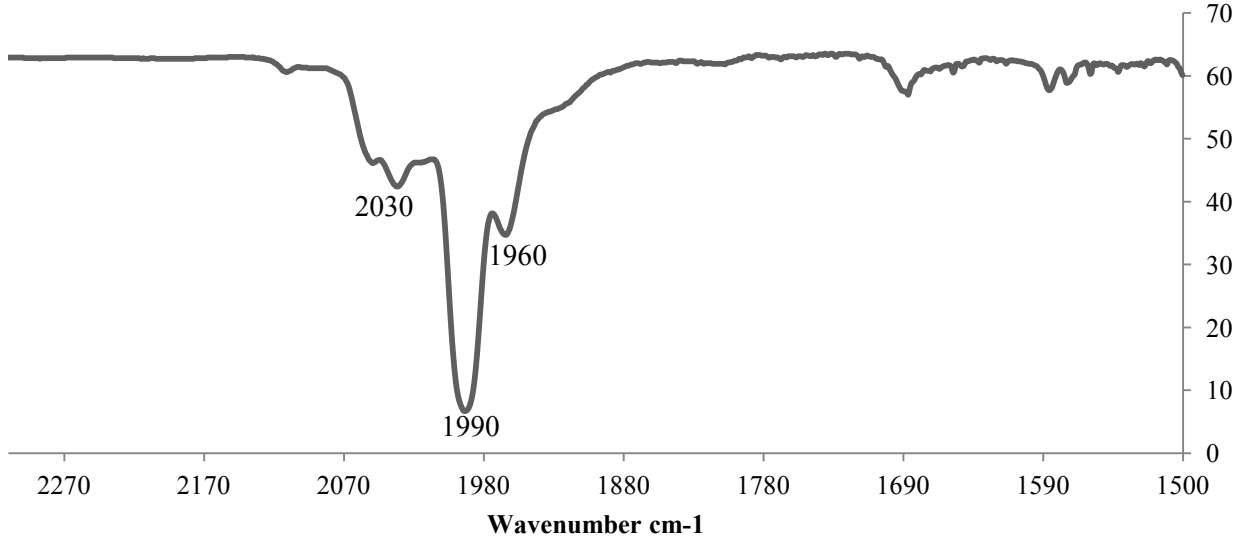

Figure A.19. IR spectrum of Fe(triphos)CO(1,2-C_4F_8), **2-5**.

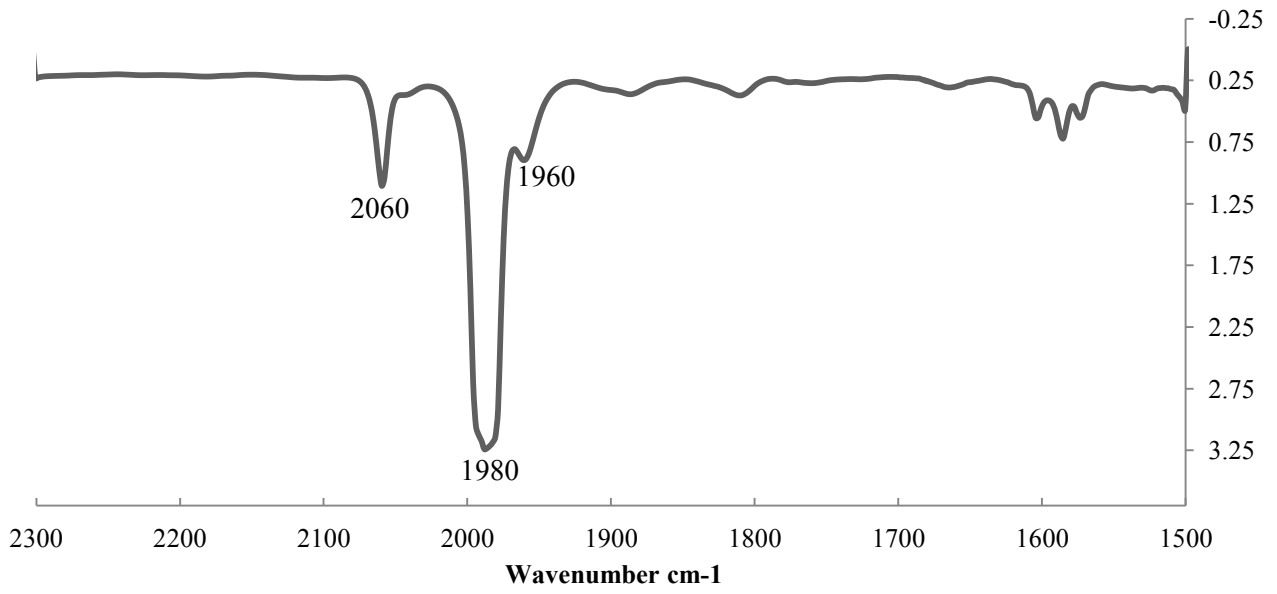

Figure A.20. IR spectrum of Fe(κ^2-tripod)$(CO)_2$(1,4-C_4F_8), **2-4**.

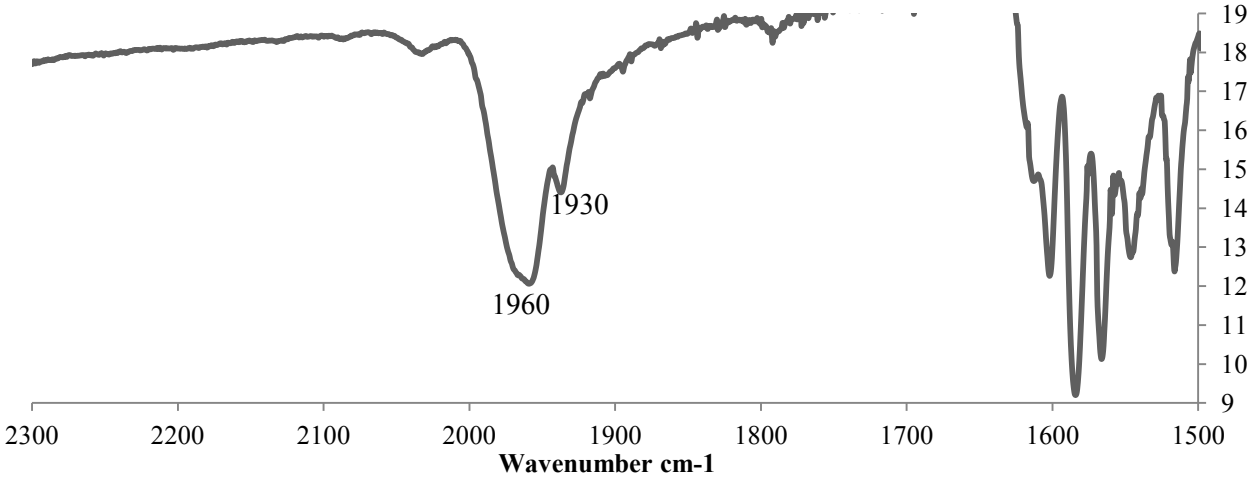

Figure A.21. IR spectrum of Fe(terpy')CO(1,4-C_4F_8), **2-9**.

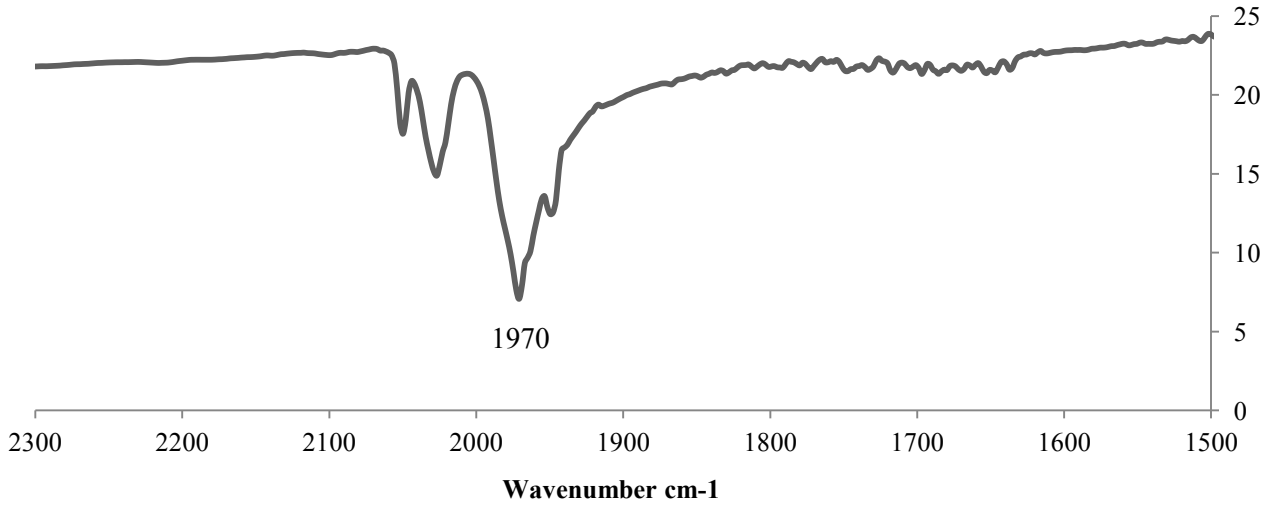

Figure A.22. IR spectrum of Fe(dibpe)(1,4-C_4F_8)$(CO)_2$, **2-3**.

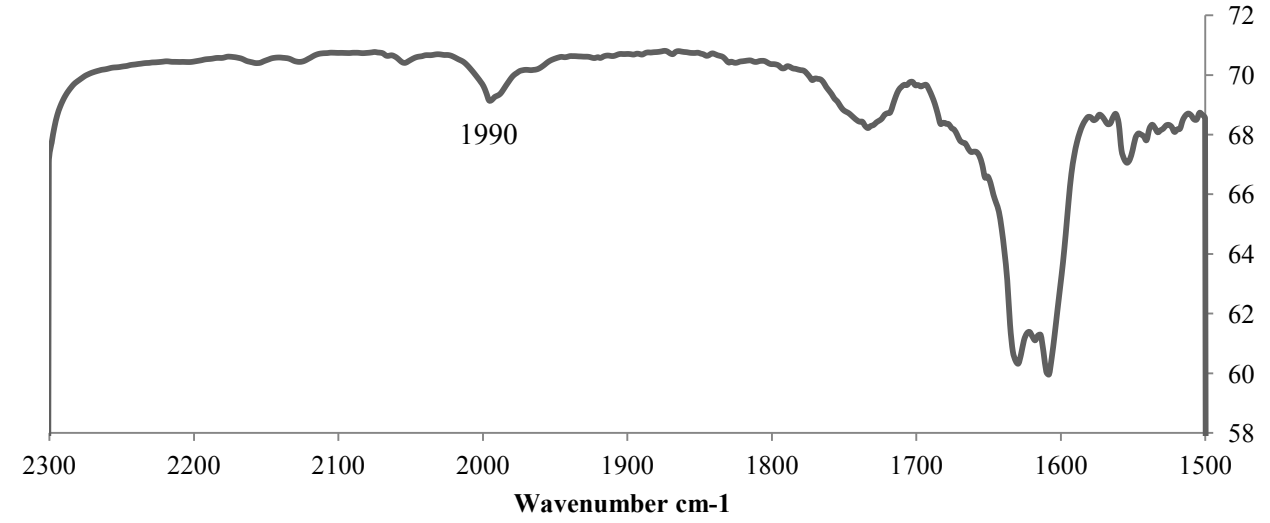

Figure A.23. IR spectrum of [Fe(terpy')(CO)(1,4-C_4F_7)]$^+$OTf$^-$, **2-10**.

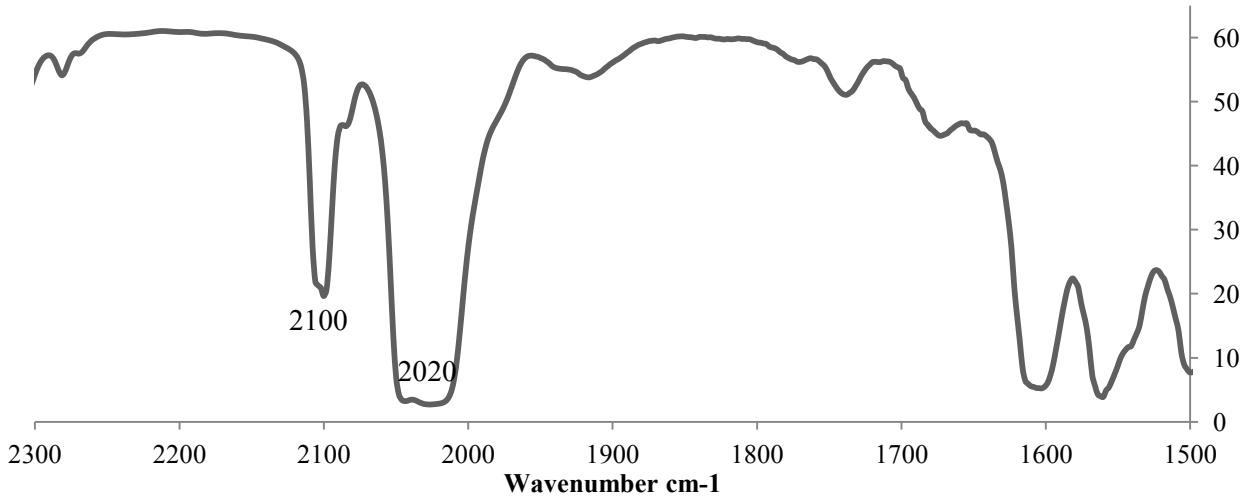

Figure A.24. IR spectrum of Fe(1,4-C_4F_7)(IMes)$(CO)_3$, **2-2b**.

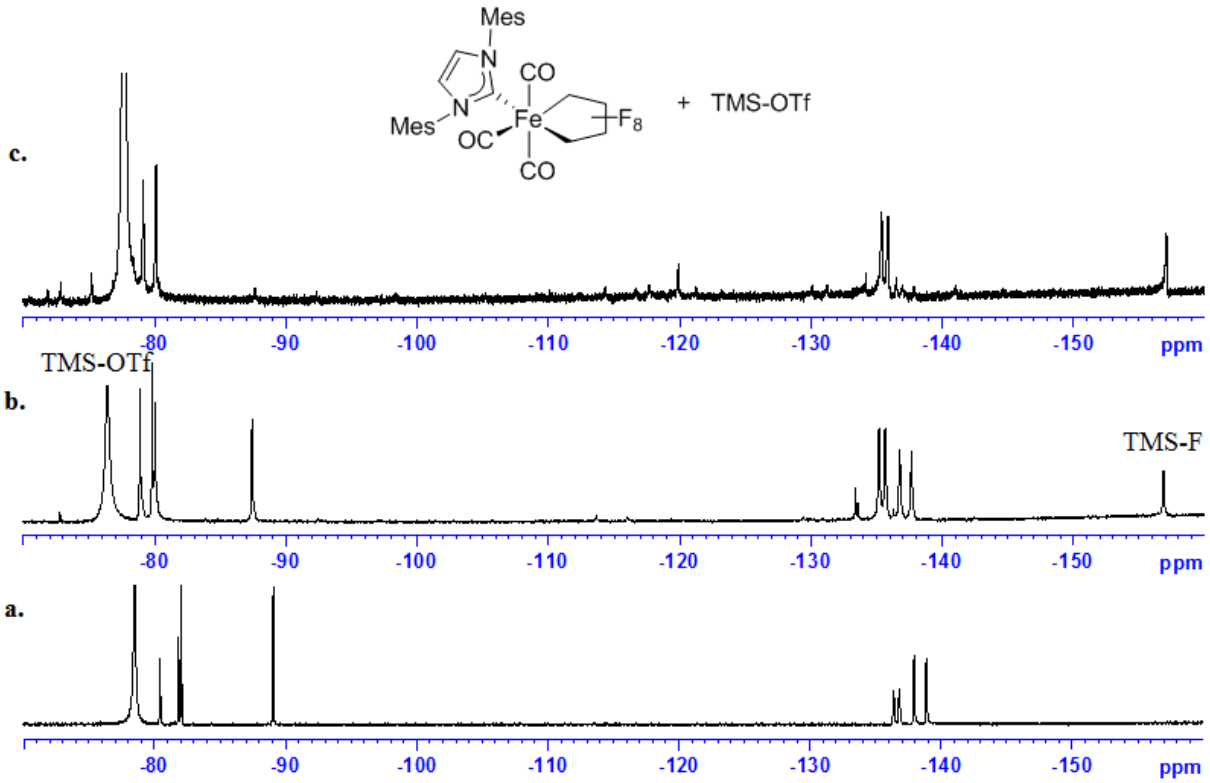

Figure A.25. ^{19}F NMR (282 MHz, toluene) spectra of Fe(IMes)$(CO)_3$(1,4-C_4F_8), **2-2b**, and TMS-OTf (a) 1 equivalent of TMS-OTf (b) excess TMS-OTf, 1 d heating (c) excess TMS-OTf, 3 d heating.

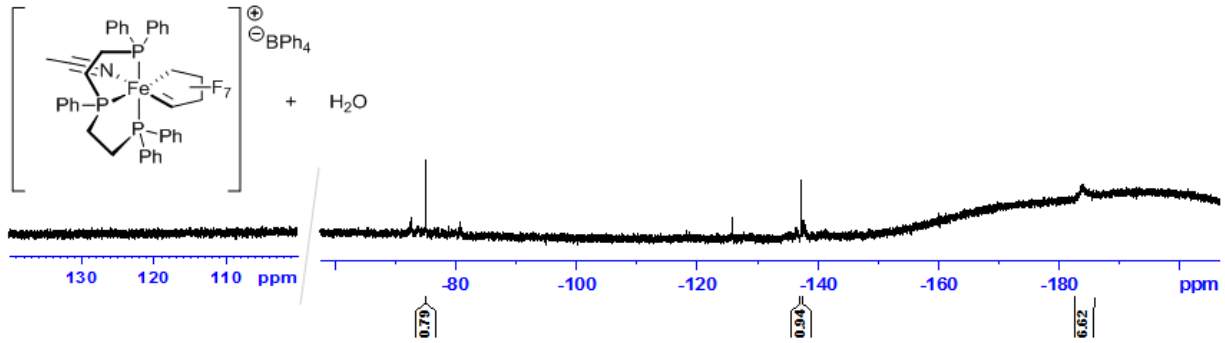

Figure A.26. ^{19}F NMR (282 MHz, THF) spectrum of the reaction [Fe(triphos)(1,4-C_4F_7)CH_3CN]$^+BPh_4^-$, **2-7**, with water.

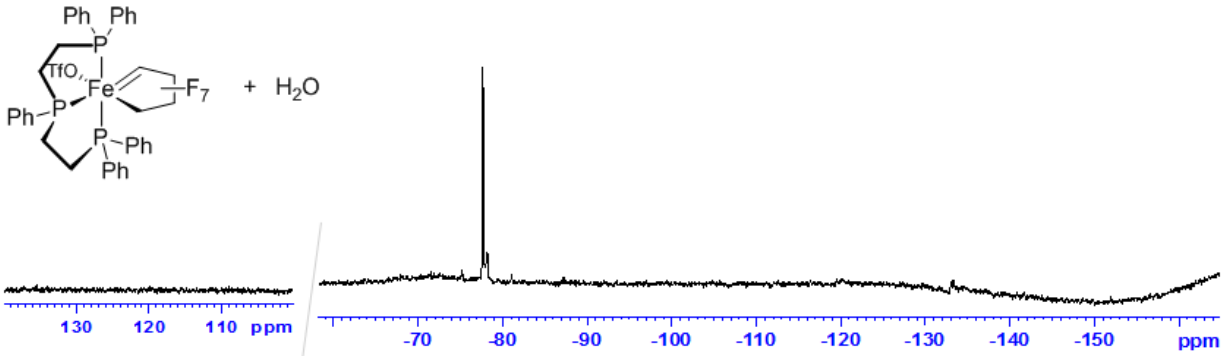

Figure A.27. ^{19}F NMR (282 MHz, toluene) spectrum of the reaction Fe(OTf)(triphos)(1,4-C_4F_7) with water.

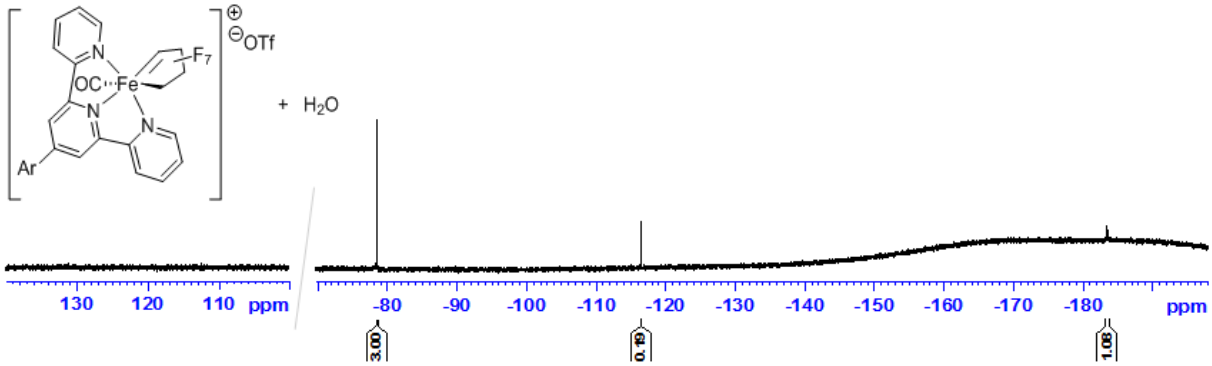

Figure A.28. ^{19}F NMR (282 MHz, THF) spectrum of the reaction [Fe(terpy')(CO)(1,4-C_4F_7)]$^+OTf^-$, **2-10**, with water.

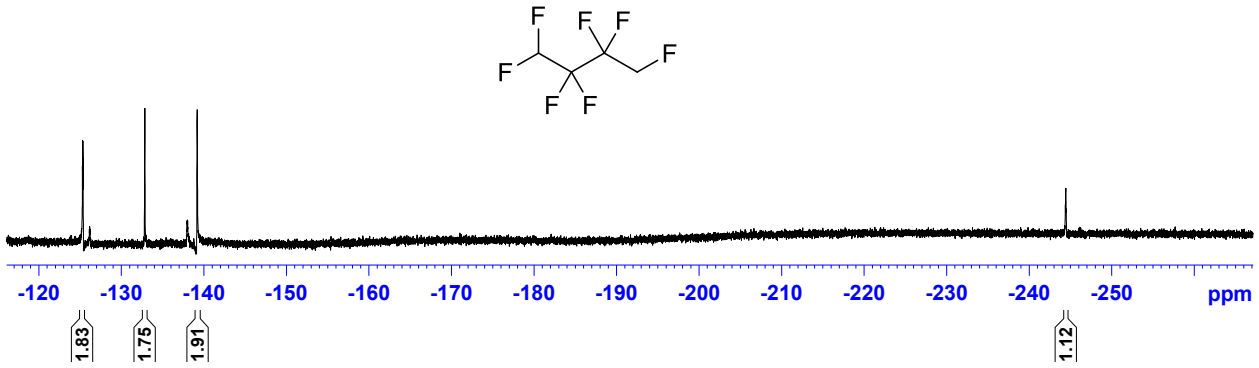

Figure A.29. $^{19}F\{^{1}H\}$ NMR (282 MHz, THF) spectrum of HCF-347pcc.

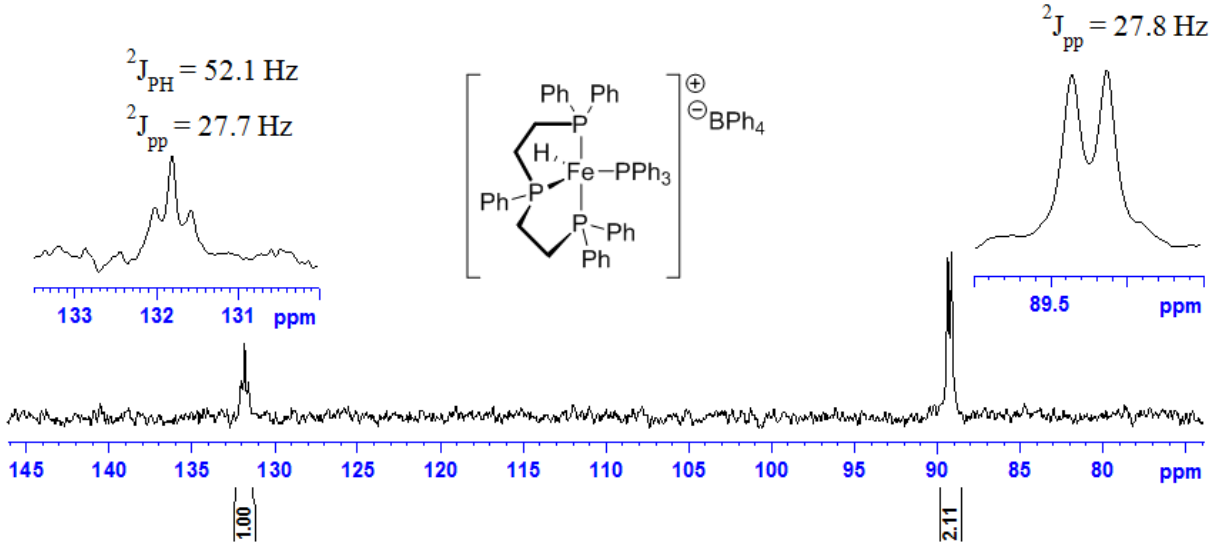

Figure A.30. $^{31}P\{^{1}H\}$ (121 MHz, THF) NMR spectrum of complex $[FeH(triphos)(CH_3CN)]^{+}$ BPh_4^{-}, **3-2**.

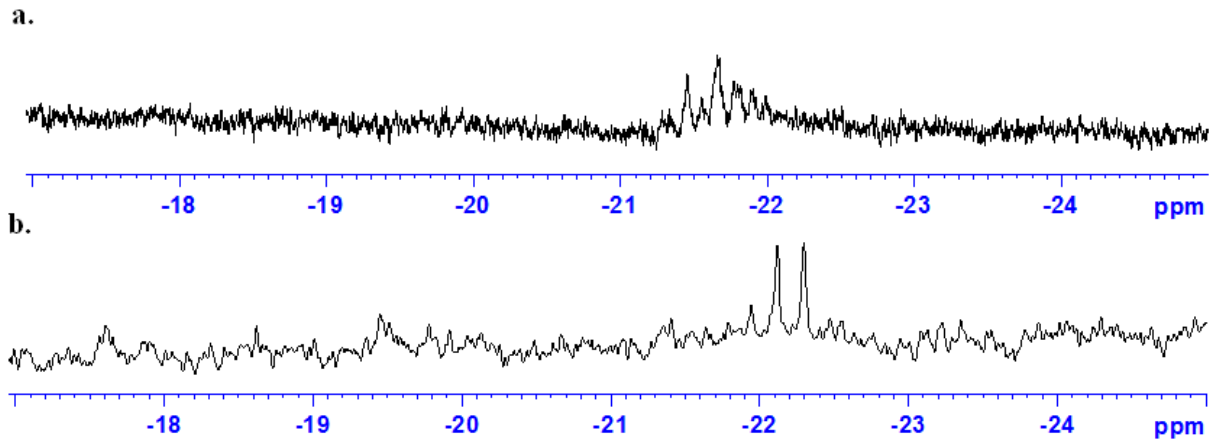

Figure A.31. ^{1}H NMR (300 MHz, THF) spectra, hydride region of (a) $[FeH(triphos)(PPh_3)]^{+}BPh_4^{-}$ (b) $[FeH(triphos)(CH_3CN)]^{+}BPh_4^{-}$, **3-2**.

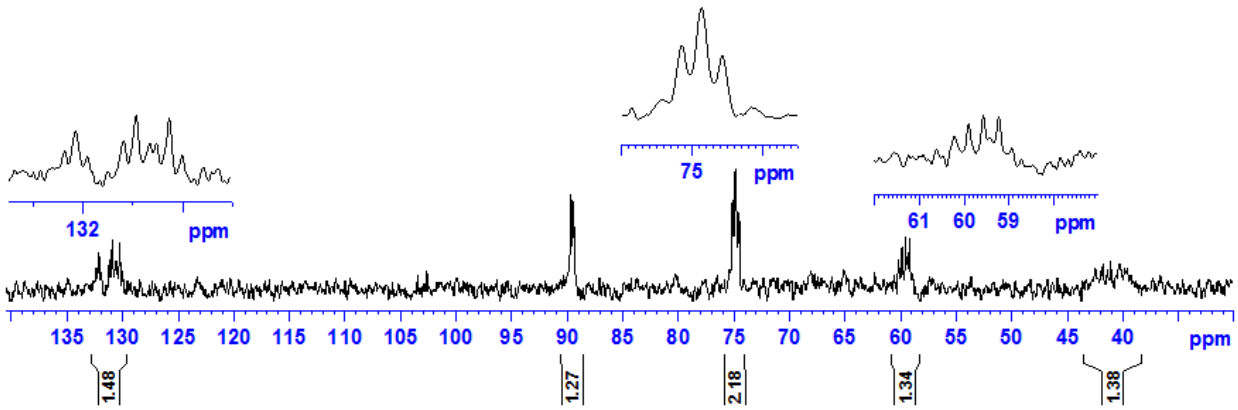

Figure A.32. $^{31}P[^{1}H]$ NMR (121 MHz, THF) spectrum of the mixture of $[FeH(triphos)(NCMe)]^{+}BPh_4^{-}$ and $[FeH(triphos)(PPh_3)]^{+}BPh_4^{-}$, **3-2**.

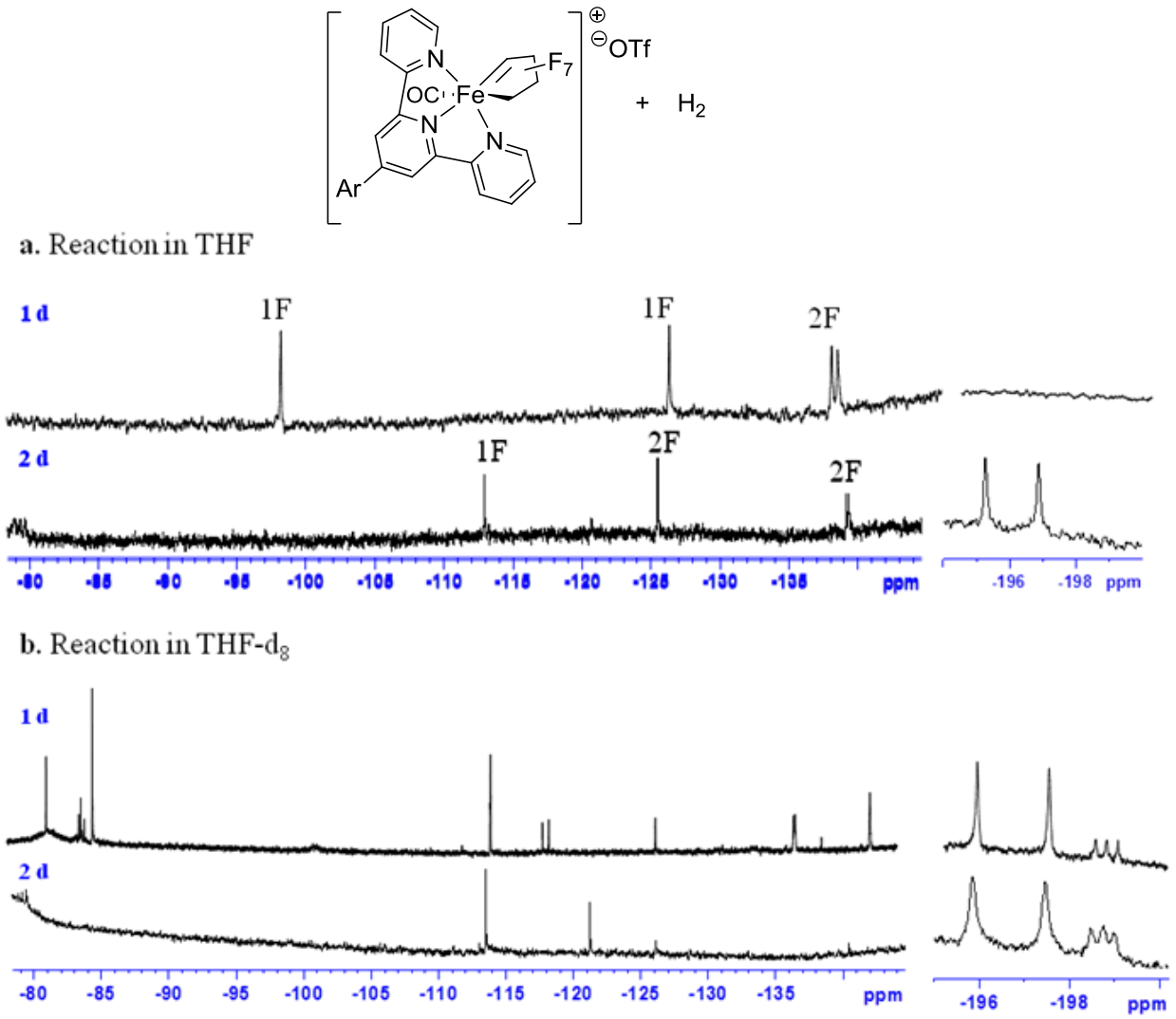

Figure A.33. (a) ^{19}F NMR (282 MHz, THF) spectra (b) ^{19}F NMR (282 MHz, THF-d_8) spectra of the reaction of [Fe(terpy')(CO)(1,4-C_4F_7)]$^+$OTf$^-$, **2-10**, and H_2.

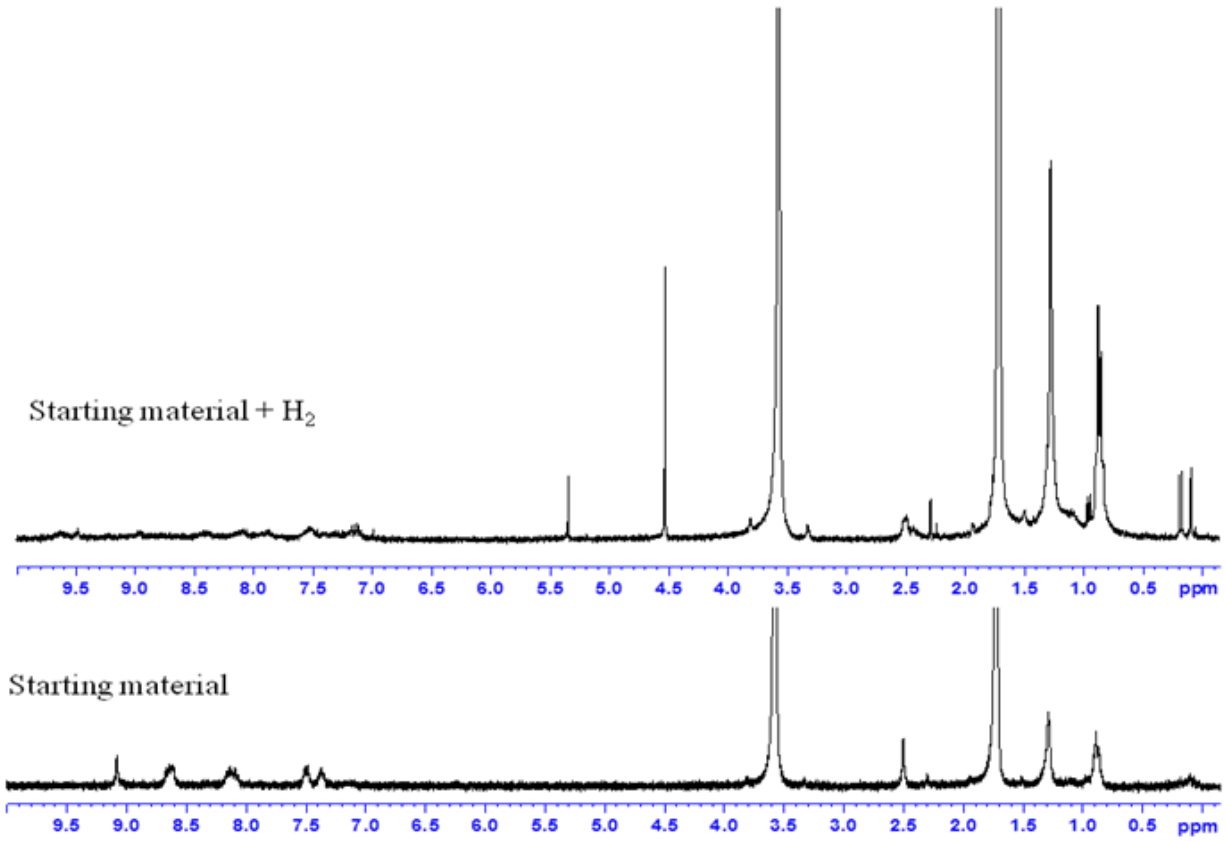

Figure A.34. ^{1}H (300 MHz, THF-d_8) spectra of **2-10** and the reaction of [Fe(terpy')(CO)(1,4-C_4F_7)]$^{+}$OTf^{-}, 2-10, and H_2.

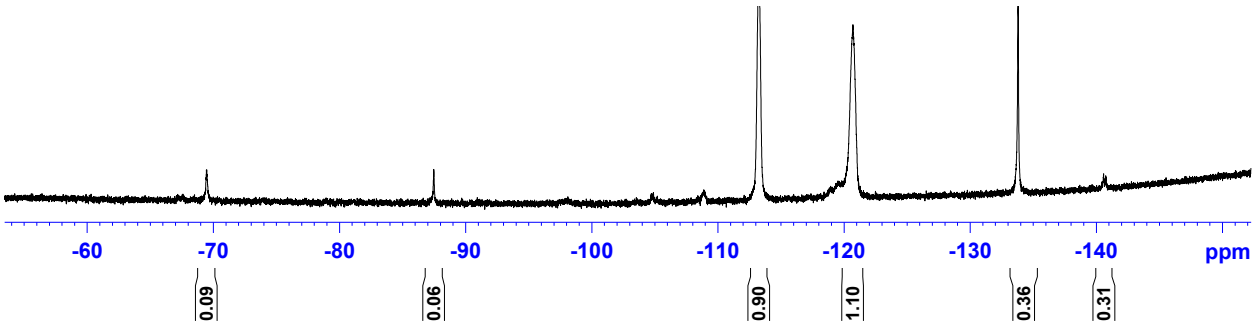

Figure A.35. ^{19}F NMR (282 MHz, THF) spectrum of $Co(PMe_3)_4$ + TFE reaction.

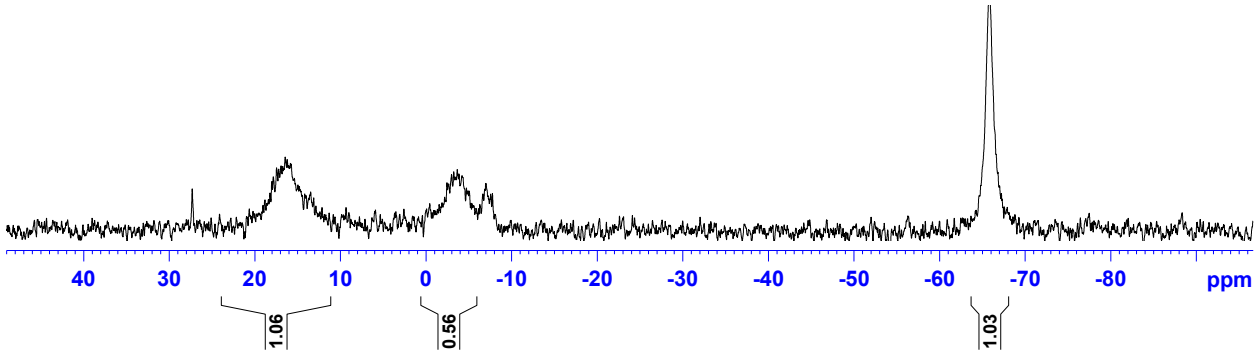

Figure A.36. $^{31}P\{^{1}H\}$ NMR (121 MHz, THF) spectrum of $Co(PMe_3)_4$ + TFE reaction.

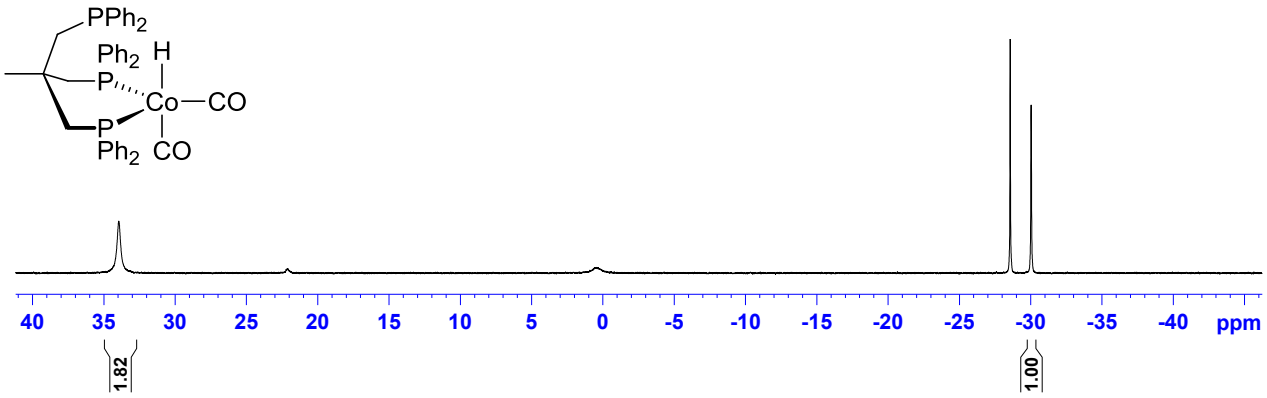

Figure A.37. $^{31}P\{^{1}H\}$ NMR (121 MHz, THF) spectrum $CoH(\kappa^2\text{-tripod})(CO)_2$, **4-1**.

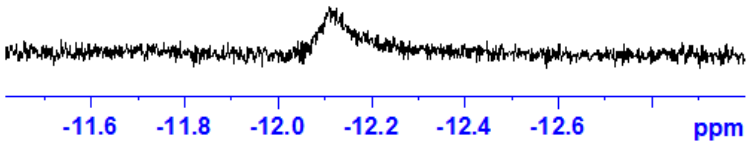

Figure A.38. ^{1}H NMR (300 MHz, THF) spectrum of $CoH(\kappa^2\text{-tripod})(CO)_2$, **4-1** (selected hydride section).

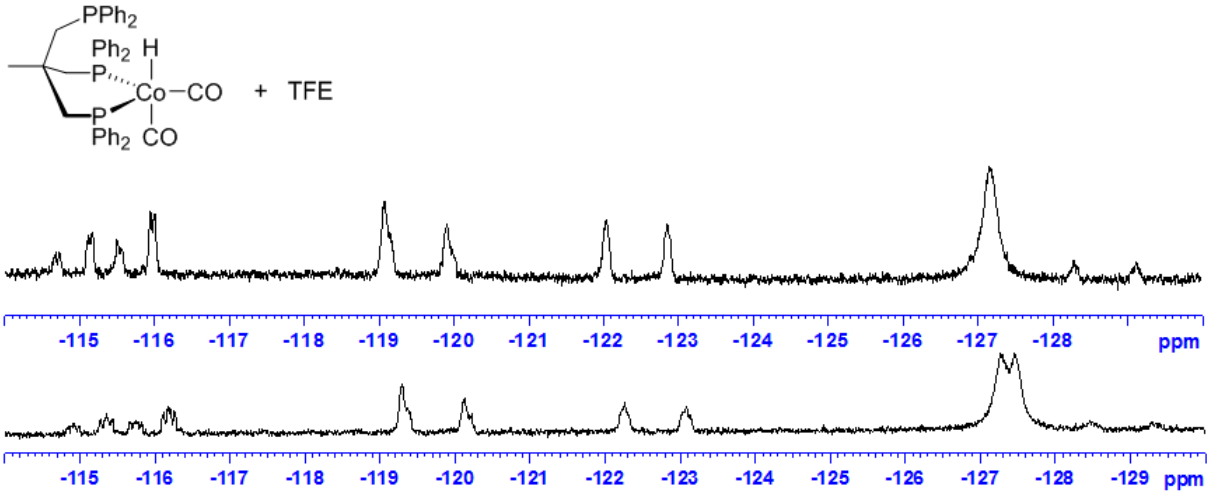

Figure A.39. ^{19}F and $^{19}F\{^{1}H\}$ NMR (282 MHz, THF) spectra of $CoH(\kappa^2\text{-tripod})(CO)_2$, + TFE reaction (selected sections) after 2 d.

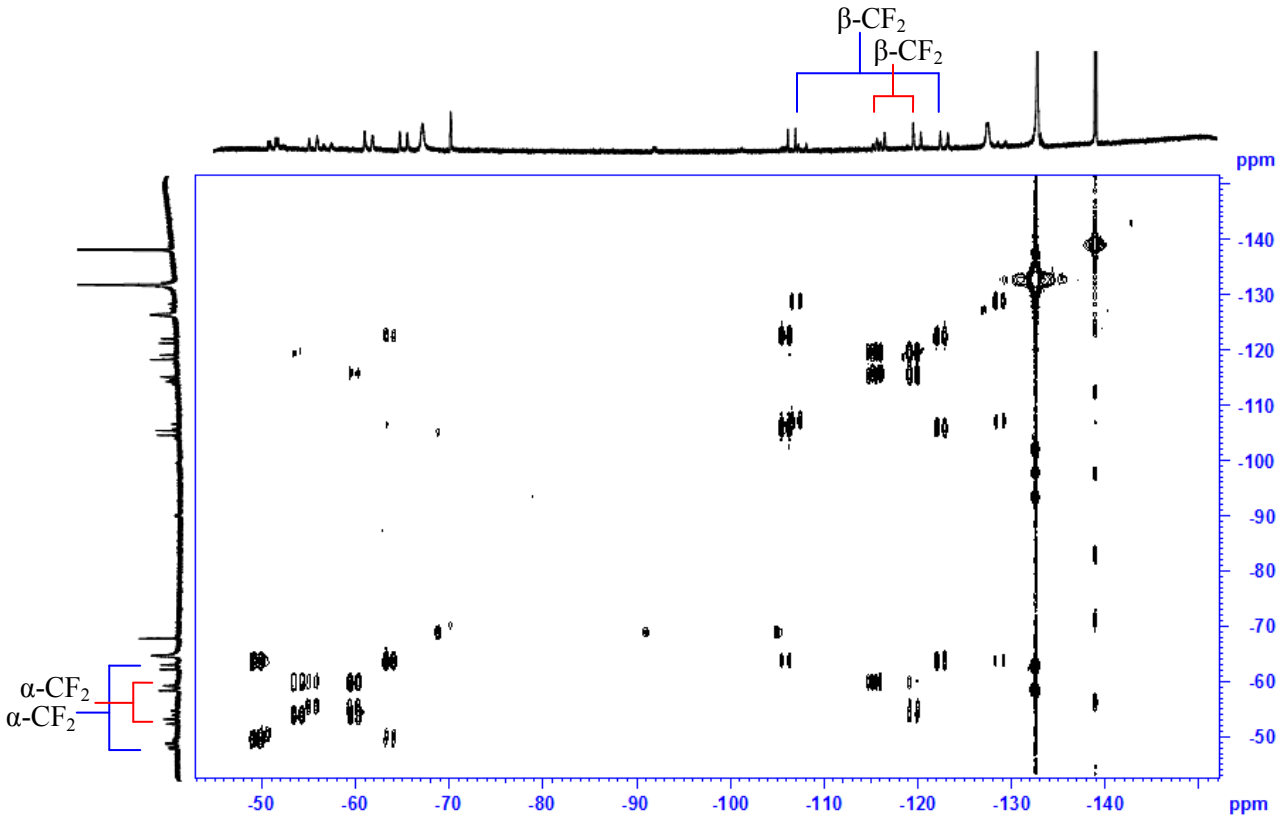

Figure A.40. ^{19}F-^{19}F COSY (282 MHz, THF) of $CoH(\kappa^2\text{-tripod})(CO)_2$, + TFE reaction.

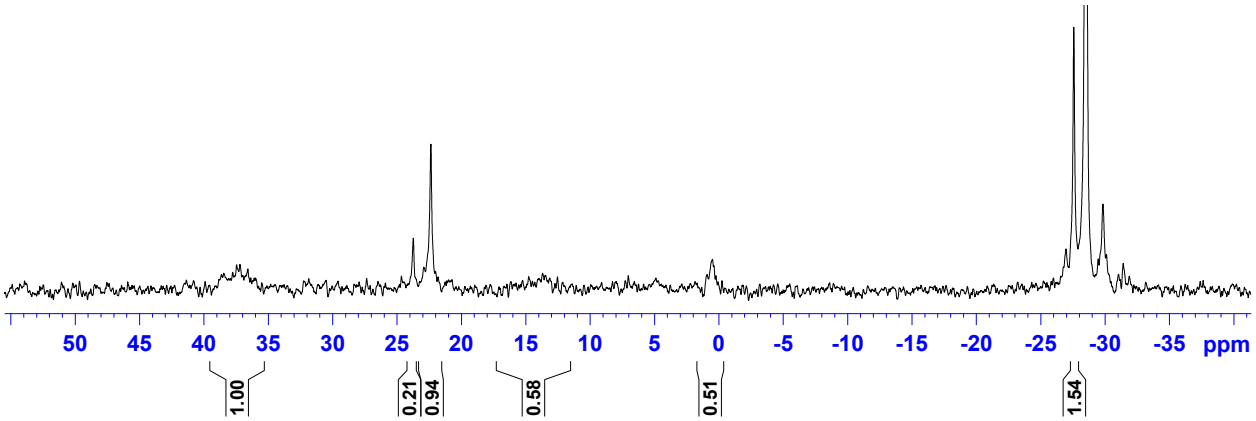

Figure A.41. $^{31}P\{^{1}H\}$ NMR (121 MHz, THF) spectrum of $CoH(\kappa^2\text{-tripod})(CO)_2$ + TFE reaction after 2 d.

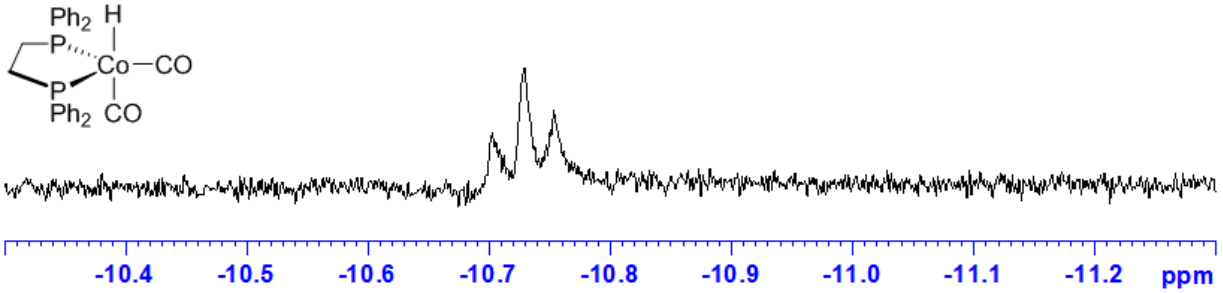

Figure A.42. ^{1}H NMR (300 MHz, Et_2O) spectrum of $CoH(dppe)(CO)_2$, **4-2**.

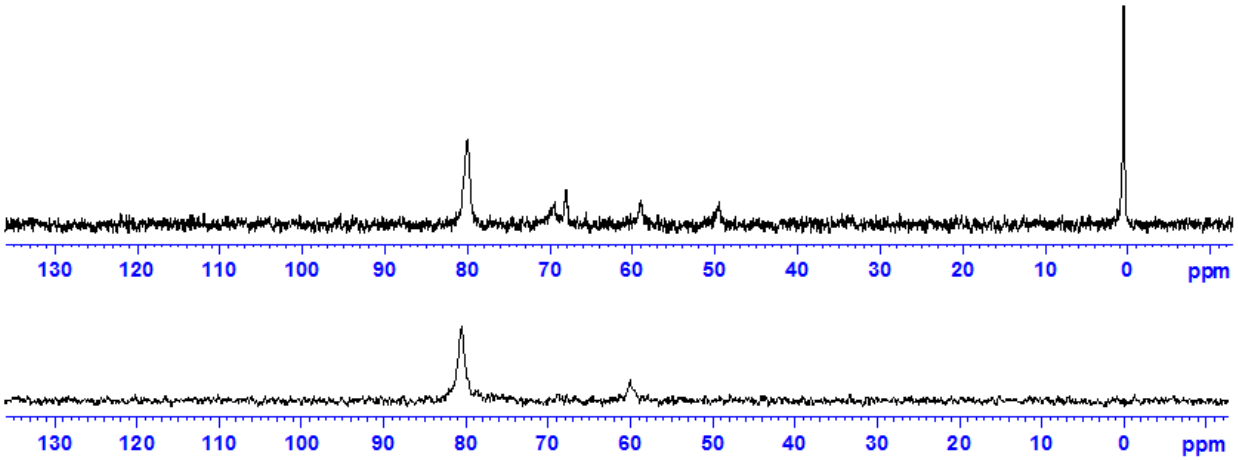

Figure A.43. $^{31}P\{^{1}H\}$ NMR (121 MHz, Et_2O) spectra of $CoH(dppe)(CO)_2$, **4-2** . Top: THF reaction mixture, bottom: after ether extraction.

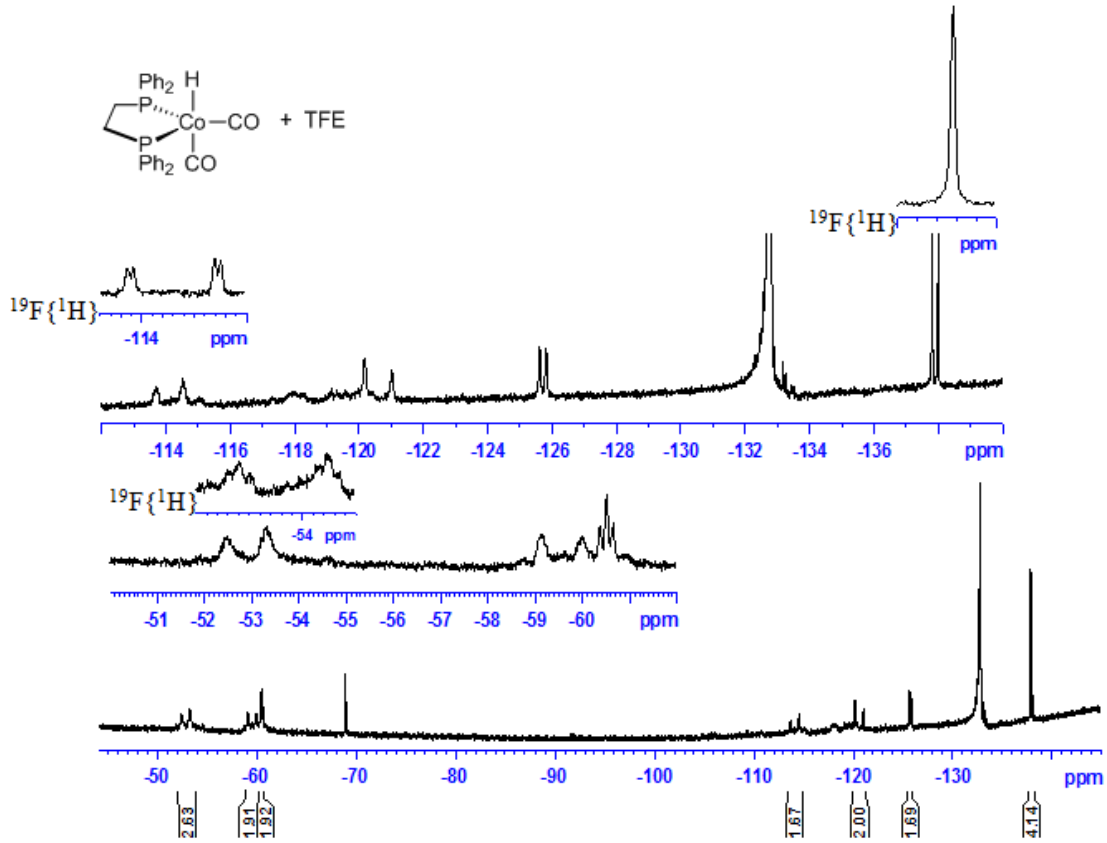

Figure A.44. ^{19}F and $^{19}F\{^1H\}$ NMR (282 MHz, THF) spectra of $CoH(dppe)(CO)_2$ + TFE reaction after 2 d.

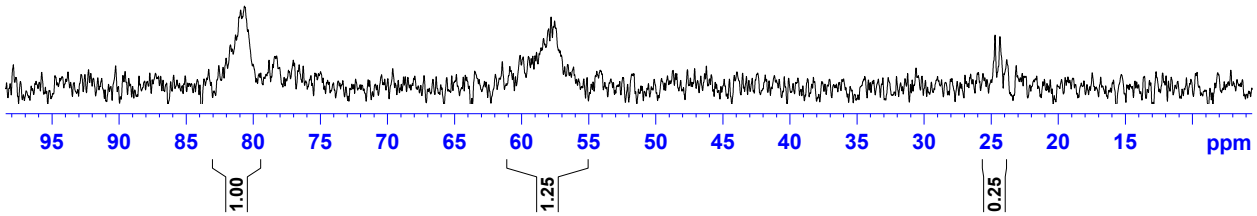

Figure A.45. $^{31}P\{^1H\}$ NMR (121 MHz, THF) spectrum of $CoH(dppe)(CO)_2$ + TFE reaction after 2 d.

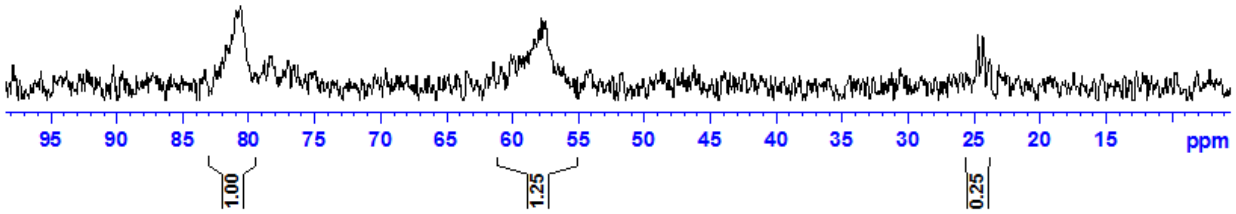

Figure A.46. ^1H NMR (300 MHz, THF) spectrum of $CoH(dcppe)(CO)_2$, **4-3**.

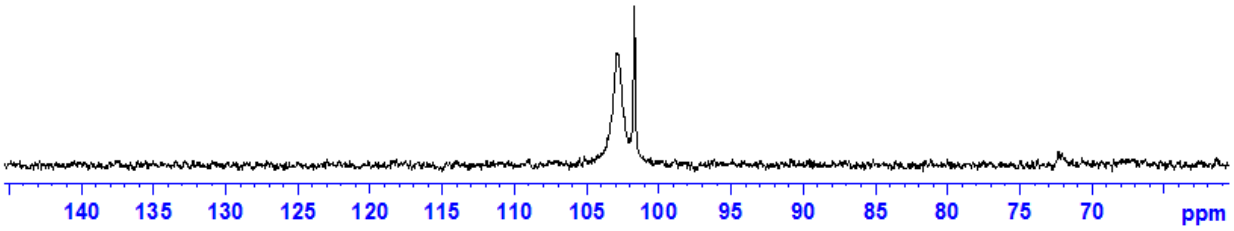

Figure A.47. $^{31}P\{^{1}H\}$ NMR (121 MHz, THF) spectrum of $CoH(dcppe)(CO)_2$, **4-3**.

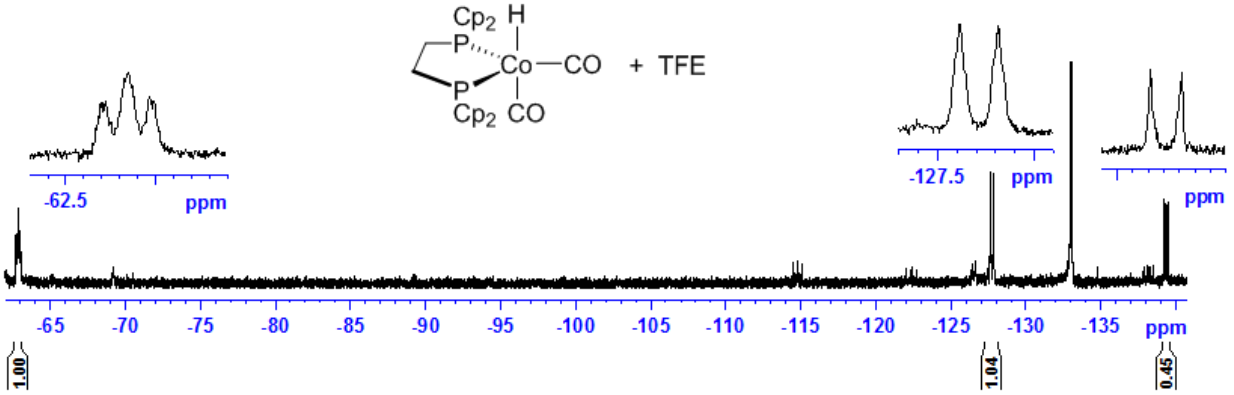

Figure A.48. ^{19}F NMR (282 MHz, THF) spectrum of $CoH(cdppe)(CO)_2$ + TFE reaction after 7 d.

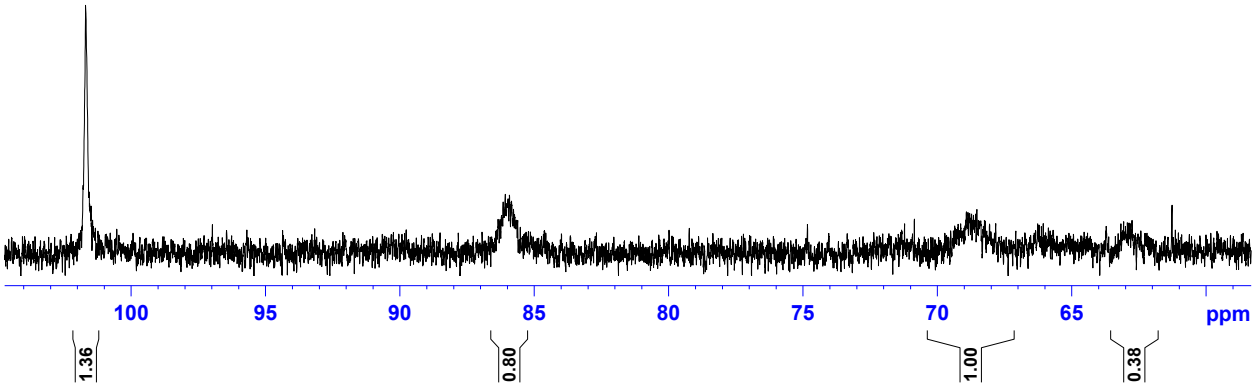

Figure A.49. $^{31}P\{^{1}H\}$ NMR (121 MHz, THF) spectrum of $CoH(dcppe)(CO)_2$ + TFE reaction after 7 d.

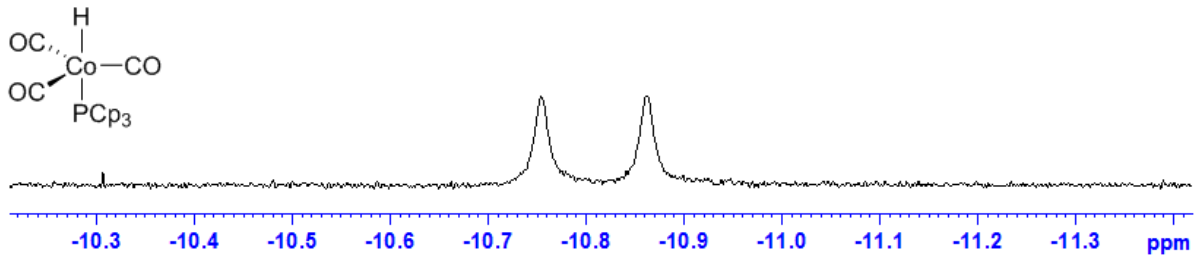

Figure A.50. ^{1}H NMR (300 MHz, THF) spectrum of $CoH(Pcp_3)(CO)_3$, **4-4**.

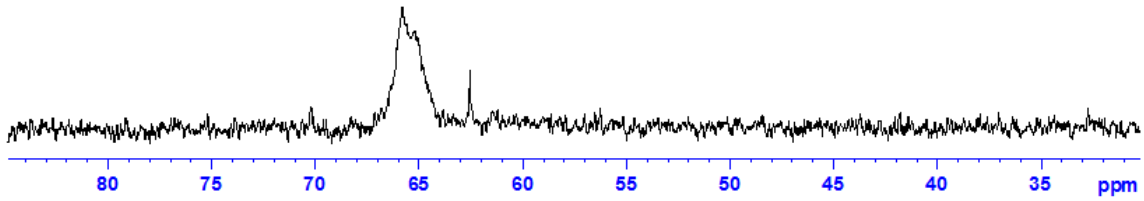

Figure A.51. $^{31}P\{^{1}H\}$ NMR (300 MHz, THF) spectrum of $CoH(Pcp_3)(CO)_3$, **4-4**.

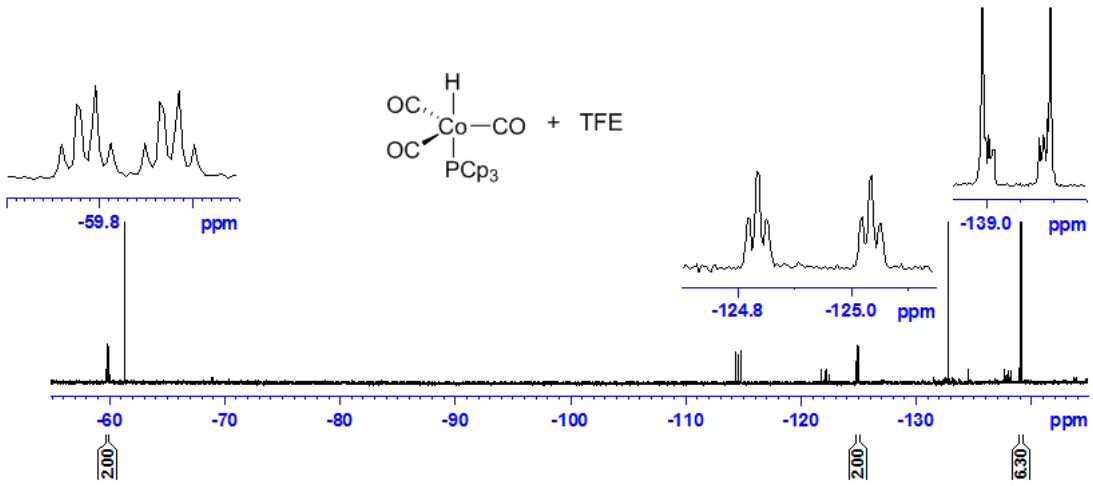

Figure A.52. ^{19}F NMR (282 MHz, THF) spectrum of $CoH(Pcp_3)(CO)_3$ + TFE reaction after 7 d.

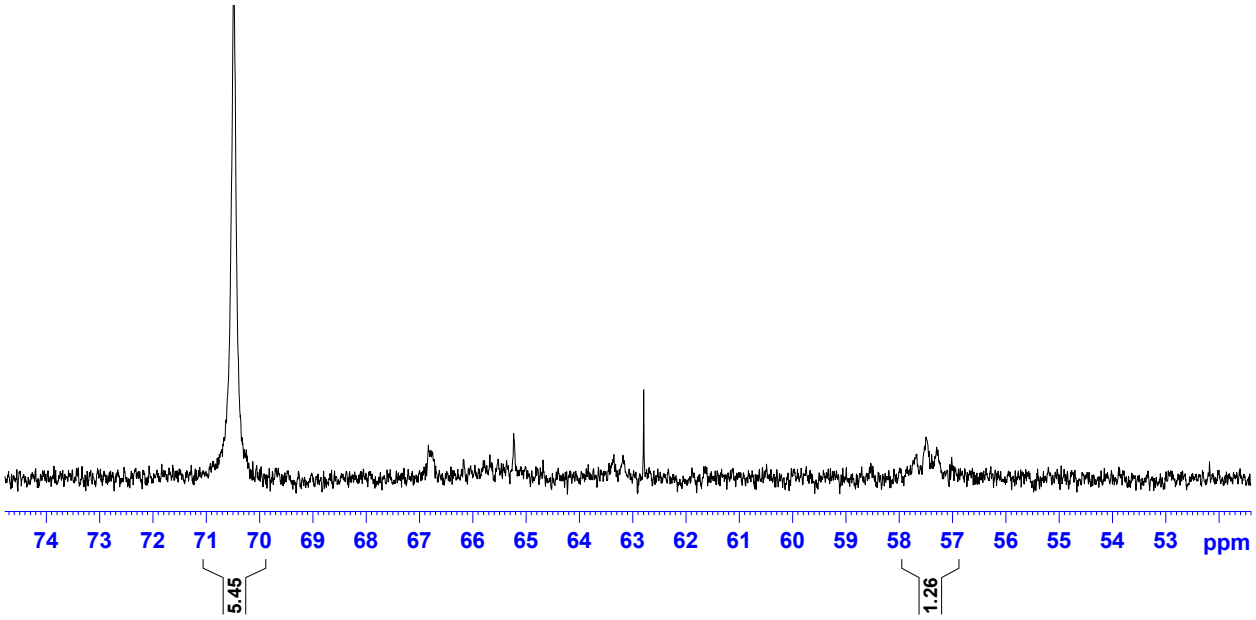

Figure A.53. $^{31}P\{^{1}H\}$ NMR (121 MHz, THF) spectrum of $CoH(Pcp_3)(CO)_3$ + TFE after 7 d.

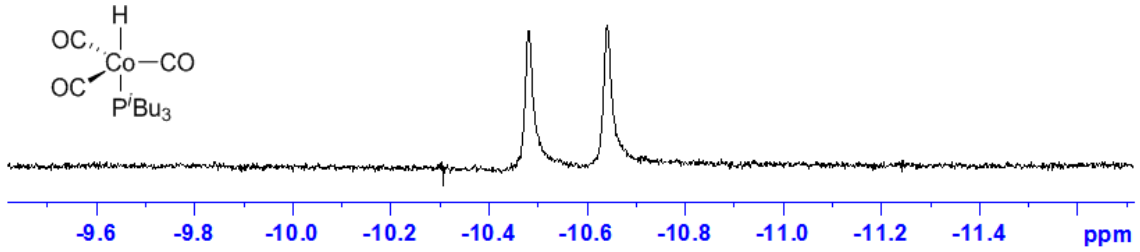

Figure A.54. ^{1}H NMR (300 MHz, THF) spectrum of $CoH(P^{i}Bu_3)(CO)_3$, **4-5**.

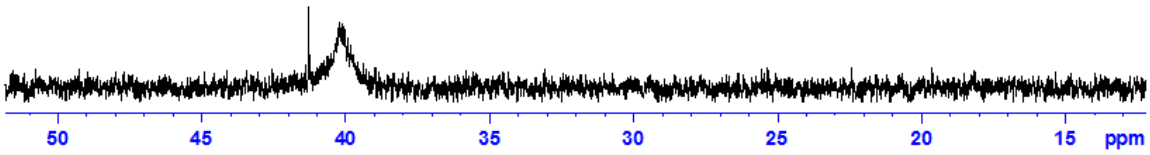

Figure A.55. $^{31}P\{^{1}H\}$ NMR (121 MHz, THF) spectrum of $CoH(P^{i}Bu_3)(CO)_3$, **4-5**.

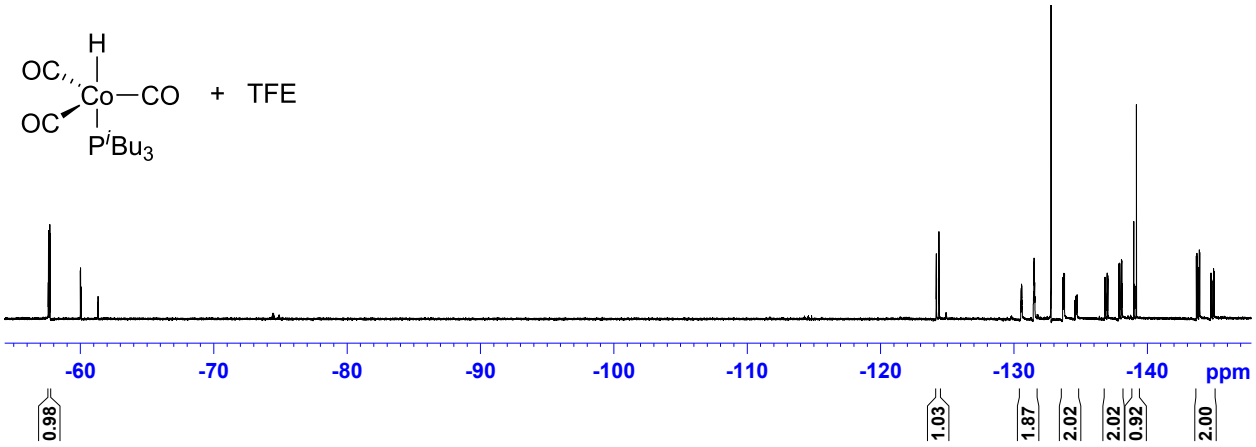

Figure A.56. ^{19}F NMR (282 MHz, THF) spectrum of CoH(P^{i}Bu$_3$)(CO)$_3$ + TFE reaction after 7 d.

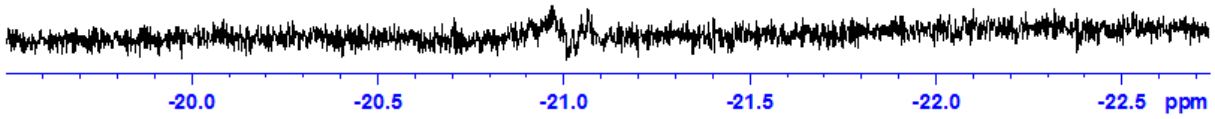

Figure A.57. ^{1}H NMR (300 MHz, THF) spectrum, hydride region, of CoH(P^{i}Bu$_3$)(CO)$_3$ + TFE reaction after 7 d.